University of Stavanger

Faculty of Science and Technology

MASTER'S THESIS

Study program/Specialization: M.Sc. Petroleum Geosciences Engineering	Spring semester, 2016 Open
Writer: Javed Iqbal	 _____ (Writer's signature)
Faculty supervisor: Alejandro Escalona External supervisor(s):	
Title of thesis: Reservoir characterization of the Lower Cretaceous clastic wedges in the southwestern Barents Sea using seismic analysis and rock physics diagnostic	
Credits (ECTS): 30	
Keywords: Barents Sea Clastic wedges Seismic analysis Rock physics diagnostics Well log facies Seismic facies Fan delta Basin floor fan	Pages: 106 + 17 front pages +enclosure: 1 CD Stavanger, 17/06/2016

Reservoir characterization of the Lower Cretaceous clastic wedges in the southwestern Barents Sea using seismic analysis and rock physics diagnostic

by

Javed Iqbal, M.Sc. Geophysics

Master Thesis

Presented to the Faculty of Science and Technology

The University of Stavanger

University of Stavanger

June, 2016

Dedication

This thesis work is dedicated to my parents, especially my mother whose prayers have always been a source of inspiration and constant support for me.

Acknowledgements

Abstract

Reservoir characterization of the Lower Cretaceous clastic wedges in the southwestern Barents Sea using seismic analysis and rock physics diagnostic

Javed Iqbal, M.Sc. Geophysics

The University of Stavanger, 2016

Supervisor: Alejandro Escalona

The southwestern Barents Sea is an underexplored area of the Norwegian continental shelf, with a few discoveries in Triassic and Jurassic reservoirs. Recently drilled exploration wells on the Loppa High and the surrounding margins have encountered hydrocarbon bearing clastic wedges in Lower Cretaceous strata. Previous studies have proposed two different depositional environments for these wedges: 1) deep marine fans and, 2) shallow marine transition with tidal influence. Consequently, further studies are required for better understanding of the depositional environment and the reservoir properties of the wedges. This study focusses on reservoir characterization of the Lower Cretaceous clastic wedges along the southern margin of the Loppa High in the Hammerfest Basin. The main objectives of this study are: 1) to define the depositional environment using well logs and seismic data and, 2) to investigate the reservoir properties using rock physics diagnostic. The dataset includes nine wells and four 3D seismic cubes which have been used to define the depositional environment of the wedges.

Ten seismic facies (SF1, SF2 …SF10) have been interpreted on the basis of seismic character and gamma-ray log response. Five types of the wedges (Type 1, Type 2…Type 5) have been identified on the basis of seismic facies whereas Type 1 and 4 also have well logs to support the interpretation. Seismic derived attributes such as variance, chaos and sweetness reveal the lobate shape fan delta (Type 4 wedge) and fan shaped submarine fans (Type 3 and 5 wedges). Sweetness attribute differentiates the fan delta and submarine fans based on their sand and shale content which further delimit these depositional bodies.

Depending upon the location of the wedges in the basin, the depositional environment ranges from transitional shallow marine to deep marine. The shallow marine environments include coastal/delta plain, fan delta, land slope aprons, and shelf canyons which are restricted

to the narrow shelf (Type 1, 2 and 4 wedges). Whereas, submarine fans and slope fans (Type 3 and 5 wedges) are dominant in deep marine environments.

Finally, rock physics analysis gives the reservoir properties from depositional (sorting) and diagenesis (cementation) points of view. Type 4 wedges (SF1 and SF4) on the narrow shelf are cemented and have porosity reduction mainly due to cementation and compaction (diagenesis effects). On the other hand, Type 1 wedges (SF2, SF3 and SF5) are not cemented and reduction in porosity is mainly due to deteriorating sorting of the grains (depositional effects). The role of diagenesis increases moving from the east to the west along the margin of the Hammerfest Basin. Therefore, the wedges on the western side have a potential of being good quality reservoirs because of porosity preservation due to cementation and well sorting of the grains.

Table of Contents

List of Figures

1 Introduction

1.1 General

Despite the exploration since 1980s in the southwestern Barents Sea, only a couple of fields have been proven commercial (Snøhvit) and (Goliat) in the Hammerfest Basin. Exploration activities have mainly focused on the western and southern parts of the Loppa High and the Hammerfest Basin targeting the Triassic and Jurassic age reservoirs. Recent discoveries (Johan Castberg & Novarg (2011), Havis (2012), Gohta and Wisting (2013), and Alta (2014)) have, once again, drawn the attention of explorationists towards the southwestern Barents Sea. Lower Cretaceous clastic wedges are one of the potential plays which are under focus in the province. Several wells have penetrated the clastic wedges in the southern and western margins of the Loppa High (7220/10-1 (Salina), 7120/1-2, 7120/2-2 and 7120/2-3S (Skalle)) as shown in Figure 1.

The Skalle well is one of the latest wells that have penetrated a wedge consisting of sandstone and siltstone of Aptian age within the Kolmule Formation, resulting into a considerable amount of gas reserves, not economical though (NPD, 2013). Other wells also have oil and gas shows from the Lower Cretaceous wedges proving the future potential of the play type. Wedges of good reservoir quality seemed to be developed on the southern bank of the Loppa High and in relatively deep western margin of the Hammerfest Basin. The analogue (a producing field) of this type of play is the Victoria Field on the United Kingdom continental shelf. However, there is no discovery of commercial importance in the Norwegian Barents Sea from this play type.

1.2 Previous work and geological problem

Rifting in overall transgressive environment in the Early Cretaceous triggered the dominance of shallow marine to marginal depositional environments on the southern margin of the Loppa High. Different studies and publications have been carried out on the characterization of the wedges in the past. Seldal (2005) discussed the Lower Cretaceous clastic wedges play with main focus on reservoir quality and its undrilled oil potential. Sattar et al. (2012) interpreted the wedges, located on the slope of the southern Loppa High, as submarine fans of reservoir quality. Sandvik (2014) suggested that the depositional environment for the Lower Cretaceous was offshore transition zone in transgressive settings with some indications of tidal influence. Wedges of similar type and age in southern margin of the Hammerfest Basin, also indicate various kinds of seismic character depending on the depositional environment e.g., chaotic high amplitudes, chaotic low amplitudes and continuous high amplitudes (Fjeld, 2014). A study

about the seismic stratigraphic interpretation of the Lower Cretaceous sediments reveals architecture of the deposits, giving indications to the depositional environment of the wedges (Marin et al., 2014). Rodriguez (2015) proposed that reservoir quality sand-rich systems may be present in the northeastern part of the Hammerfest Basin and become mixed submarine fans of lower reservoir quality while moving towards the southwestern side along the Loppa High. Matthews et al. (2015) carried out provenance studies about the possible source of the Cretaceous sediments in the Barents Sea. All of these studies have been used as basis to build on, especially one's from Sandvik (2014) and Rodriguez (2015) focusing on the depositional environment and the reservoir properties respectively. Most of these studies are part of the LOCRA project jointly managed by the University of Stavanger (UiS) and the University Center in Svalbard (UNIS) in cooperation with other universities. It has helped in understanding the Lower Cretaceous sediments from various perspectives as described earlier. However, the depositional system and intrinsic reservoir properties of the wedges are still least understood from seismic attributes and rock physics perspective. Understanding of these aspects of the wedges is crucial to find the true potential of this type of play in the Barents Sea.

1.3   Objectives and significance

This project focusses on characterization of the Lower Cretaceous clastic wedges in the southern margin of the Loppa High, especially those penetrated by wells 7120/1-2, 7120/2-3S and 7120/2, using an integrated analysis of well and seismic data. There are two main objectives of this project; 1) define the depositional system of the wedges and their evolution based on seismic facies and attributes integrated with well data, and 2) apply rock physics analysis for evaluation of the reservoir properties of the wedges.

Seismic facies and attributes, integrated with well data, define the depositional environment on the basis of morphology of the response from various lithologies. An integrated rock physics analysis is then helpful to characterize the reservoir potential of the wedges in the wells that have penetrated the wedges. This approach may help understanding the depositional environment and intrinsic reservoir properties of the wedges under investigation which might lead to successful targeting of prospects for petroleum exploration in this play type.
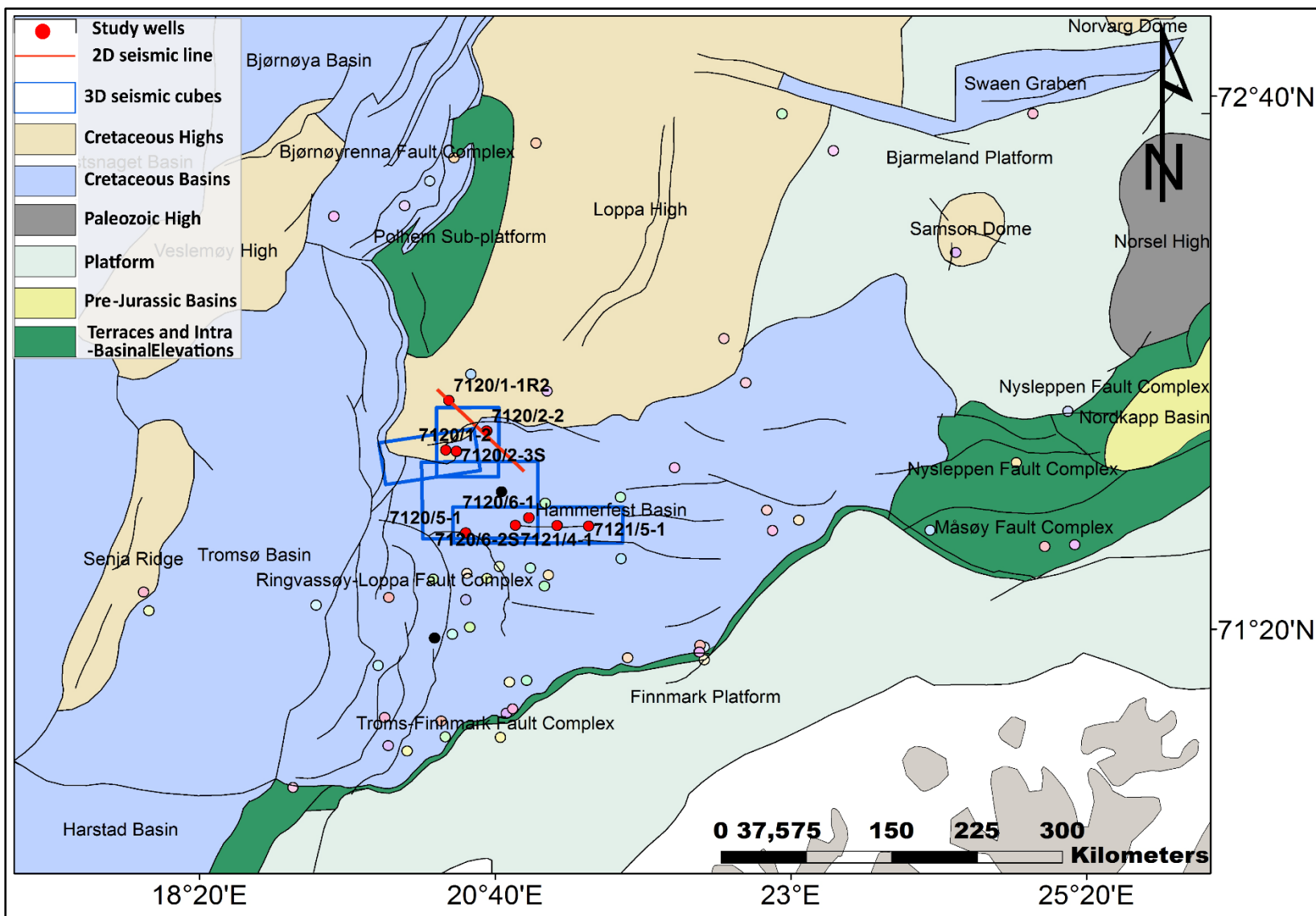
Figure 1: Location of the southwestern Barents Sea with structural elements and wells drilled in the area. 3D Seismic data (blue rectangles), 2D seismic line (red) and wells (red dots) used in this study are highlighted.

2   Regional background

2.1   Regional structural geology

The Barents Sea is the northwestern part of the Eurasian plate which is bounded by the North Atlantic Ocean (Norwegian/Greenland Sea) and Svalbard to the west and northwest respectively and Novaya Zemlya to the East (Figure 2). The continental shelf of the western Barents Sea is bounded by three major fault zones, the Senja Fracture Zone (SFZ) and the Hornsund Fault Zone (HFZ) to the west and northwest respectively, and the Troms-Finnmark Fault Complex (TFFC) to the south (Gabrielsen, 1984). The Senja Fracture Zone and the Hornsund Fault Zone may be considered the most fundamental, as they are the transition zone between the oceanic and continental crust at the western margin of the continental shelf (Gabrielsen, 1984). The sedimentary basins at the conjugate continental margins of Norway and Greenland and in the western Barents Sea developed as a result of a series of post-Caledonian rift episodes until the Early Cenozoic time, when the complete continental separation took place (Faleide et al., 2008). The southern Barents Sea is divided into two parts, differing in tectonic and stratigraphic development, by the Ringvassøy-Loppa and the Bjørnøyrenna Fault Complexes. The area to the west of this boundary was tectonically very active throughout the Late Mesozoic and the Cenozoic times, with the deposition of enormous thicknesses of Cretaceous, Paleogene and Neogene sediments in the Harstad, Tromsø and Bjørnøya basins. NNE-SSW, NE-SW and locally N-S trending faults dominate in this western part. In contrast, the area to the east is dominated by thick Upper Paleozoic and Mesozoic sequences in the Hammerfest and Nordkapp basins, where E-W, WNW-ESE to ENE-SSW fault trends dominate (Halland et al., 2014).

The Hammerfest Basin is a fault controlled basin bounded by the Ringvassøy-Loppa Fault Complex (RLFC) to the west, the Troms–Finnmark Fault Complex (TFFC) to the south, the Asterias Fault Complex (AFC) to the north and the Bjarmeland Platform to the east. AFC is a complex network of faults that controlled the deposition of the Lower Cretaceous sediments (Faleide et al., 1993). The basin was established due to rifting in Early to Late Carboniferous. The internal part of the basin is characterized by the east-west striking faults (probably flexural faults) related to tectonic activity in the Upper Jurassic. Thicker sediment packages of the Triassic, Jurassic and Lower Cretaceous are preserved, and are covered by thin/condensed section of the Upper Cretaceous and the Paleocene shale. There are no evidences of the Paleozoic evaporites in the basin unlike Tromsø and Nordkapp basins to the west and east respectively (Halland et al., 2014). The Lower Cretaceous is composed of overall fine grained

transgressive sediments with occasional input of reservoir quality sand wedges. The Lower Cretaceous deposits consist mainly of three formations as discussed in the next section (Figure 3).
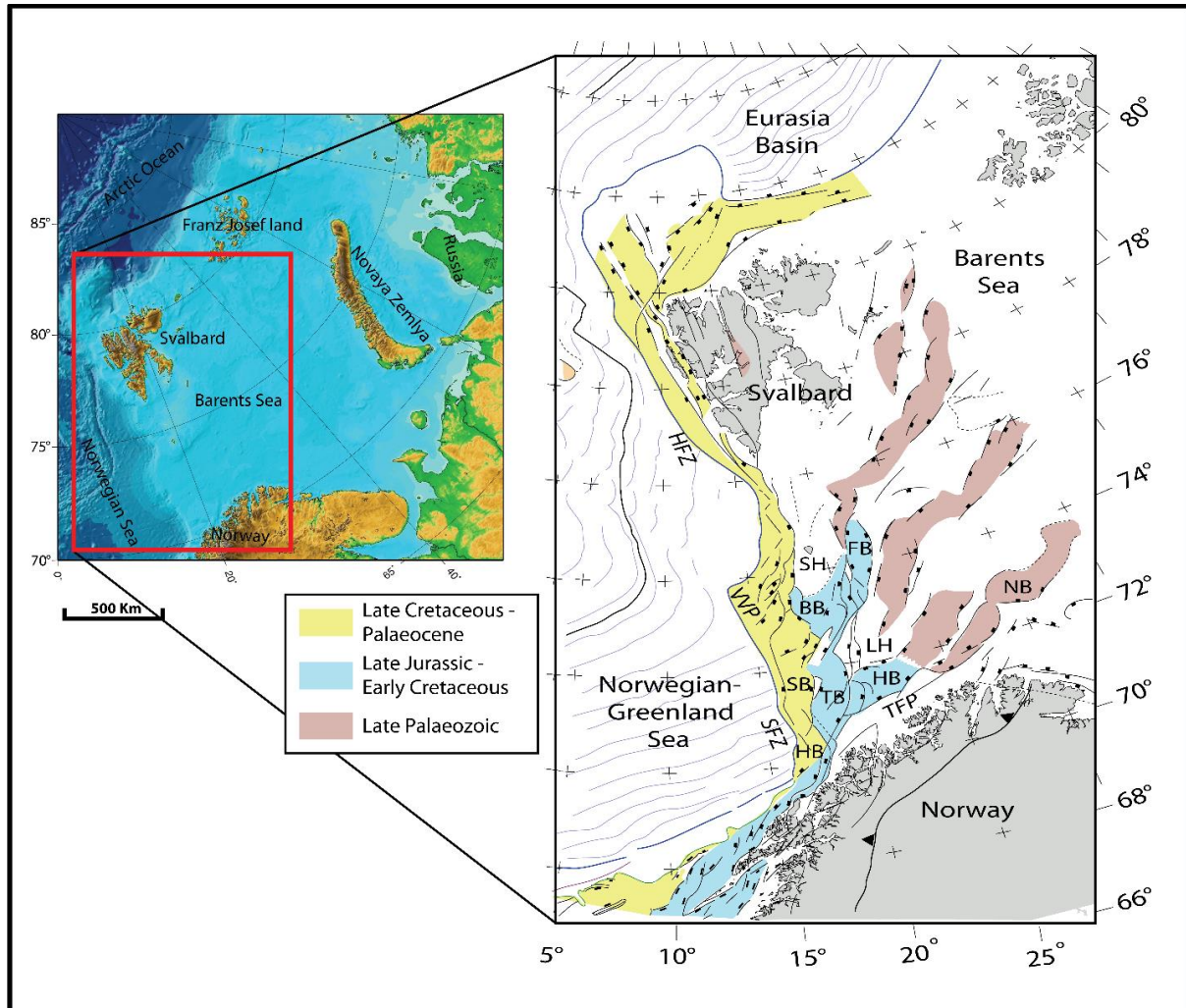
Figure 2: Location map of structural elements in the western Barents Sea. Main structures and basins are Troms-Finnmark platform (TFP), Harstad Basin (HB), Sørvestsnaget Basin (SB), Tromsø Basin (TB), Hammerfest Basin (HB), Loppa High (LH), Nordkapp Basin (NB), Fingerdjupet sub-Basin (FB), Bjørnøya Basin (BB), Vestbakken Volcanic province (VVP), Senja Fracture Zone (SFZ), Hornsund Fracture Zone (HFZ), and Stappen High (SH). Different colors show the basins developed in different ages. (Modified from Faleide et al., 2010 and Jakobsson et al., 2012)

2.2 Lower Cretaceous stratigraphy

2.2.1 Knurr Formation

The Knurr Formation (Berriasian/Valanginian to lower Barremian) is distributed over the southwestern part of the Barents Shelf, mainly in the Hammerfest Basin which contains dark grey to greyish claystone with thin beds of limestone and dolostone. It also contains sandstone clastic wedges pinching out towards the center of the basin (Dalland et al., 1988). It overlies the Upper Jurassic Hekkingen Formation, top of which is interpreted as Base Cretaceous Unconformity (BCU). The formation was deposited in an open generally distal marine environment with local restricted bottom conditions (Dalland et al., 1988).

2.2.2 Kolje Formation

An Early Barremian to Late Barremian/Early Aptian age, Kolje Formation dominantly consist of dark brown to dark grey shale and claystone with minor beds of pale limestone and dolomite. The upper part of the formation also contains thin beds of light grey to brown siltstone and sandstone. The formation thickness increases westwards but become thin towards the central part of the Hammerfest Basin. The lithology remains relatively similar regionally (Dalland et al., 1988).

2.2.3 Kolmule Formation

An Aptian to mid-Cenomanian age is assigned to the Kolmule Formation and is composed of dark grey to green claystone and shale, silty in parts with minor thin interbeds of siltstone and limestone and dolomite stringers. Traces of glauconite and pyrite can also be found.

Thickness of the formation increases towards and into the Tromsø Basin and shows a small increase in thickness in the eastern margin of the Hammerfest Basin (Dalland et al., 1988). A relatively clean sandstone has been penetrated by the Skalle well i.e. 7120/2-3S in the Lower Kolmule Formation, which is gas discovery (NPD, 2013). Open marine depositional environment is suggested for the formation on regional scale (Dalland et al., 1988).
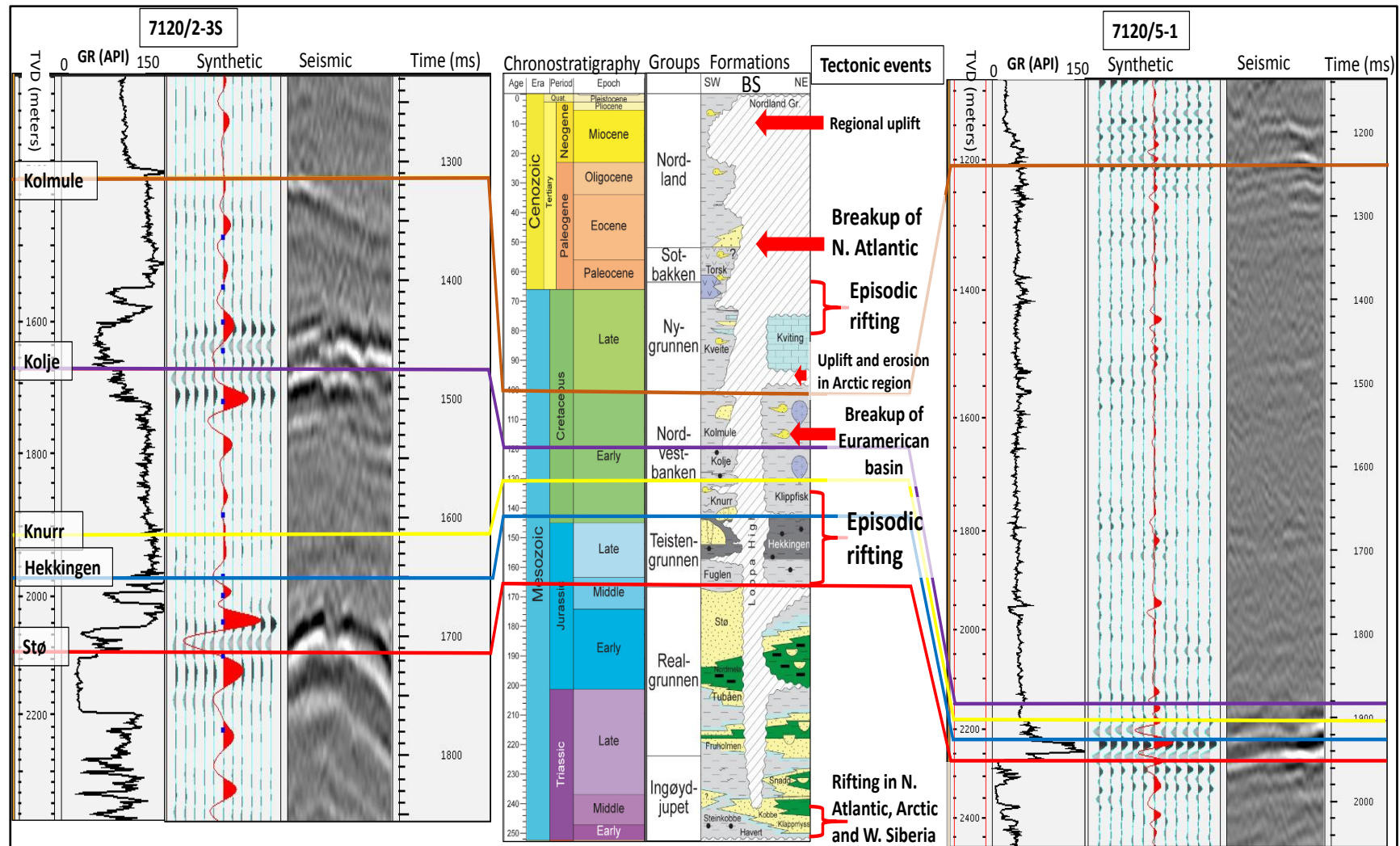
Figure 3: Lithostratigraphy of the Barents Sea. Formations of the Lower Cretaceous are correlated and synthetic seismograms are shown for two of the wells. Well 7120/2-3S is located on the narrow shelf whereas well 7120/5-1 is located in the Hammerfest Basin. Notice the thickening of the strata between the Hekkingen and the Kolje formations in well 7120/2-3S. Lithostratigraphic column is modified from Smelror et al. (2009).

2.3 Background of depositional environments in tectonically active settings

2.3.1 Transitional shallow marine environments

2.3.1.1 Fan deltas

Fan deltas are coarse grained deltas which are formed where alluvial fans prograde directly into a standing body of water from adjacent highlands (Wescott and Ethridge, 1980). They mainly occur in tectonically active areas such as the rift basins, pull apart basins and back arc basins (Hwang et al., 1995). Fan deltas produce small wedge shaped bodies of sediment displaying abrupt changes in the facies and a high variability in the paleocurrent patterns (McPherson et al., 1987). They commonly act as indicators of tectonic activity during the deposition. The location of the sediment source area and the depocenter of a fan delta depend on the basin wide tectonic activities, such as hanging wall subsidence and footwall uplift (Hwang et al., 1995). The fan deltas associated with rift basins are shown in Figure 4. The deposits are generally coarse grained, very poorly sorted, matrix rich, heterolithic and partially cemented by carbonate, depositing concurrently. As a result, they usually have very low porosity and permeability (McPherson et al., 1987). Progradational patterns and internal geometries of depositional systems are related to the timing, style and magnitude of tectonic movements (Hwang et al., 1995). A slight variation in the base level and the sediment supply can affect progradational patterns and architecture of sedimentary facies (Hwang et al., 1995).

Fan deltas can be deposited in lowstand, transgressive and highstand system tracts depending on their proximal and distal locations (Hoy and Ridgway, 2003). Distal fan deltas may also deposit during forced regression during rapid sea level fall.
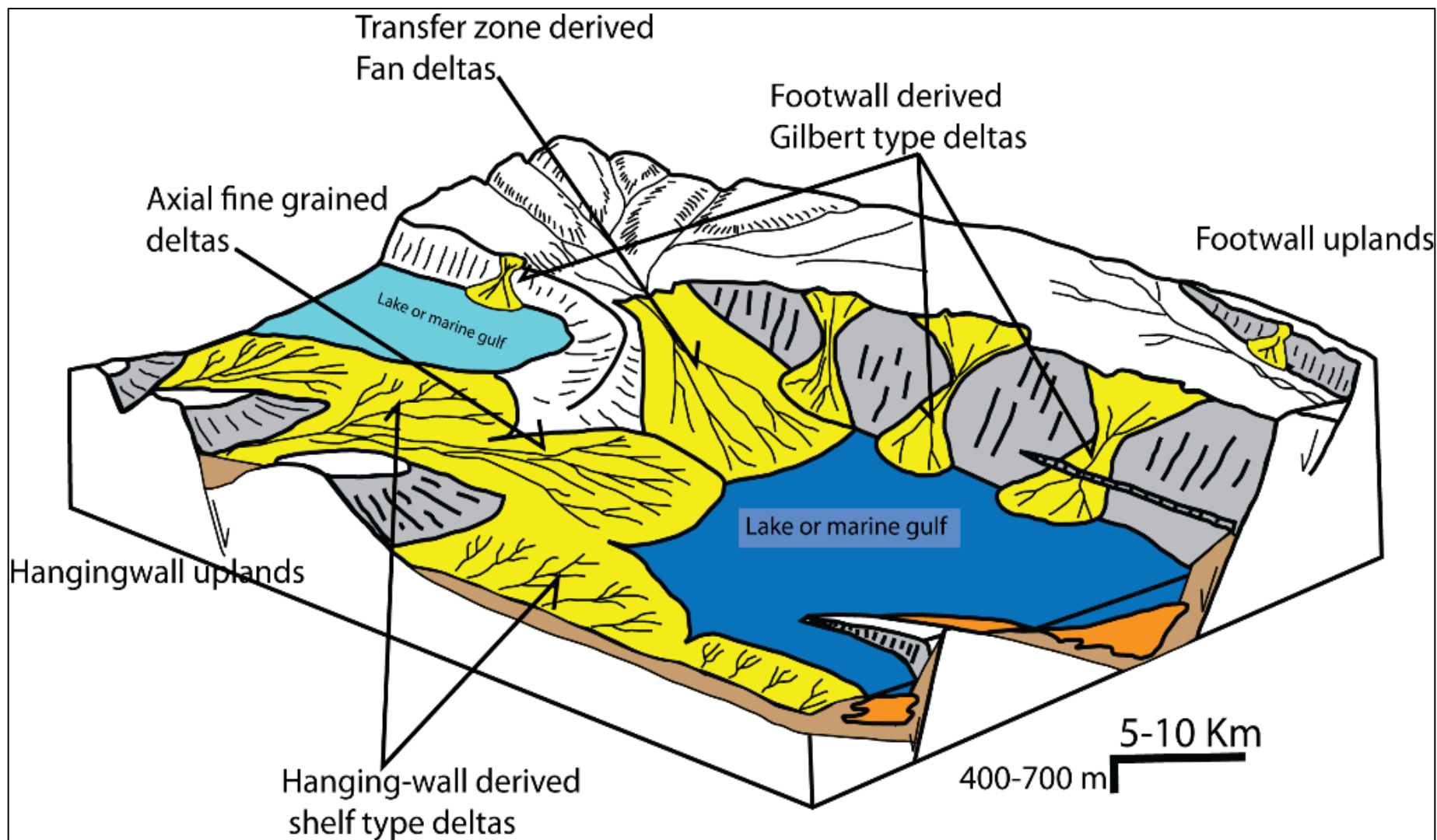
Figure 4: Types of fan deltas in a rift basin. Deltas may be sourced from footwall uplands, hanging wall uplands or the transfer zones between two en-echelon fault segments. (digitized from Reading (2009)

2.3.1.2 Slope aprons

Slope aprons lie between the shelf or land area and the basin floor, both small shelf basins and large ocean basins. They are distinguished from ramps by being fed from an essentially continuous linear source. However, it is difficult to distinguish between the two at coarser end of the spectrum. They extend from 2 to 200 km into the basin with a relatively high gradients of 10-150 m/km. (Reading, 2009).

Slope aprons are divided into four types on the basis of dominant grain size: mud rich slope aprons, mixed mud/sand rich slope aprons, sand rich slope apron sand gravel rich slope aprons. Sand/mud rich slope apron in deep marine settings is shown in Figure 5.
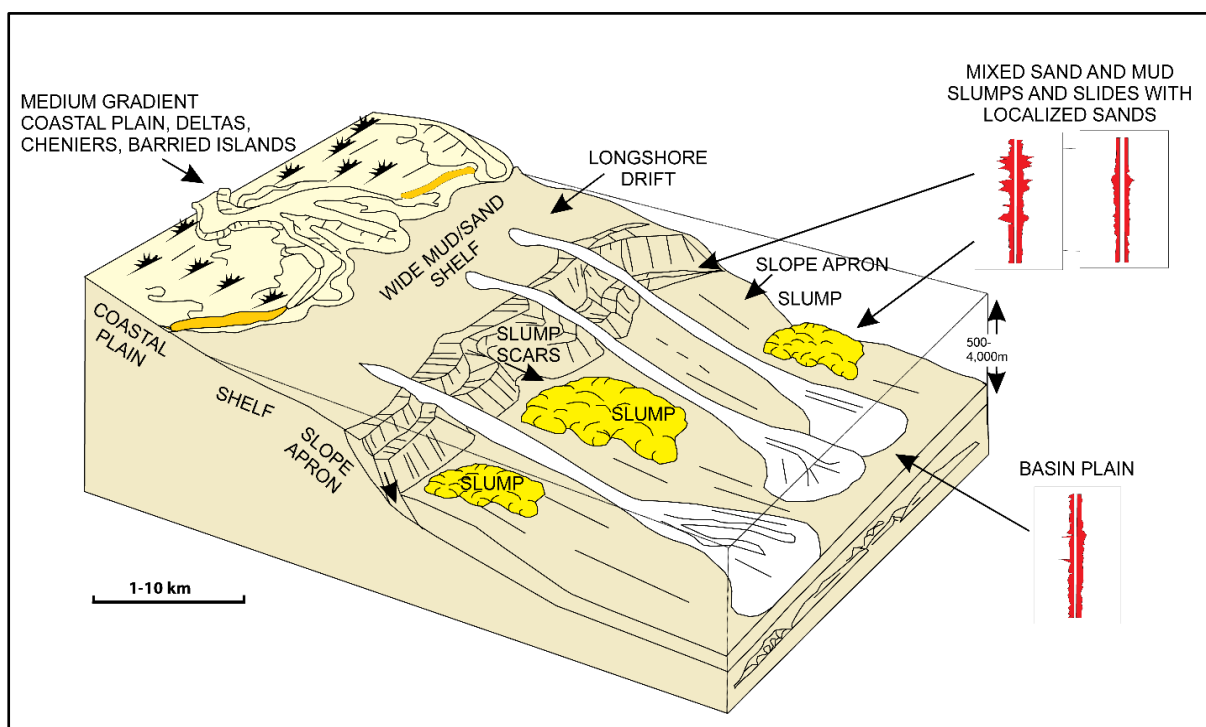
Figure 5: Sand/mud rich slope apron. The sediments deposits on the slope by debris flow, slumps and multi-point sources from the shelf or land. This is an example of deep marine apron , however similar kind of aprons may develop between highlands and shallow platform such as between Loppa High its narrow shelf to the south. (Weimer et al., 2007)

2.3.1.3 Straind-plains

Strandplains are marine dominated processes depositional features welded to coastal mainlands in linear shape along the shoreline. They are classified into two main groups: sand rich beach ridge plains and mud rich chenier plains (Figure 6). Both of them are dominantly progradational features shaped by interplay of sediment texture/rate of supply, coastal physiography and wave and tidal energy (Tyler and Ambrose, 1985). Chenier plains are formed when there is an abundance supply of mud to the system. Beach ridge plains are sand dominated and the corresponding facies are: 1) sandy beach ridge complex, which is the most widespread of

10

strandplain facies, 2) crosscutting fluvial-deltaic complexes, and 3) sand shoreface. Chenier plains consist of: 1) tidal or storm influenced interridge mud flats, 2) cheniers, 3) fluvio-estuarine complexes, and 4) sandy to silty shoreface (Tyler and Ambrose, 1985). The strandplains can be observed in the seismic data used in this study and are clearly visible in seismic derived attributes discussed in coming sections.
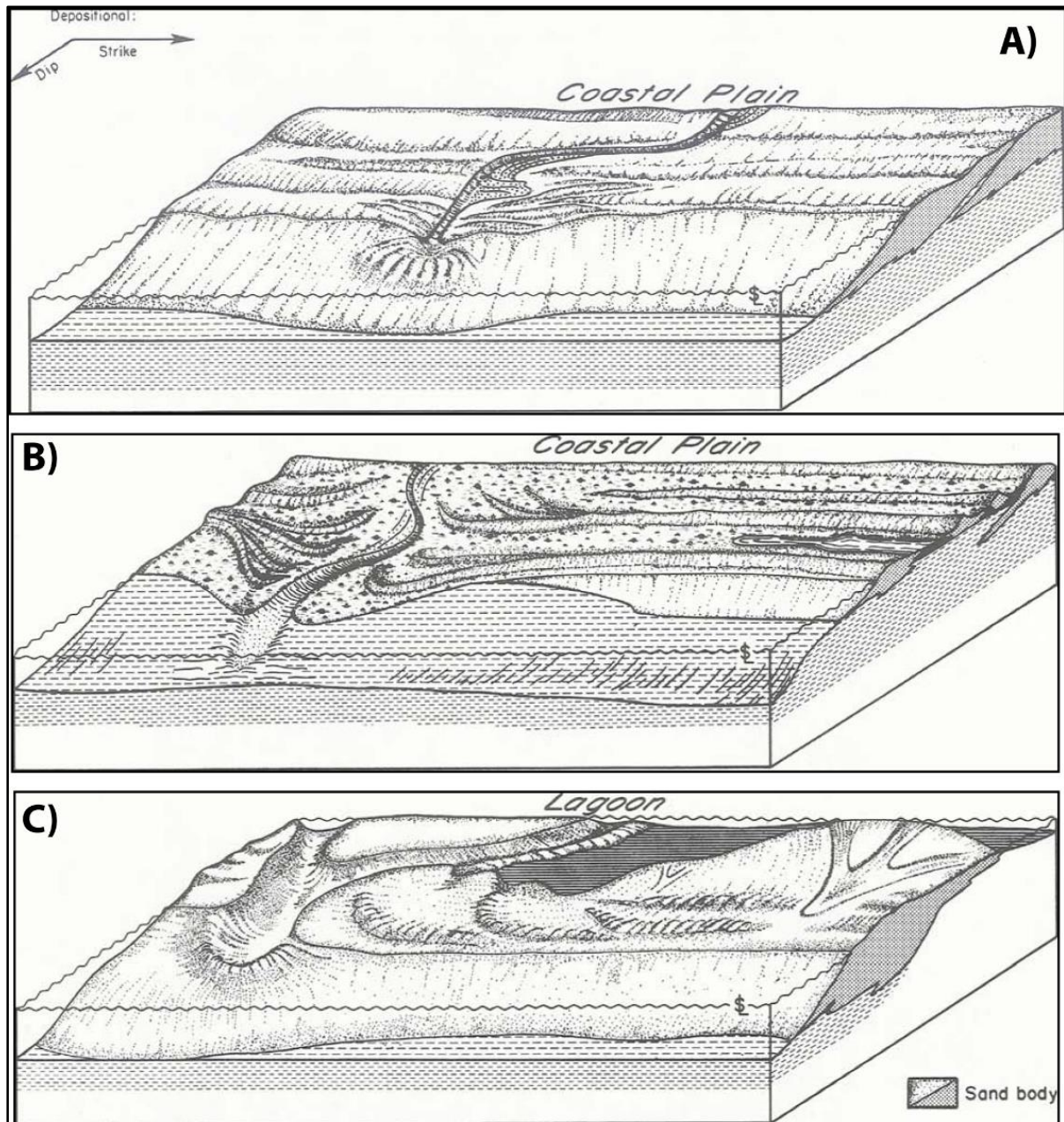
Figure 6: A) Sand-rich strandplain, B) Mud-rich strandplain and C) Barrier island (Tyler and Ambrose, 1985)

2.3.2 Deep marine environments

2.3.2.1 Submarine fans

Submarine fans are the deep water accumulation of sediments in the shape of fans. The main sediment transport mechanism for these fans is turbidity currents and through suspended load (Reading, 2009). They have three parts based on the environment of deposition and sediment texture: inner fan, mid fan and outer fan as shown in Figure 7.

Submarine fans can also be divided into four types like slope aprons: mud rich fans, mixed sand/mud rich fans, sand rich fans and gravel rich fans (Reading, 2009). Figure 7 shows various sub environments for the mixed sand/mud submarine fans along with log responses.
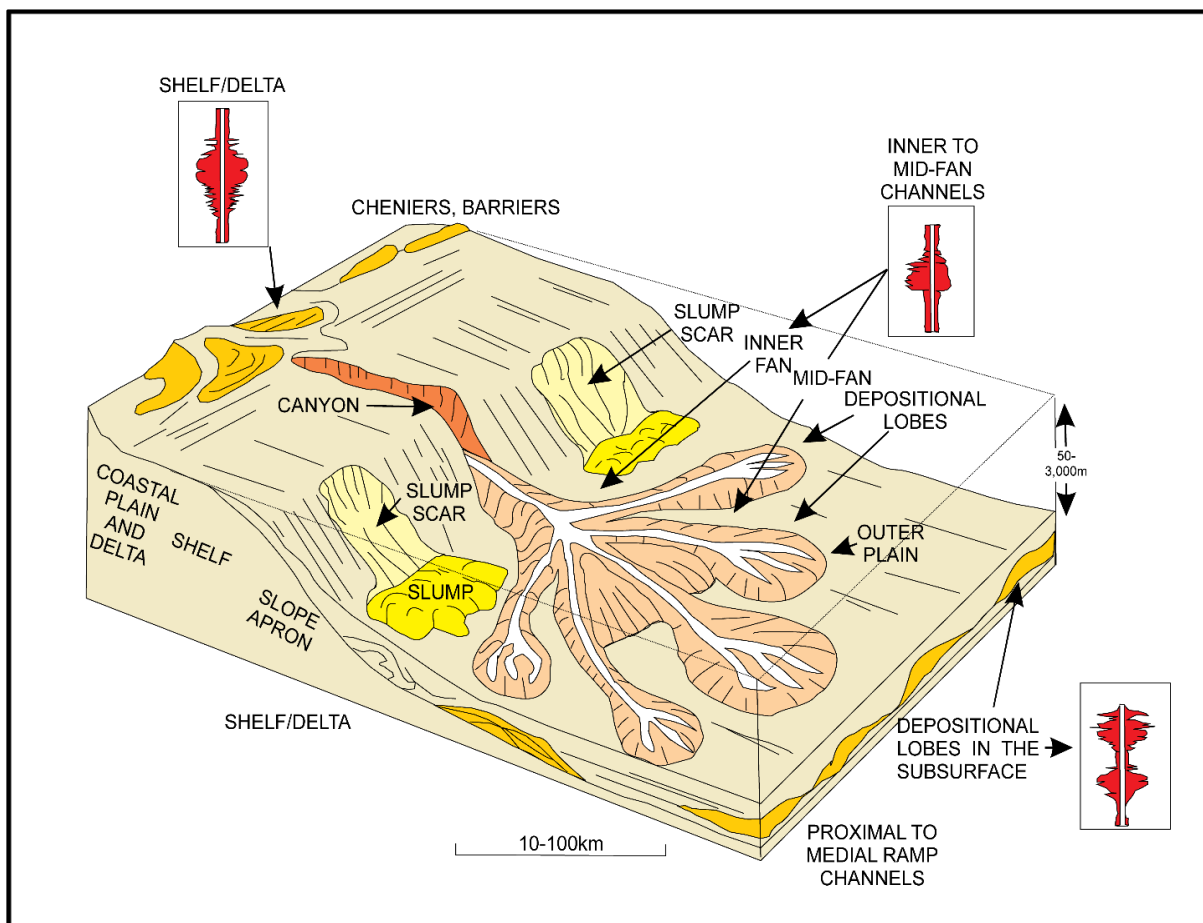
Figure 7: Sand/mud rich submarine fan. Various sub-environments have been highlighted with well log responses. Notice the difference in log responses of the channelized and lobe part of the fan (Weimer et al., 2007).

2.4 Rock physics diagnostics

Rock physics relates porosity, mineralogy, fluid saturation and their properties to the elastic properties of the rock which is helpful in interpreting the connection between seismic impedance and velocity inversion/reservoir properties (Avseth et al., 2010). Rock physics

12

diagnostics explains the differences in the depositional and diagenetic properties of the rocks through interpretation of various trends of the data in velocity-porosity, impedance-porosity and/or elastic moduli-porosity plane. Identification of these trends from the data and assigning it to appropriate depositional sequences is called rock physics diagnostics (Avseth et al., 2000). Rock physics diagnostics is performed on well log and core data and various relations between porosity and elastic properties are generated. These relations are helpful in understanding the behavior of the rocks with varying elastic properties. Fundamental elastic properties include p-wave velocity (Vp), s-wave velocity (Vs) and density (ϱ). Once these relations are found, texture of the rock i.e. diagenetic cement, grain size sorting, volume of clay etc. is easy to define with accuracy. For example, well sorted grains correspond to high energy environments whereas poorly sorted grains are product of low energy depositional environments (Avseth et al., 2010).

The relationships between porosity and elastic properties of the rocks can be obtained using following data:

1. Velocity, density, porosity and mineralogical measurements from core data and/or,
2. Velocity, density, porosity and mineralogical (Gamma Ray) logs from well log curves.

In this project, well log data is used to generate cross plots, then the rock physics models are superimposed on the data for interpretation of depositional and diagenetic properties of the clastic wedges encountered in three of the study wells. It is worthy to note that the interpretations using these models may not be the best because of uncertainties in the models which are based on assumptions and the data itself. However, they are helpful in estimating the rock properties within acceptable limits of errors.

2.4.1 The friable sand model

Dvorkin and Nur (1996) proposed friable sand model for unconsolidated high porosity sands. The velocity-porosity relation for this model changes as the sorting deteriorates. These sand are bounded by confining pressure to a rock under reservoir conditions otherwise they are likely prone to sanding if pressure is removed. This model assumes that porosity of sandstone decreases due to deposition of solid matter away from the grain contacts (Figure 8). Reduction in porosity may correspond to deteriorating grain sorting in low energy depositional environment. This non-contact additional solid matter weakly affects the stiffness of the rock (Dvorkin and Nur, 2002).

This model connects two end points in elastic moduli- porosity plane: critical porosity at one end and zero porosity at the other. The elastic moduli of the dry rock at critical porosity end are described by the moduli of a pack of elastic spheres which is subject to confining pressure (Fanka, 2012). These moduli are given by Hertz-Mindlin theory as follows (Mindlin, 1949);
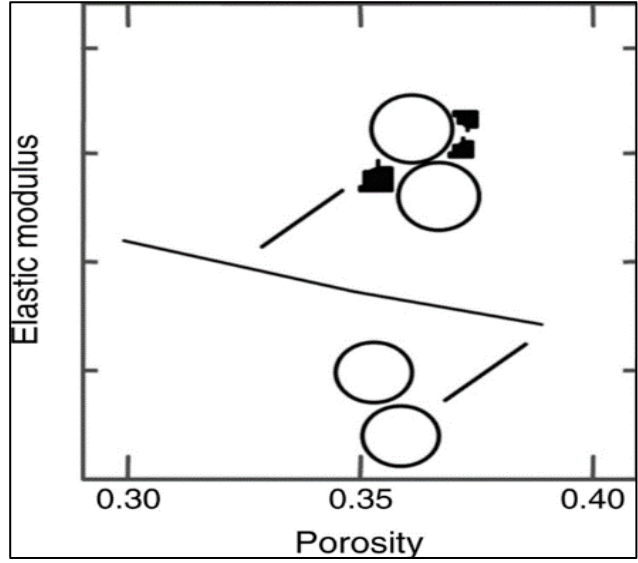
Figure 8: Schematic depiction of the friable sand model and corresponding sedimentological variation (Avseth et al., 2005)

$$K_{HM} = \left[\frac{n^2(1-\phi_c)^2 G_{MIN}^2}{18\pi^2(1-v)^2} P \right]^{\frac{1}{3}} \tag{1}$$

$$G_{HM} = \frac{5-4v}{5(2-v)} \left[\frac{3n^2(1-\phi_c)^2 G_{MIN}^2}{2\pi^2(1-v)^2} P \right]^{\frac{1}{3}} \tag{2}$$

Where

K_{HM} = Bulk modulus of dry rock

G_{HM} = Shear Modulus of dry rock

ϕ_c = Critical porosity

P = Effective pressure i.e. difference between overburden and pore pressures

G_{MIN}= Shear modulus of mineral phase

v =Poisson's ratio of mineral phase

n = Coordination number i.e. average number of contacts per grain at given porosity

For the zero porosity end, the elastic moduli (K and G) represent the mineral point which are usually available from laboratory measurements.

The elastic moduli between these two ends are computed using a combination of Hertz-Mindlin contact theory and Hashmin-Shtrikman lower bound. The following equations are used for the calculation of elastic moduli;

$$K_{dry} = \left[\frac{\frac{\phi}{\phi_c}}{K_{HM} + \frac{4}{3}\,G_{HM}} + \frac{\frac{1-\phi}{\phi_c}}{K_{HM} + \frac{4}{3}\,G_{HM}} \right]^{-1} - \frac{4}{3}\,G_{HM} \tag{3}$$

14

$$G_{dry} = \left[\frac{\frac{\phi}{\phi_c}}{G_{HM} + Z} + \frac{\frac{1-\phi}{\phi_c}}{G_{HM} + Z} \right]^{-1} - Z \qquad (4)$$

Where

$$Z = \frac{G_{HM}}{6} \left[\frac{9K_{HM} + 8G_{HM}}{K_{HM} + 2G_{HM}} \right]$$

K_{dry}= Bulk modulus of dry frame of the rock

G_{dry}= Shear modulus of dry frame of the rock

ϕ= Porosity of the rock which is mixture of elastic sphere pack and the solid phase, always less than critical porosity.

The upper bound can easily be calculated using the same equations (3) and (4) and Z by replacing G_{HM} with G_{MIN}. Hertz-Mindlin theory tends to overpridict the shear modulus, therefore a correction factor has to be applied which is equal to G_{HM}=0.5 G_{HM} (Fanka, 2012). Dvorkin and Gutierrez (2002) proposed that friable sand model can also be applied to generate constant clay lines for shaly sands to sandy shales. Critical porosity of clean sands ϕ_c is replaced with porosity of clean shale ϕ_{shale} and the fraction of clay (C) in the rock. Volume of clay (C) is inversely related to the porosity of clean shale conditioned that silt grains are dispersed in clay matrix and is as follows;

$$C = \phi/\phi_{shale} \qquad (5)$$

Elastic moduli for this shale dominated rock can be calculated using following equations;

$$K_{MIX} = \left[\frac{C}{K_{SHALE} + \frac{4}{3} G_{SHALE}} + \frac{1-C}{K_{QTZ} + \frac{4}{3} G_{SHALE}} \right]^{-1} - \frac{4}{3} G_{SHALE} \qquad (6)$$

$$G_{MIX} = \left[\frac{C}{G_{SHALE} + \frac{4}{3} Z_{SHALE}} + \frac{1-C}{G_{QTZ} + \frac{4}{3} Z_{SHALE}} \right]^{-1} - Z_{SHALE} \qquad (7)$$

Where

$$Z_{SHALE} = \frac{G_{SHALE}}{6} \left[\frac{9K_{SH} + 8G_{SH}}{K_{SH} + 2G_{SH}} \right]$$

C= Volume of shale as given by equation 5.

K_{MIX}= Bulk modulus of mixture rock

G_{MIX}= Shear Modulus of mixture rock

K_{SHALE}= Bulk modulus of pure shale

15

G$_{SHALE}$= Shear modulus of pure shale

K$_{QTZ}$= Bulk modulus of silt grains (100% quartz)

G$_{QTZ}$= Shear modulus of silt grains (100% quartz)

Bulk density for the mixture can be calculated using following formula;

$$\rho_b = \rho_{qtz}(1-C) + C(1-\phi_{SHALE})\rho_{clay} + C * \phi_{SHALE} * \rho_{fl} \qquad (8)$$

Where

ρ_{qtz}= Density of quartz

ρ_{clay}= Density of clay

ρ_{fl}= Density of fluid

Figure with clay models.

2.4.2 The contact cement model

The contact cement model was also proposed by Dvorkin and Nur (1996) which describes the behavior of high velocity/porosity sands in relation with cement volume. Deposition of even small amount of cement at the grain contacts causes a rapid stiffening of the rock with minute decrease in porosity and a significant increase in velocity (Figure 9). This model explains that after this small decrease in porosity, further decrease is caused by diagenesis and deteriorating sorting of the grains. An assumption has to be made that porosity is almost same as for well sorted friable sand model. Well sorted friable sand is well sorted packing of similar grains and has a critical porosity from 36 to 40% for sandstones and 60% for shales (Fanka, 2012). More poorly sorted cemented sandstones are modelled using constant cement model (Avseth et al., 2005).
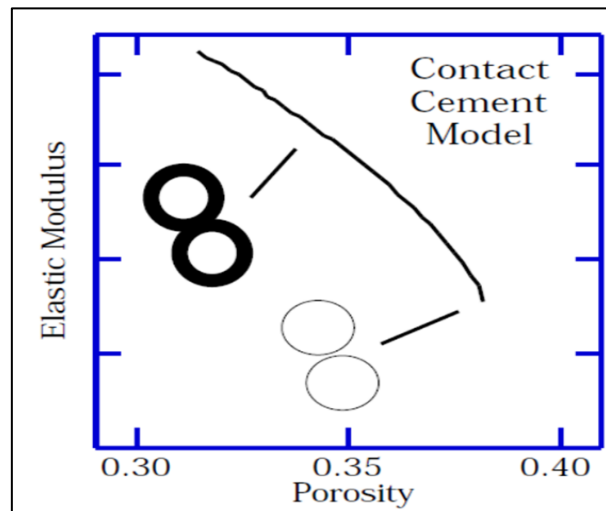
Figure 9: Schematic depiction of the contact cement model and corresponding diagenetic variation (Dvorkin and Nur, 2002).

The contact cement model assumes that the layer of cement is uniformly deposited on the grain contacts, decreasing the porosity from an initial critical porosity value. The cement could be quartz, calcite or a reactive clay e.g. illite (Dvorkin and Nur, 1996). The following equations for the elastic moduli are based on rigorous contact problem solution by Dvorkin et al. (1994) and the error does not exceed 1%.

16

$$K_{Dry} = \frac{1}{6}n(1 - \phi_c)M_cS_n \tag{9}$$

$$G_{Dry} = \frac{3}{5}K_{Dry} + \frac{3}{20}n(1 - \phi_c)G_cS_\tau \tag{10}$$

Where

$$M_c = \rho_c V_{Pc}{}^2$$

$$G_c = \rho_c V_{Sc}{}^2$$

ρ_c, V_{Pc} and V_{Sc} are the density, P-wave and S-wave velocity respectively. K_{Dry} and G_{Dry} are the effective bulk and shear moduli respectively. S_n and S_τ are proportional to the normal and shear stiffness respectively of a cemented two-grain combination. They depend on the amount of contact cement and properties of the cement and the grains (Dvorkin and Nur, 1996). They can be calculated using following equations;

$$S_n = A_n(\Lambda_n)\alpha^2 + B_n(\Lambda_n)\alpha + C_n(\Lambda_n)$$

Where

$$A_n(\Lambda_n) = -0.024153 * \Lambda_n{}^{-1.3646}$$

$$B_n(\Lambda_n) = 0.20405 * \Lambda_n{}^{-0.89008}$$

$$C_n(\Lambda_n) = -0.00024649 * \Lambda_n{}^{-1.9846}$$

$$S_\tau = A_\tau(\Lambda_\tau, v)\alpha^2 + B_\tau(\Lambda_\tau, v)\alpha + C_\tau(\Lambda_\tau, v)$$

Where

$$A_\tau(\Lambda_\tau, v) = 10^{-2} * (2.26v^2 + 2.07v + 2.3) * \Lambda_\tau{}^{0.079v^2 + 0.1754v - 1.342}$$

$$B_\tau(\Lambda_\tau, v) = (0.0573v^2 + 0.0937v + 0.0202) * \Lambda_\tau{}^{0.0274v^2 + 0.0529v - 0.8765}$$

$$C_\tau(\Lambda_\tau, v) = 10^{-4} * (9.654v^2 + 4.945v + 3.1) * \Lambda_\tau{}^{0.01867v^2 + 0.4011v - 1.8186}$$

$$\Lambda_n = \frac{2G_c(1 - v)(1 - v_c)}{\pi G\,(1 - 2v_c)}$$

$$\Lambda_\tau = S\frac{G_c}{\pi G}$$

$$\alpha = \left[\frac{2S\phi_c}{3(1 - \phi_c)}\right]^{0.5}$$

2.4.3   The constant cement model

The constant cement model was introduced by Avseth et al. (2000) which assumes that sands of varying porosity have the same amount of contact cement. Porosity variations are solely due to non-contact pore-filling material e.g. deteriorating sorting (Figure 10). Mathematically, this model is a combination of the contact cement model and the friable sand models. This model

explains the porosity reduction from the initial sand pack critical porosity to ϕ_b (initial cement porosity) due to contact cement deposition, and further decrease from ϕ_b due to deposition of solid phase away from the grain contacts. Bulk and shear moduli of dry rock can be computed using the following formulas;

$$K_{dry} = \left[\frac{\frac{\phi}{\phi_b}}{K_b + \frac{4}{3} G_b} + \frac{\frac{1-\phi}{\phi_b}}{K_{MIN} + \frac{4}{3} G_b} \right]^{-1} - \frac{4}{3} G_b \tag{11}$$

$$G_{dry} = \left[\frac{\frac{\phi}{\phi_b}}{G_b + Z} + \frac{\frac{1-\phi}{\phi_b}}{G_{MIN} + Z} \right]^{-1} - Z \tag{12}$$

Where

$$Z = \frac{G_b}{6} \left[\frac{9K_b + 8G_b}{K_b + 2G_b} \right]$$

ϕ_b = Porosity of well sorted end member

K_b = Bulk modulus of dry rock at ϕ_b which is calculated by using contact cement model equation

G_b = Shear modulus of dry rock at ϕ_b which is calculated by using contact cement model equation

K_{dry} = Bulk modulus at lower porosity ϕ

G_{dry} = Shear modulus at lower porosity ϕ

K_{MIN} = Bulk modulus of the mineral grain

G_{MIN} = Shear modulus of the mineral grain

These three rock physics models have been used in this project with different combinations of cement volume, fluid saturation, and mixture of minerals. The fluid saturation, mineral content and porosity logs have been generated using interactive petrophysics (IP) senergy software as shown

Figure 10: Schematic depiction of three effective medium models for high porosity sands in the plane of elastic modulus versus porosity, and corresponding diagenetic transformations (Avseth et al., 2009).

in Appendix I (Figure 55). The constant cement model has been found to be fitting the crossplots for most of the clastic wedges showing presence of cement at the grain contacts and between the grains.

3 Dataset and methodology

3.1 Dataset

The data set used in this project has been provided by Norwegian Petroleum Directorate (NPD) at the University of Stavanger (UiS) (Figure 11).

- 3D seismic data consists of NH9605 (approx. area 282 Km2), SH9301 (approx. area 272 Km2) and LN0901 (approx. area 352 Km2) and ST9705 (approx. area 485 km2), only one 2D seismic line (NH8610-406) is used for well correlation purposes.

- Well data includes a complete suite of logs from the wells 7120/1-1R, 7120/2-2, 7120/1-2, 7120/2-3 S, 7120/5-1, 7120/ 6-2S, 7120/6-1, 7121/4-1 and 7121/5-1. Interpretation of cores by Sandvik (2014), and that of thin sections and petrophysical analysis of wells 7120/1-2 and 7120/2-2 by Rodriguez (2015) have been used in this study.
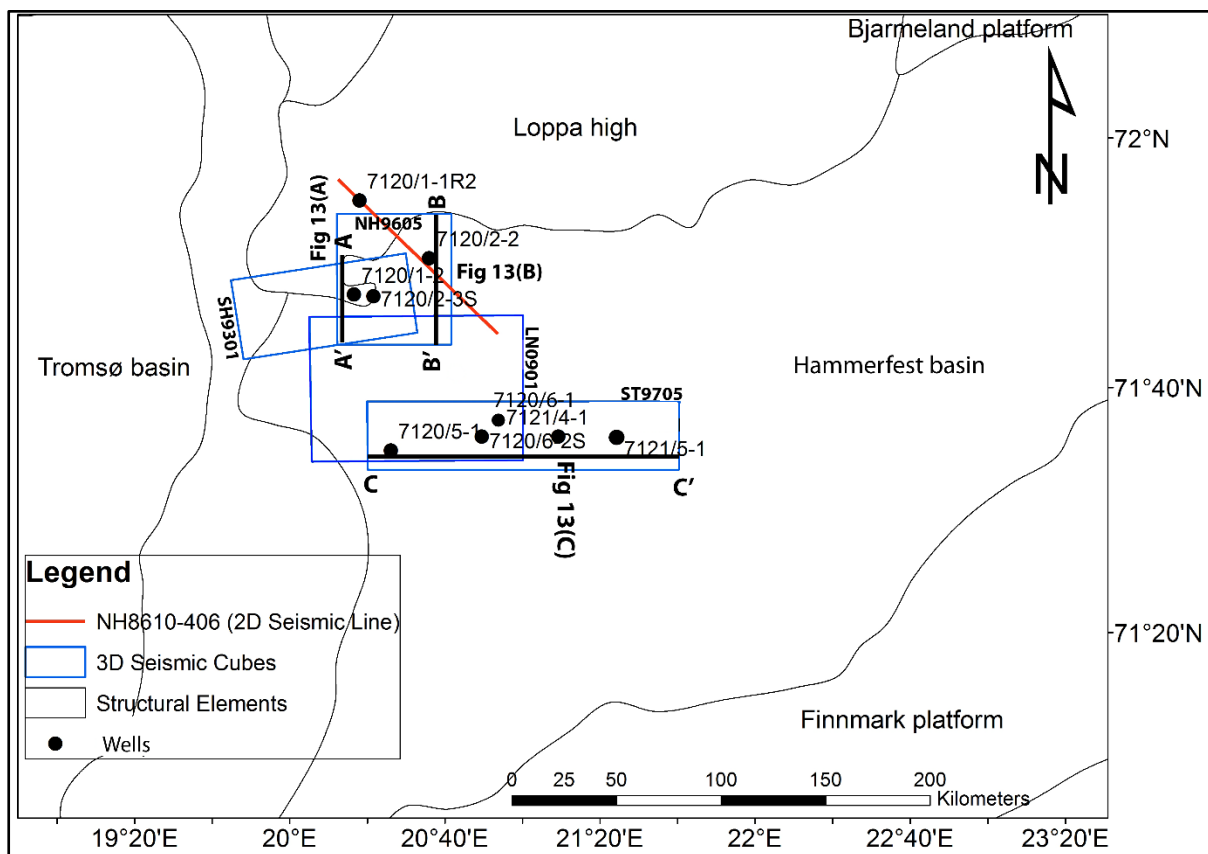
Figure 11: Dataset used in this study (four 3D seismic cubes, one 2D seismic line and nine wells) is shown. The wells 7120/1-2, 7120/2-3S and 7120/2-2 have been drilled through the Lower Cretaceous clastic wedges.

3.2 Bandwidth of 3D seismic data

Spectral analysis of 3D seismic data was carried out, in the target zone, to analyze the frequency bandwidth of the data.

- NH9605 has been acquired by Norsk Hydro Production AS in 1996. The data is of fair to good quality with frequency bandwidth of 7 to 35 Hz.
- SH9301 was acquired by A/S Norske shell in 1993, spectral analysis shows a frequency bandwidth of 5 to 45 Hz.
- LN0901 is a multiclient 3D seismic data which is acquired by Fugro multiclient services AS in 2009. Data is of good quality with frequency bandwidth of 5 to 45Hz.
- ST9705 was acquired by Den Norske Stats Oljeselskap AS in 1997. Spectral analysis of the dataset shows that maximum energy is focused at frequencies between 5 to 65 Hz as shown in Figure 12.
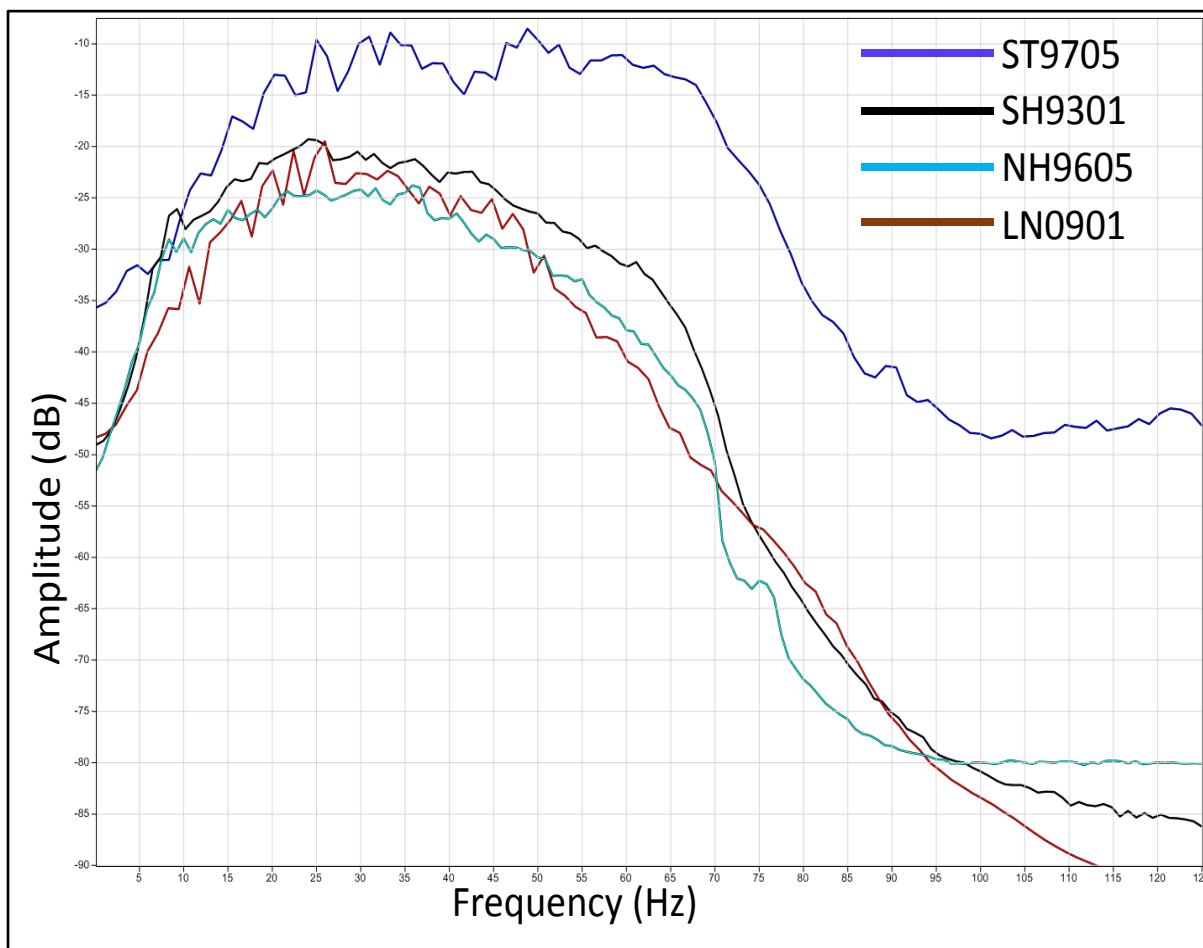
Figure 12: Frequency spectrum of the 3D seismic data. All the cubes have a good frequency bandwidth in the target zone averaging between 5 to 45 hertz.

3.3 Seismic data limitations

The data was acquired in 1990s and has some processing and noise problems except surveys LN0901 and SH9301. The prominent issues observed in the seismic cubes are listed below (Figure 13);

1. NH9605 has strong multiples and diffractions from the edges of faults and canyons. Diffractions are misleading and obscuring the reflections from subsurface rocks as shown in Figure 13A. Bow-tie reflections can also be observed from the edges of canyons which is additional source of noise. The multiples are masking the key reflections in the zone of interest and causing problem in visibility in time slices as well (Figure 13B).The seismic cube also has some places where data is missing due to acquisition geometry, which is causing difficulties when combing with other surveys (Figure 13D).

2. ST9705 has some chaotic and transparent patches in the data in the vicinity of faults and under the bright reflectors as shown in Figure 13C. This might be related to energy penetration issues due to presence of hard and reflective lithologies on top such as basalts or salt layers. The other possibilities may also be considered such as gas chimneys.

All the surveys have incoherent noise and has to be removed using noise suppression techniques such as filtering and structural smoothing. Structural smoothing has been applied for noise suppression in this project.

3.4 Methodology

3.4.1 Integrated well correlation

Well correlation is performed using the nine wells from the study area. Wells are selected such that they give a complete picture of the Cretaceous sediments along the depositional dip from source to sink. Sonic (DT), Gamma-ray (GR), density (RHOB) and neutron (NPHI) logs were used to carry out the correlation. GR is the main log which is used to interpret changes in lithology with the support of other log responses. The Kolmule formation is selected as datum for well correlation which is helpful in differentiating the sediment fill of the basin relative to the basin topography.
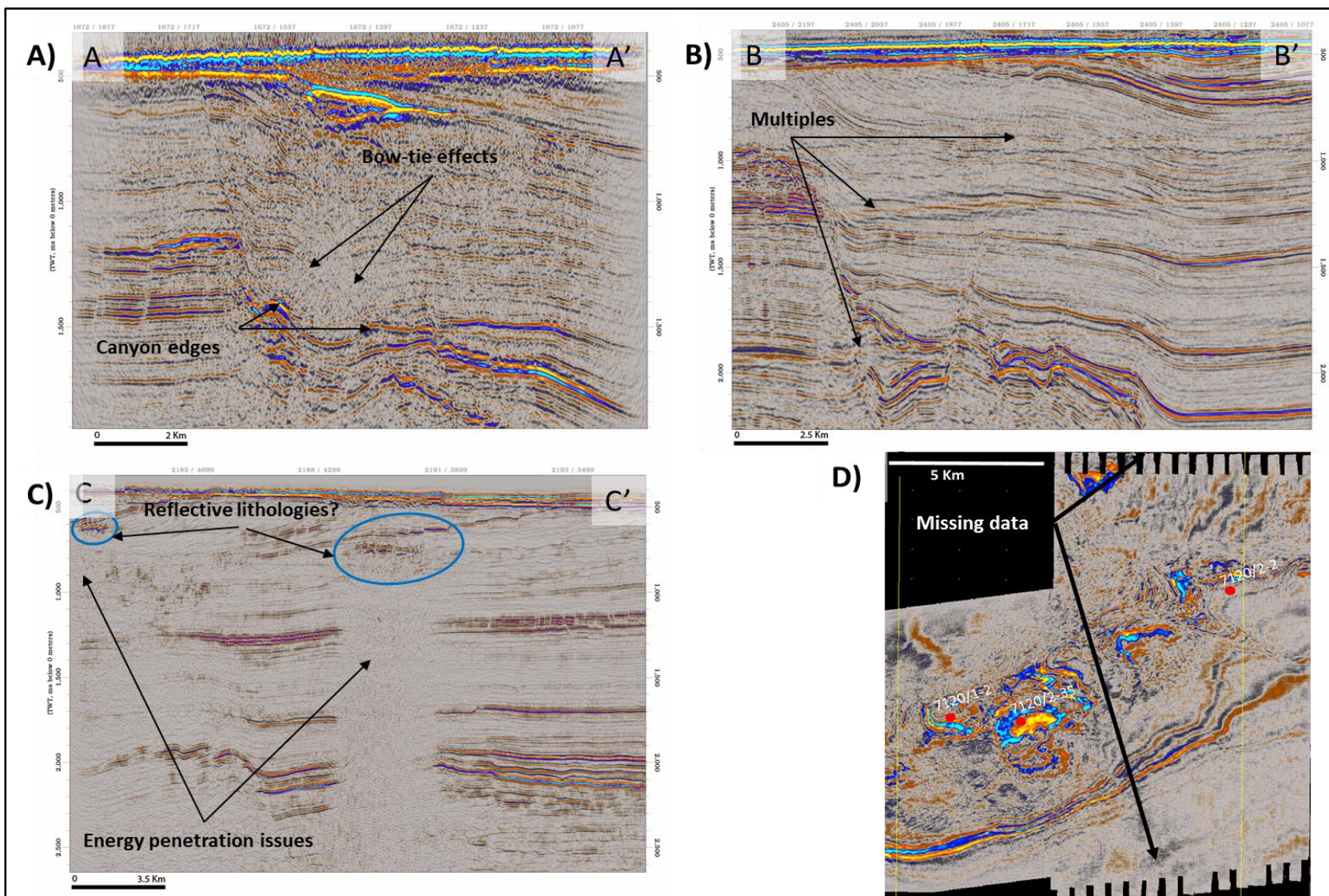
Figure 13: Observed problems in the seismic data. A) Diffractions from the edges of a canyon, B) very strong multiples of seabed affecting the target zone, C) transparent areas possibly because of presence of very reflective lithologies on top hindering passage of energy downwards and D) patches with no data due to acquisition geometry. See Figure 11 for location of the seismic lines. The time slice is from seismic cube NH9605.

Four formations (Top Hekkingen, Top Knurr, Top Kolje and Top Kolmule) from the Lower Cretaceous have been correlated which gives an overall picture of the sedimentation. The Hekkingen Formation has a suggested age of Late Oxfordian to Ryazanian and is a regional source rock for the area (Dalland et al., 1988). Knurr Formation has been suggested to be deposited during Ryazanian/Valanginian to Early Barremian times. It consists of coarse grained clastic wedges of reservoir quality (Dalland et al., 1988). The Kolje Formation has an age of Late Barremian to Early Aptian and the top part of the formation is composed of coarse grained clastic wedges penetrated in well 7120/2-3S. Finally, the Kolmule Formation is of Aptian to mid-Cenomanian age and has clastic wedges in the lower part of the formation.

Six sequences have been interpreted to subdivide the Lower Cretaceous into smaller packages on the basis of sequence stratigraphic framework from the LOCRA project (Marin et al., 2014) as shown in Figure 14. These sequences are K0, K1, K2, K3, K4, and K5 and are correlated between Top Hekkingen (BCU) and Top Kolmule formations (Figure 15). These subdivisions help to localize the clastic wedges inside the sequences. Almost all the wedges fall between the Top Hekkingen and the Top K2 as can be observed in Figure 15.
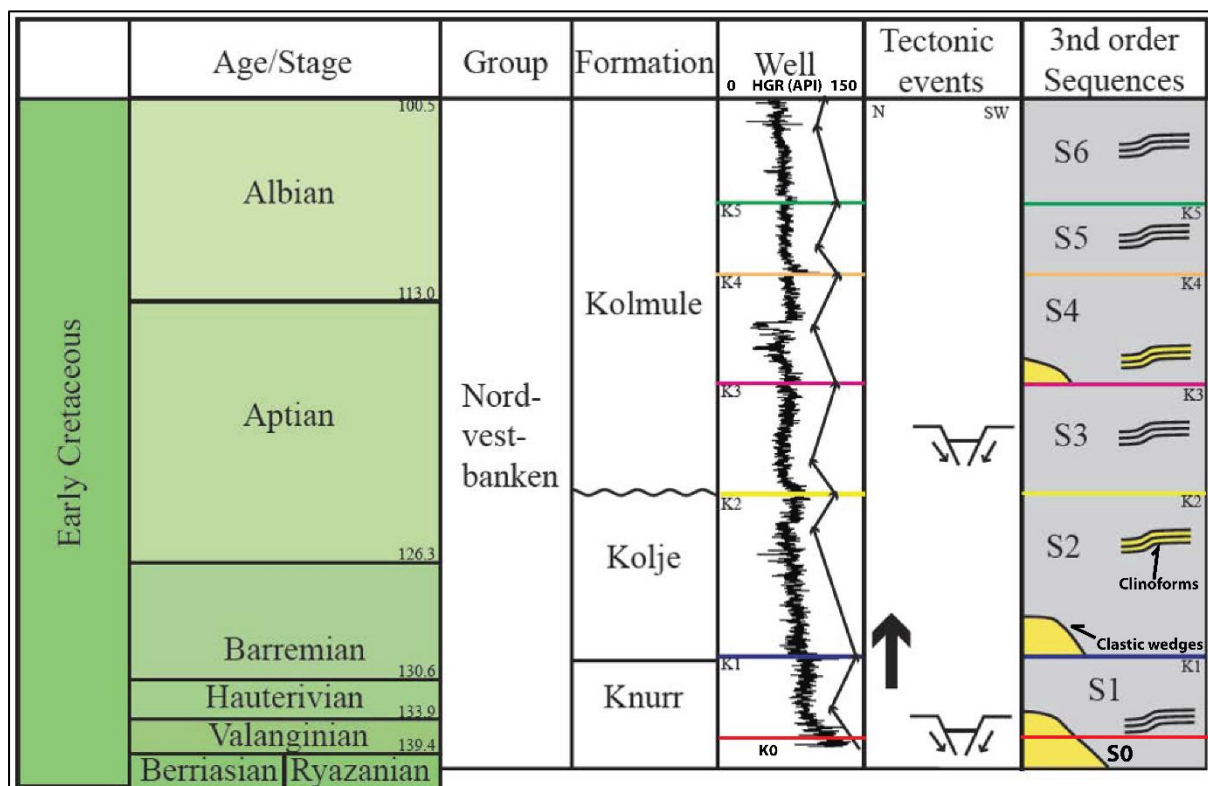
Figure 14: The Lower Cretaceous 3rd order sequences with clastic wedge and clinoforms. These sequences have been extended to the wells used in this study (Marin et al., 2014).
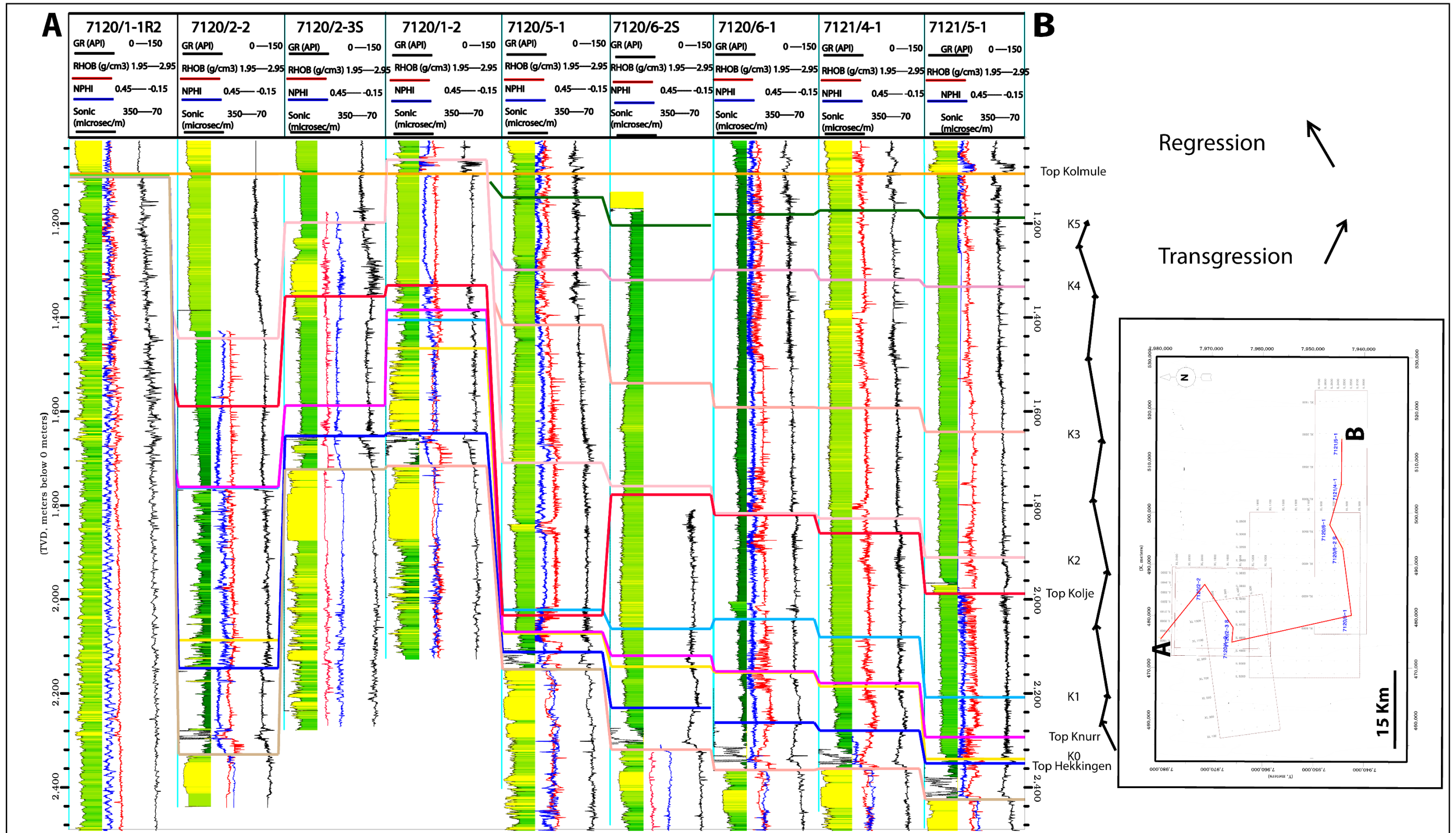
Figure 15: Integrated well correlation for the Lower Cretaceous sediments. It can be observed that the Lower Cretaceous is dominated by fine grained shale sediments (note GR response). Localized wedges of coarse grained sediments are found mainly in few of the wells such as 7120/2-3S, 7120/1-2 and 7120/2-2. Difference in DT, NPHI, density and GR log can be observed for the wedges drilled in wells 7120/2-3S, 7120/1-2 and 7120/2-2.

3.4.2 Synthetic seismograms and seismic-well tie

Synthetic seismograms are generated for all the wells under study. However, only three of them, containing the clastic wedges, are shown in Figure 16. Sonic and density logs were used to generate the synthetic seismograms and then corrected for time-depth using time-depth relations of the wells. A wavelet has been extracted from seismic data, at each well location, for convolution with the reflectivity series obtained from sonic and density logs. The extracted wavelet is of reverse polarity as indicated by negative amplitudes for a change from soft to hard lithology. The seismograms are, then, correlated with surface seismic data. The synthetics are matching well with the surface seismic data as shown in Figure 16. Decisionspace module of Landmark interpretation software has been used to generate the synthetic seismograms.

The seismic character of the clastic wedges in wells 7120/1-2, 7120/2-3S and 7120/2-2 is very different from one another as can be observed in Figure 16. The wedges encircled with blue color are shallower falling at the depths of around the Kolje Formation of Early Barremian to Early Aptian age. The red circles show the wedges having reflections in the internal part which shows changes in lithology as indicated by the GR response in Figure 16. The wells in which wedges have not been encountered are not included in the synthetic correlation.

It can be observed that the surface seismic response is much brighter in well 7120/2-3S for blue circled wedge than the equivalent wedges in wells 7120/1-2 and 7120/2-2 as shown in Figure 16. Whereas, the wedges encircled with red color have reflections in the internal part of the wedges in wells 7120/1-2 and 7120/2-2 and almost no reflections in well 7120/2-3S.

Top of the wedge in well 7120/2-3S can be characterized by a trough indicating a change from soft to hard lithology for reverse polarity. Whereas, bottom is defined by a peak showing a change from hard to soft lithology. The wedge is characterized by strong internal reflections as shown in Figure 16. Top and base of other wedges are also characterized by trough and peak respectively.
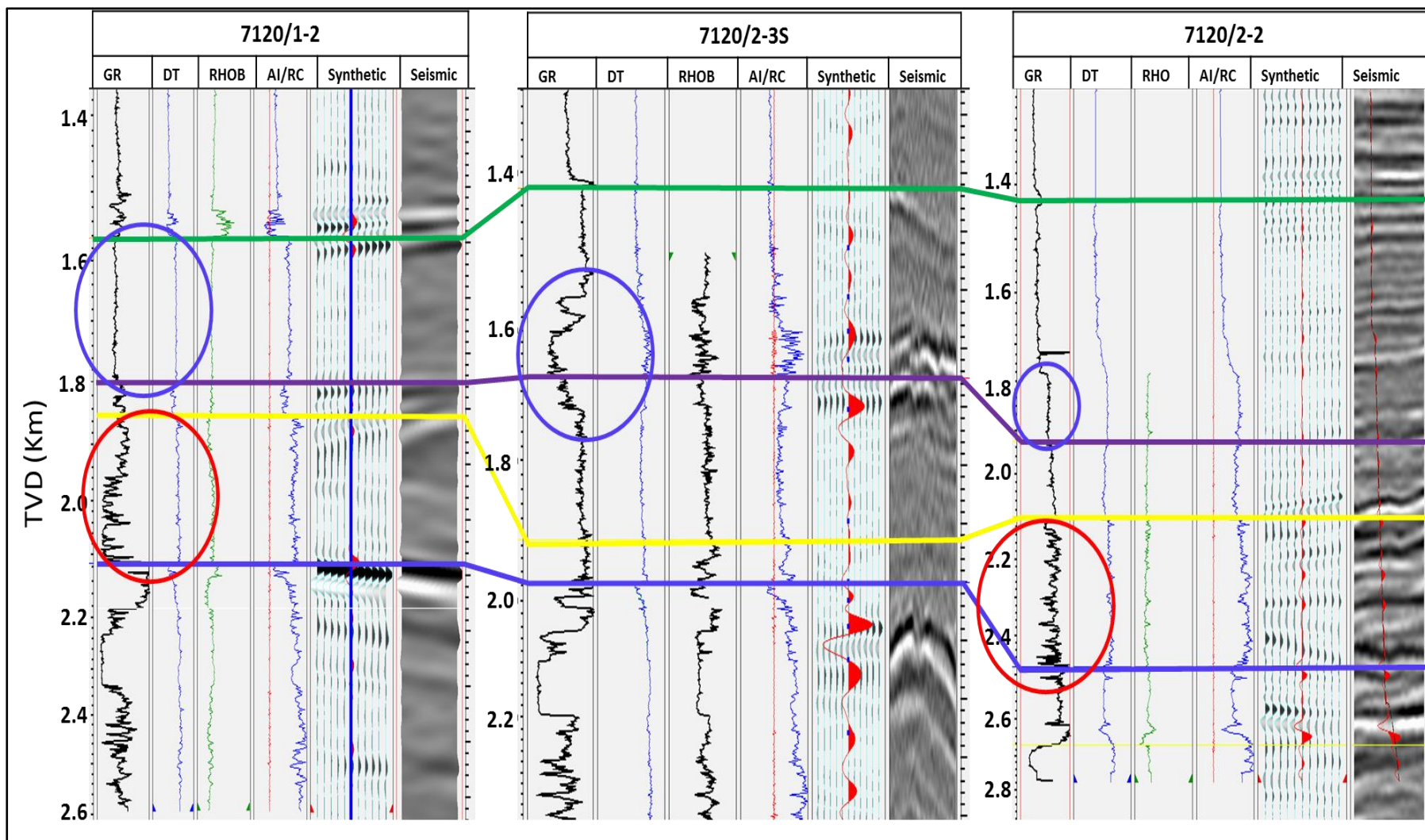
Figure 16: Synthetic seismograms correlated along the strike of deposition of the wedges. Blue circles highlight the wedges related to same depositional event whereas red circles show for a different environment. Prominent surfaces have been correlated Top BCU (blue), Top Knurr (yellow), Top Kolje (violet) and Top Kolmule (green). See Figure 15 for location of the profile along the correlated wells.

3.4.3   Seismic Attributes

Seismic attributes assist in both quantitative and qualitative interpretation of seismic data. Quantitative interpretation includes estimation of physical properties of the rocks such as porosity and lithology. Qualitative uses include description of geometries that can be correlated with stratigraphic and structural features such as channels, deltas, strand-plains, basin floor fans and many more (Hart, 2008). All seismic attributes are derived mainly from the basic seismic trace properties like time, amplitude, frequency, phase and attenuation (Brown, 1996). According to Radovich and Oliveros (1998), pseudo-color techniques used in satellite image processing can be applied to seismic attributes to create combination of displays that are both more informative and more concise than traditional display methods. These visualization techniques have made it easier to interpret the depositional elements i.e., channels, point bars, canyons etc., from seismic data. Seismic attributes, which are used in this study, are full spectrum seismic attributes.

In reality, conventional seismic amplitudes display may not reveal subtle features such as minor faults and stratigraphic boundaries (thin sand bodies and other depositional features). Therefore, seismic attributes are used to enhance one or more components of seismic amplitude such as phase and structural relationships (Chopra and Marfurt, 2005). Petrel software has been used for generation of the attributes.

3.4.3.1   Structural smoothing

The 3D seismic data is noisy and have processing issues as described in the data section. These data pitfalls were masking the signal which was a hindrance in proper analysis of the data. The data quality is not so good in time slices, in particular. Slices were noisy which, at some places, overprint the structural and stratigraphic features. Particularly, the key cube NH9605 is very noisy probably due to diffractions from the intensely faulted narrow shelf on south of the Loppa High.

Due to presence of complex faulting in the narrow shelf area, dip-guided structural smoothing was applied to remove noise which made geological features more interpretable as shown in Figure 17. Notice that the noise has been removed and some linear and stratigraphic features have been uncovered after structural smoothing.

Figure 17: Time slice at 1508 milliseconds. A) Noise is masking structural and stratigraphic features in original seismic cubes, B) Noise has been removed and minor faults and depositional features such as channels are clearer in structurally smoothed cube.

28
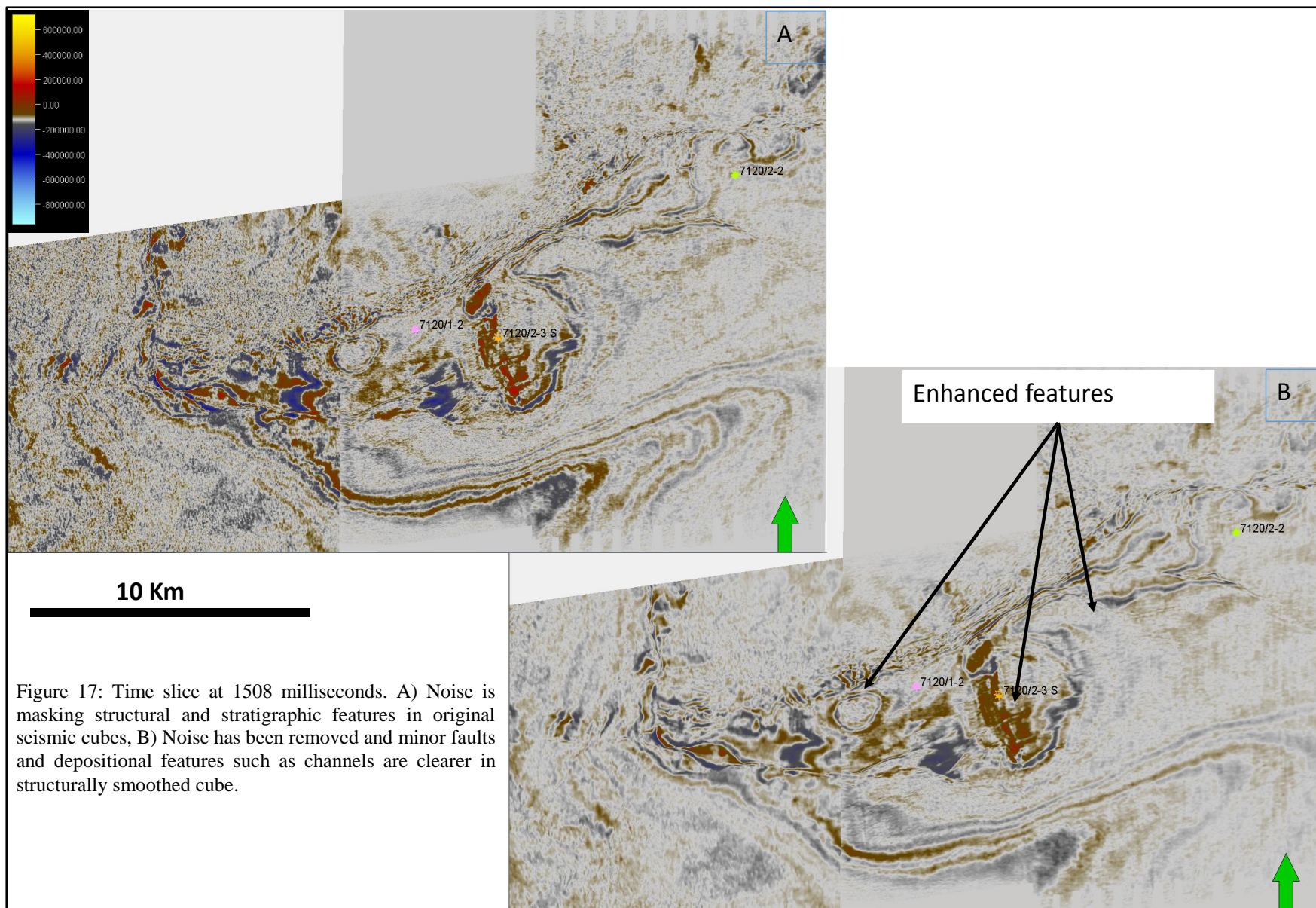
3.4.3.2 Structural smoothing followed by coherence/variance

Semblance/coherence is a non-interpretation seismic multi-trace attribute i.e. it can be obtained from seismic data without any interpretation beforehand. The main concept behind this attribute is the localized waveform similarity which is calculated in both inline and crossline directions to estimate three dimensional seismic coherence (Bahorich and Farmer, 1995). Small regions of seismic traces cut by a fault surface generally have a different seismic character than the corresponding regions of neighboring traces on other side of the fault plane. This difference results in a sharp discontinuity in trace to trace coherence due to lineaments of low coherence along faults. Boundaries of stratigraphic and depositional features such as channels, deltas, canyons, and coastal plains also create the similar continuity or discontinuities (Bahorich and Farmer, 1995).

Variance attribute seems to resolve subtle features from the seismic data (Figure 18 (A) and Figure 19 (A)). It is scaled between 0 and 1. 0 represents maximum possible coherence/similarity or the lowest value of variance. Whereas, 1 represents minimum possible coherence/similarity or the highest value of variance. Figure 18 (A) shows that the faults and depositional features such as channels are resolved in addition to the fan shape bodies. However, coherence works on the principle of local waveform similarity as described earlier and might not resolve closely related sediment fills such as submarine fan deposits. Therefore, it is necessary to apply other attributes such as chaos and sweetness for the possible value addition to the interpretation.

3.4.3.3 Structural smoothing followed by chaos

Chaos attribute is helpful in differentiating the homogeneous from heterogamous sediments. It is scaled between 0 and 1; the lower the value is, the more homogenous the deposits will be. Deposits from channels, delta lobes and submarine fans are usually homogeneous whereas slump and debris flows are more chaotic probably because of similar type of sediments. Chaos attribute estimate chaoticness of the objects using local variations in dip and azimuth. These variations might be caused by channel fills, delta lobes, slumps, debris flows, gas migration paths, salt structures, reefs and slope aprons (Ferguson et al., 2010). Figure 18 (B) shows the fan shaped, elongated linear features along the faults with low chaoticness indicating a homogenous sediment fill.

It implies that the chaos attribute helps in differentiating homogeneous channel and lobe fills from heterogeneous slope apron and debris flow deposits. In addition, it resolves features

present in the deep basin clearly compared to variance, proving its usefulness for refining the interpretations as an additional seismic attribute.

3.4.3.4 Structural smoothing followed by sweetness

The sweetness attribute is a good sale-sand indicator and can be used in conjunction with coherency for channel detection in deep water clastic and coastal plain settings (Hart, 2008). Mathematically, sweetness is derived by dividing reflection strength by the square root of instantaneous frequency (Hart, 2008). Therefore, zones of seismic volume with high amplitudes and low frequency will have high sweetness and the opposite is true for low sweetness. Isolated sand bodies in shale successions tend to generate stronger and broader reflections than the surrounding shales making it convenient for detection by sweetness attribute due to high sweetness. On the other hand, sweetness becomes less effective for the zones where acoustic impedance contrast between shales and sands are low or when they are highly interbedded (Hart, 2008). It is scaled between 0 and 1, higher values indicate sand prone areas. The threshold for sand is chosen to be around 0.05 as shown in Figure 19 (B).

This multi-trace attribute is found to be good at differentiating between shale and sand deposits. Figure 19 shows that the sand content decrease moving from SW to NE. It is also observable from the well correlation in Figure 15 that the wells 7120/1-2 and 7120/2-3S are more sand prone than the well 7120/2-2.
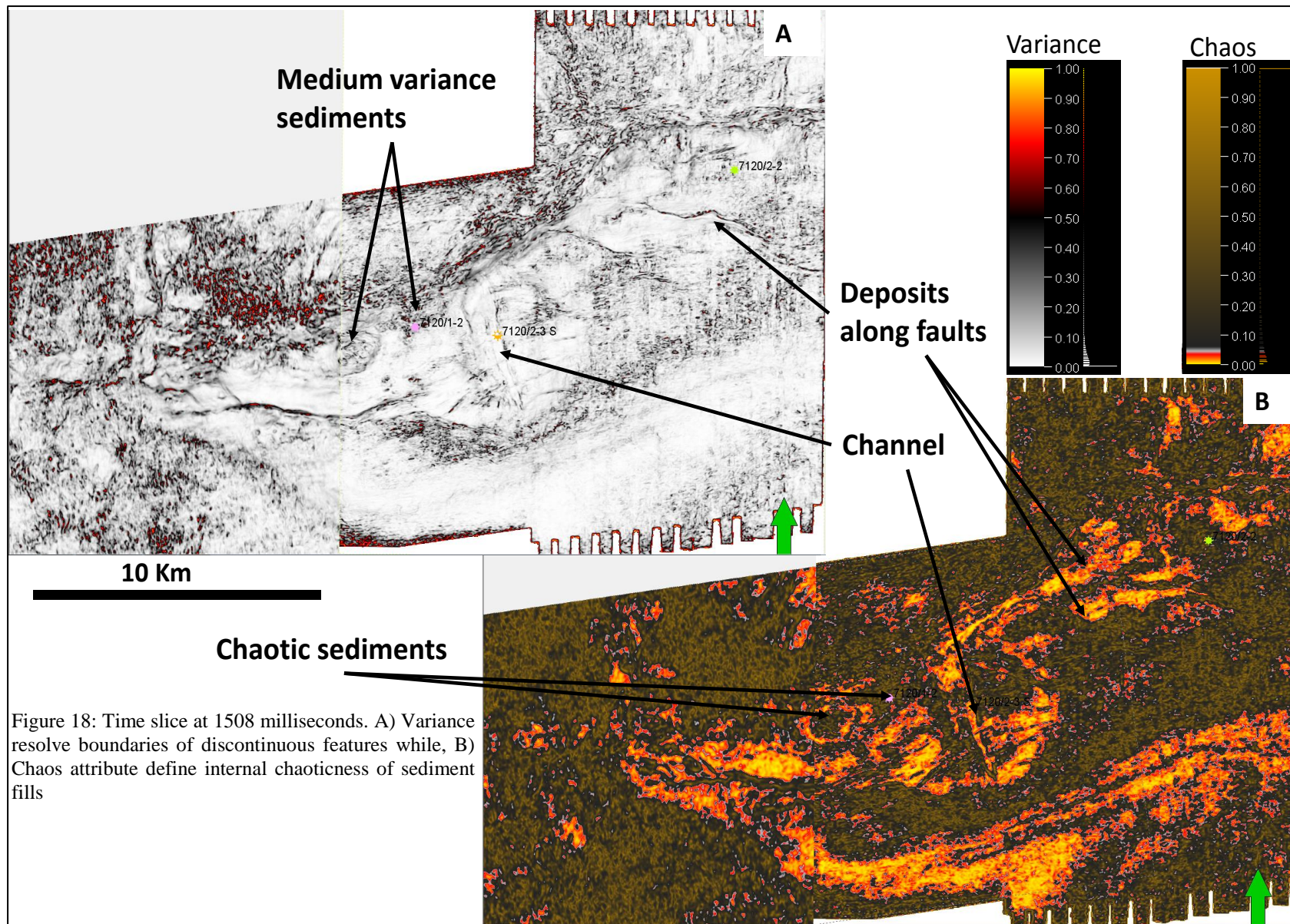
Figure 18: Time slice at 1508 milliseconds. A) Variance resolve boundaries of discontinuous features while, B) Chaos attribute define internal chaoticness of sediment fills
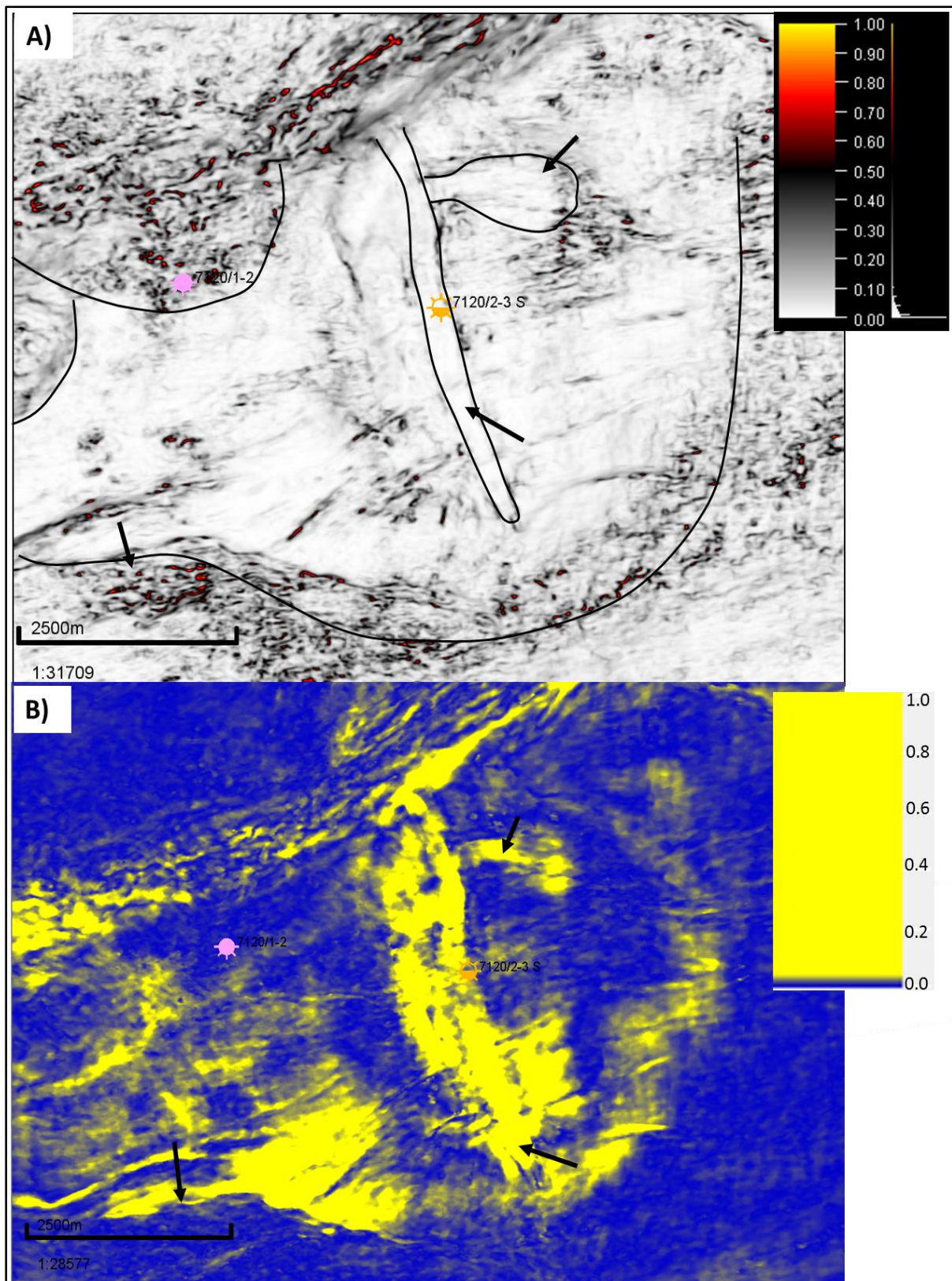
Figure 19: Time slices at 1508 milliseconds. A) Variance time slice shows features with small values of variance, B) Sweetness attribute resolve these features more clearly and add value to interpretation.

3.4.4   Rock Physics Diagnostics

Firstly, the density-porosity plots have been generated to check the homogeneity/heterogeneity of the wedges. The wedges are very heterogeneous as shown in appendix II (Figure 56 and Figure 57). Then, the rock physics diagnostics has been used for lithological and fluid characterization of the clastic wedges encountered in three wells. However, focus has been given to the recently drilled well 7120/2-3S for complete rock physics analysis. The Blue Back Rock Physics module, a plugin of petrel software, has been used for rock physics analysis. The main steps involved are listed as follows;

- Quality Control (QC) the sonic, density, Gamma Ray (GR) logs for any erroneous measurements.

- Generation of P and S-wave logs for sonic and shear sonic (only 7120/2-3S) logs.

- Generation of porosity log from density log and calibrate it with the one generated using Interactive Petrophysics (IP®) software (Appendix I (Figure 55)). Porosity log derived from density log has been used as there is no significant difference between the two.

- Generation of a crossplot between porosity and P-wave velocity. The trends in the Porosity-velocity plane can be used to differentiate between sand of different qualities and shale. Interactive facies have been generated using Blueback Rock Physics plugin of petrel interpretation software (appendix III (Figure 58).

Superimpose friable sand, contact cement and constant cement models on the crossplot which is then used to separate the crossplot into sand zones of different reservoir qualities.

3.4.5   Rock Physics Template

Rock physics templates (RPT) are used to classify the rocks into different lithologies and fluids based on their elastic properties. Various RPTs can be used but the most commonly used is an Acoustic Impedance (AI)-VP/Vs ratio plane. Petrel software has been used for generating RPT and the main steps involved are as follows;

- Bulk and shear moduli of quartz and clay have been used from literature to calculate the moduli of the clastic wedges under investigation. Hashmin-Shtrikman lower bound has been used for friable sands and shale elastic properties. Hashmin-shtrikman upper bound was used for cemented sandstones.

- The bulk modulus of fluid was estimated using the Brie model of mixing the fluids which is between Reuss/Wood and Voigt mixing models.

- The next step is to apply Gassman's fluid substitution to estimate the bulk moduli with the various fluid saturations. The Workflow for fluid substitution is listed below;

    1. Calculate bulk and shear moduli for saturated rock
    2. Calculate K_{dry} by inverted Gassman equation
    3. Calculate saturated bulk modulus for new fluid using Gassman equation
    4. Calculate bulk rock density for new pore fluid
    5. Calculate P and S-wave velocities.

- Generation of an AI-Vp/Vs crossplot for well 7120/2-3S and superimpose the rock physics template to interpret the mineralogical composition of the sandstone and the possible geological trends. The Blue Back Rock Physics module from petrel has been used for calculation of all the above stated steps.

The methodology is summarized in the integrated workflow as shown in Figure 20.
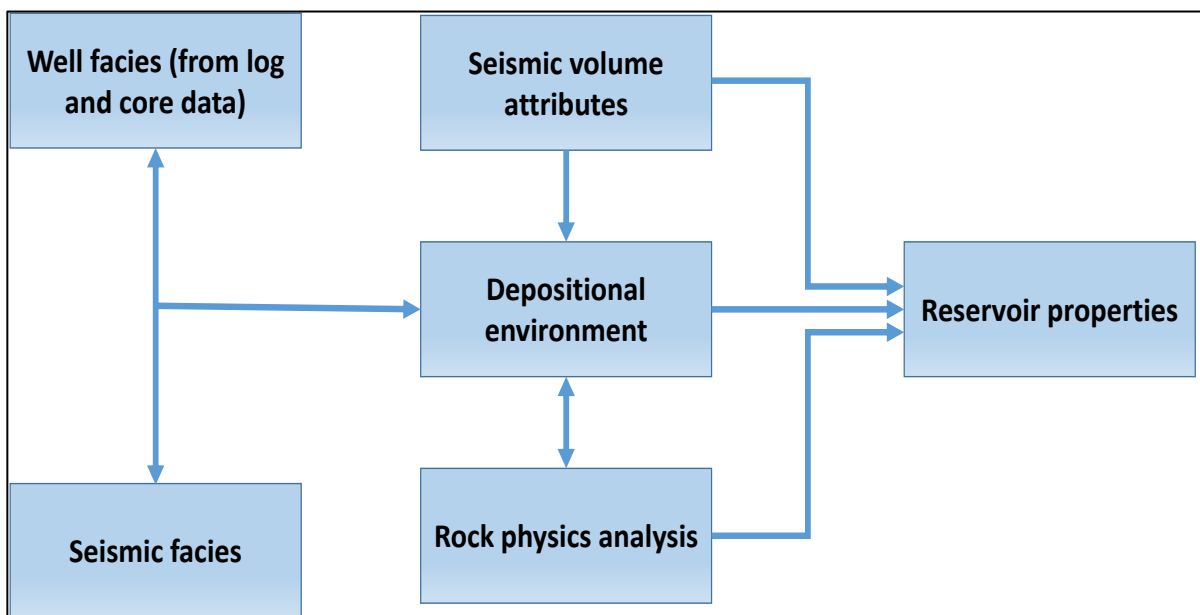
Figure 20 : Workflow of methodology employed during this study

4 Observations and Interpretations

4.1 Structural complexity of the narrow shelf (faulted terrace)

The narrow shelf (faulted terrace), to the south of the Loppa High, is confined by Ringvassøy-Loppa Fault Complex (RLFC) and Asterias Fault Complex (AFC) to the west and north respectively (Figure 21). These bounding faults are named as fault family 1 (F1). F1 family is composed of regional faults and controls the tectonic activity on the narrow shelf. RLFC is north-south running fault complex located to the west of the narrow shelf whereas AFC is an east-west running fault complex located to the north of the narrow shelf and the Hammerfest Basin. A complex network of faults can be observed on the narrow shelf as shown in Figure 21 (red colored faults). These faults are named as fault family 2 and are striking mainly in two directions (NE-SW and NW-SE) on the narrow shelf. F2 family and AFC are collectively known as the southern Loppa High Fault System (Gabrielsen, 1984).

Figure 21 shows two way time (TWT) map of Base Cretaceous Unconformity (BCU) for the study area. Faults of family 1 and 2 are marked with black and red colors respectively. It can be observed from the map that the development of main AFC gives rise to the formation of a narrow shelf to the south of the Loppa High. Tectonics along RLFC and AFC generate fault family 2 (F2) which are running mainly in two directions on the narrow shelf. Some of them are striking in NE to SW direction (same as AFC) whereas others are striking NW-SE direction (same as RLFC). These faults of F2 were acting as weak zones for development of canyons, gullies and fluvial incisions. An intensive system of canyons can be observed on seismic data along these faults as shown in the seismic line in Figure 22. Fault families F1 and F2 can also be observed and interpreted on the variance map as shown in Figure 23. F2 family of faults played a key role in the sedimentation during the Early Cretaceous times. Therefore, it can be concluded that the F2 family of faults is the main controlling mechanism for the transport of the sediments to the deeper basin through gullies/canyons and fluvial incisions (developed along these faults).
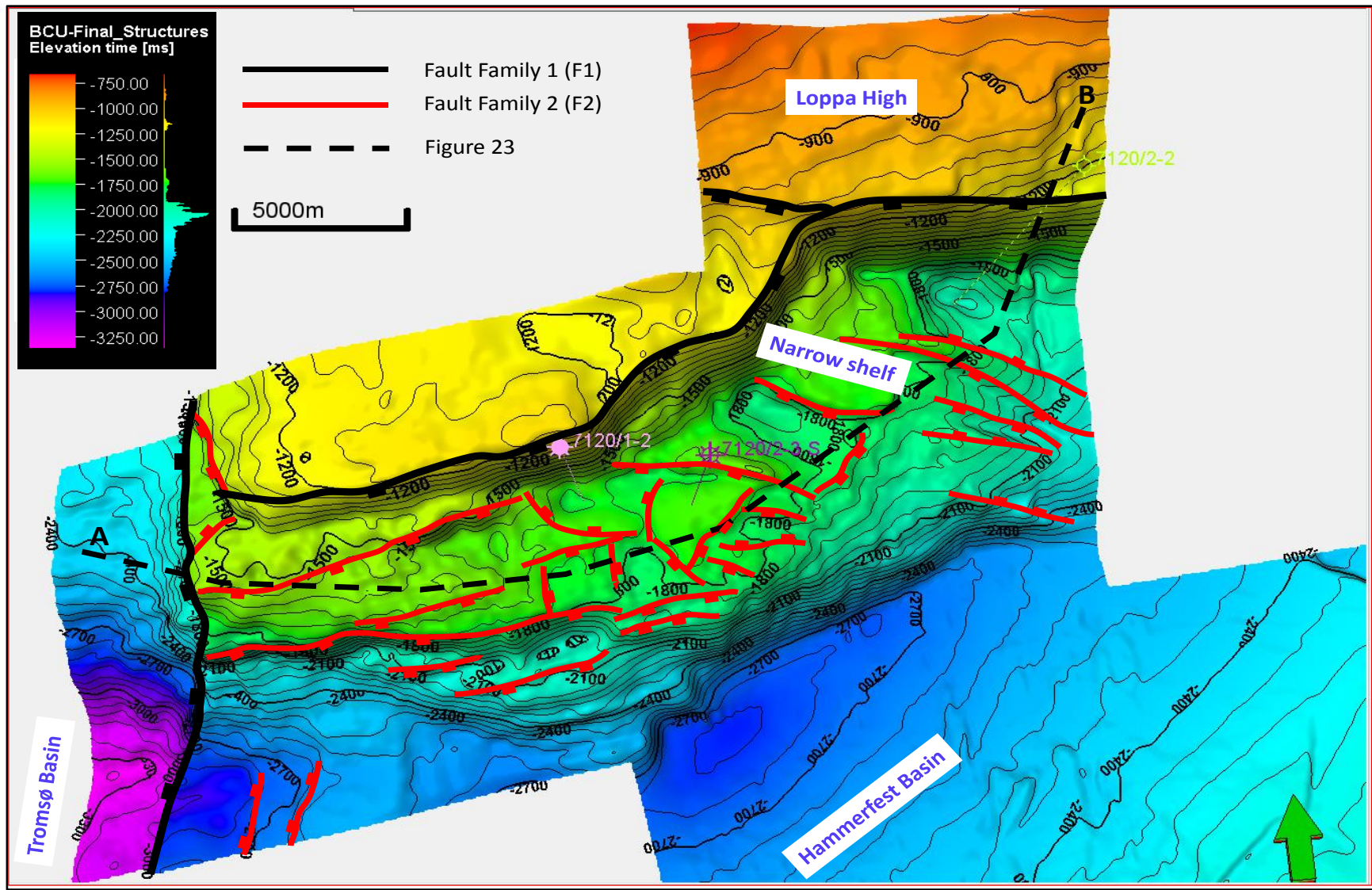
Figure 21: Structural complexity of the southern margin of the Loppa High. Notice that the narrow shelf has been intensely faulted by fault family 2 (F2). These faults controlled the deposition of sediments both in dip and strike directions during the Early Cretaceous times. Fault family 1 (F1) is shown in black color.
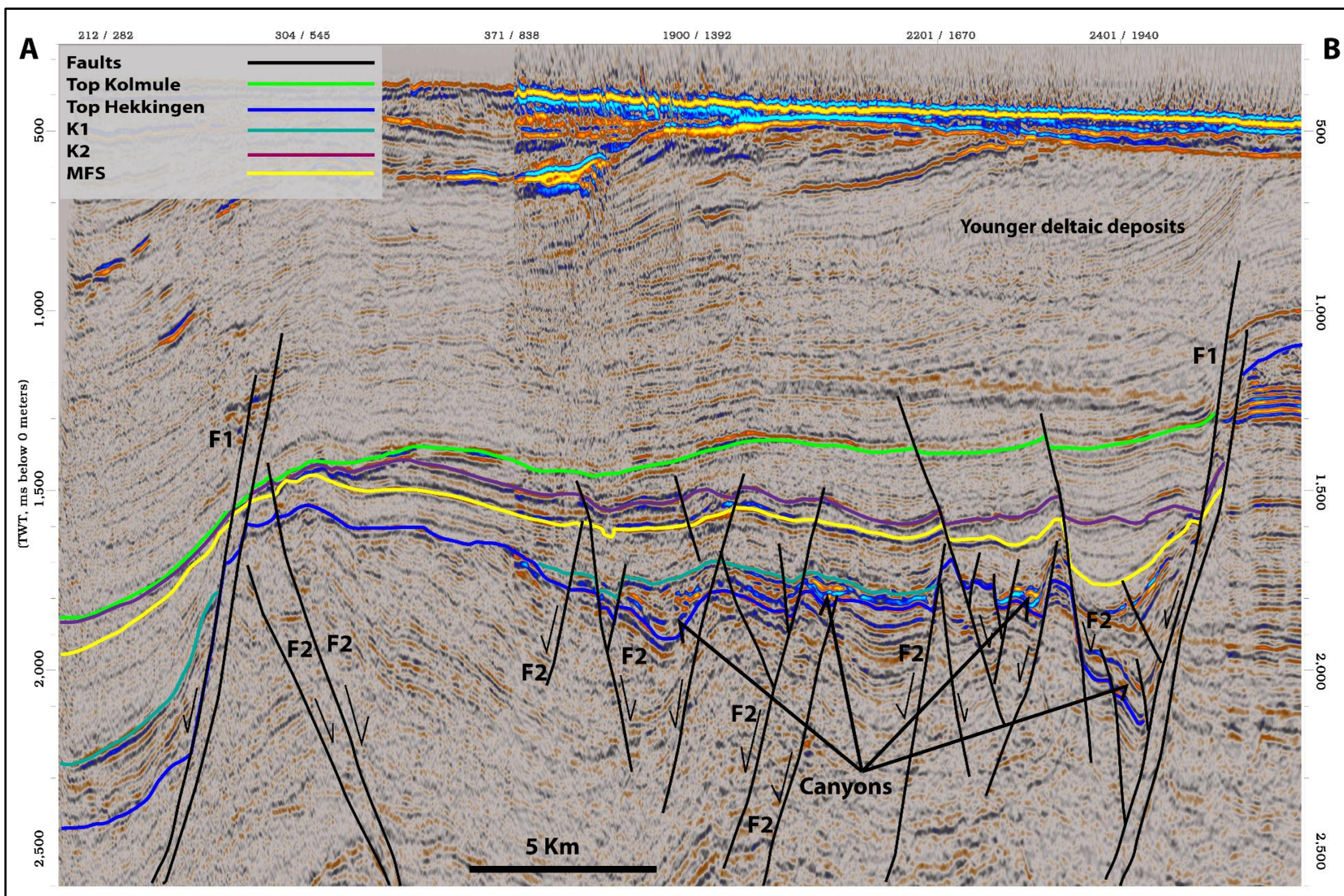
Figure 22: Seismic line along the strike of deposition of the clastic wedges. Structural complexity of the shelf is evident by intense faulting at BCU level. Canyons incisions along the faults of family 2 (F2) are highlighted. See Figure 21 for location of the seismic line.

37
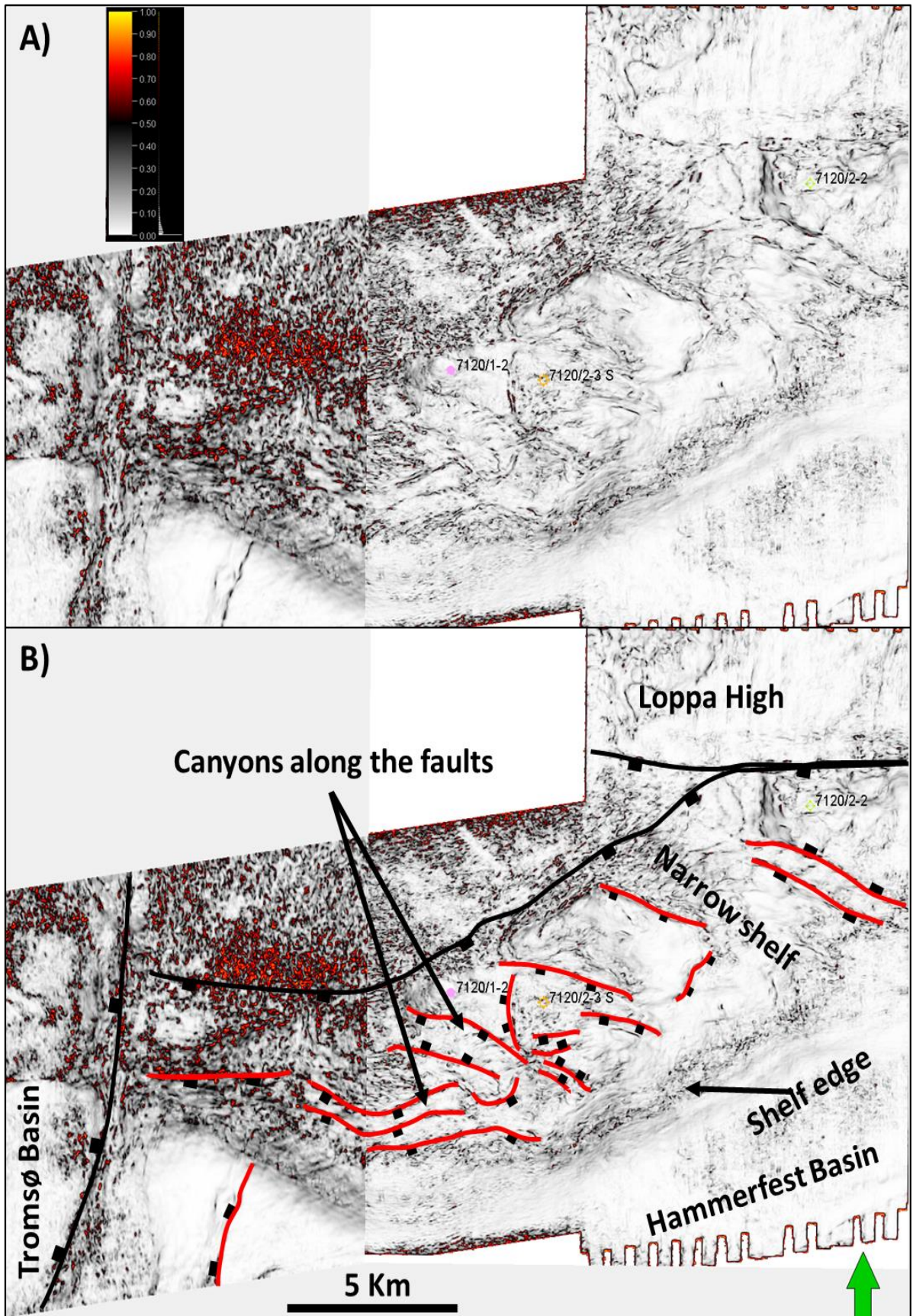
Figure 23: Variance attribute time slice at 1820 milliseconds. A) Un-interpreted variance map for surroundings of the Loppa High showing intense faulting, B) prominent faults of F1 and F2 family are interpreted on the same slice.

4.2 Seismic facies interpretation based on well logs

Almost all the wedges have distinct seismic response moving from west to east. Some of the wedges are chaotic and transparent while others have strong continuous reflections. Response of GR log has been used (where available) while defining the seismic facies. Seismic facies related to clastic wedges found in the study area are summarized alongwith well log facies in Figure 24.

Seismic Facies 1 (SF1)

SF1 is identified on the narrow shelf associated with a channelized incision. It can only be observed along the channel incision on the shelf. The reflections are subparallel-to-parallel and continuous with strong amplitudes. It is quite extensive on the shelf and can be identified as elongated shape of about 5 km length. Well 7120/2-3S has penetrated this facies. It is characterized by coarsening-up with blocky top response from GR log as shown in Figure 24. It is interpreted as delta front deposits with an amalgamated channel fills on top.

Seismic Facies 2 (SF2)

SF2 is identified along the main Asterias Fault, separating the Loppa High from the shallow shelf of the Hammerfest Basin. This facies is characterized by chaotic and discontinuous reflections with medium amplitude strength. Well 7120/1-2 has penetrated this facies. It is described by spiky and coarsening-up response from GR log as shown in Figure 24. It is interpreted as ponded deposits, slope aprons, footwall-derived sediments deposited as clastic wedges.

Seismic Facies 3 (SF3)

SF3 is identified as lower part of SF2 along the main fault. It is classified separately on the basis of its internal geometry and reflection amplitude. It is characterized by subparallel to parallel and sub-continuous reflections with weak amplitude. The reflections are dipping towards north (opposite to that of SF2). It is described by blocky and fining-up response from GR log as shown in Figure 24. It is interpreted as amalgamated channel fill with a clean sand as indicated by GR log.

Seismic Facies 4 (SF4)

SF4 is characterized by dipping and continuous reflections with weak amplitude. It is identified along the main Asterias Fault building out on the narrow shelf. It is quite extensive on the shelf and has an area of around 20-40 Km2. Well 7120/1-2 has penetrated this facies. It is defined by smooth and blocky response from GR log as shown in Figure 24. It is interpreted as foresets of fan delta as indicated by slightly concave-up shape of the foresets.

Seismic Facies 5 (SF5)

It is identified adjacent to the main fault along the Loppa High. The reflections are chaotic and transparent (weak amplitude). It is not so extensive and is bounded by faults on both sides . It has an area of approximately 10-15 Km2. It is penetrated by the well 7120/2-2. The GR log response is highly spiky with overall fining-upward shape (Figure 24). It is interpreted as delta-plain/interdistributary bay deposits with a mud dominated lithology.

Seismic Facies 6 (SF6)

SF6 is identified on top of SF5 in the same location of well 7120/2-2. The reflections are dipping, subparallel and continuous with weak amplitudes (transparent) bounded by main fault to the north and an antithetic fault to the south. The GR log character has spiky and fining-up response (serrated) for this facies (Figure 24). The log response indicates a lower delta plain depositional environment for this facies.

Seismic Facies 7 (SF7)

SF7 is characterized by sub-horizontal, parallel to subparallel and continuous reflections with strong amplitudes. It is composed of doubly downlapping convex-up reflections. These facies are not penetrated by any of the wells drilled in the study area (Figure 24). It is interpreted as basin floor fan deposits.

Seismic Facies 8 (SF8)

SF8 is bounded by incision walls on both sides and are identified on the narrow shelf. The reflections are sub-parallel to parallel and continuous with medium amplitude. It is interpreted as canyon fill deposits with coarse-grained sediments. This facies is also not drilled by any well (Figure 24).

Seismic Facies 9 (SF9)

SF9 is composed of subparallel to parallel, chaotic and continuous reflections bounded by incision walls from both sides. The amplitude strength of the reflections is weak (transparent). It is located on the narrow shelf near to the shelf edge. It is not drilled by any well drilled in the study area (Figure 24). It is interpreted to be deposited in canyons/gullies close to edge of the faulted terrace.

Seismic Facies 10 (SF10)

SF10 is characterized by sub-horizontal, parallel and continuous reflections with very strong amplitude. It is located in the deeper basin next to the shelf edge. Sheet like reflections can be seen in the wedge with bidirectional downlapping. It is not penetrated by any well drilled in the area to date (Figure 24). It is interpreted as basin floor fan with coarse-grained sediments.
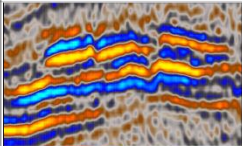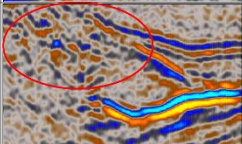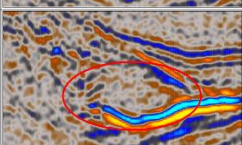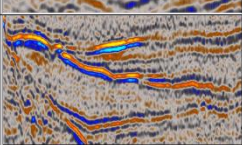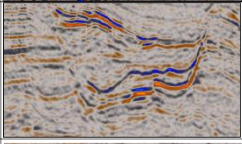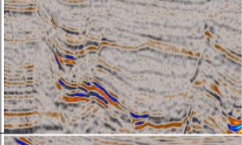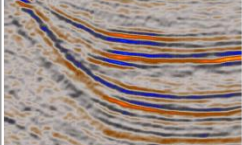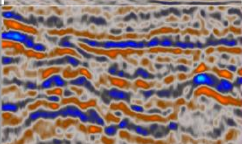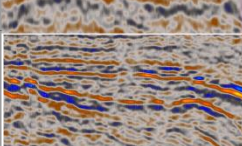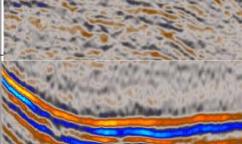
Seismic Facies	Gamma ray (GR) response	Seismic facies description	Gamma-ray (GR) response	GR description	Interpretation
SF1		High amplitude, continuous with incisions		coarsening-up with spikes and blocky top	Delta front, mouth bar with amalgamated fluvial channels on top
SF2		Inclined, discontinuous reflection with medium amplitude		Spiky and coarsening-up	Gravity flow, slope aprons and debris flow deposits
SF3		Horizontal to dipping, continuous with occasional breaks and weak amplitude		Blocky and fining-up with spikes	Amalgamated fluvial channel fill, ponded deposits
SF4		Dipping, parallel and continuous, reflections with weak amplitude		Smooth, blocky and fining-up	Distal foresets of fan deltas with intercalations of silt and sand.
SF5		Chaotic and transparent reflections with weak amplitude		Highly spiky and fining-up	Middle to lower delta plain with abundance of silt and shale
SF6		Dipping and subparallel reflections with weak amplitude		spiky and fining-up	Lower delta plain with abundance of shale and silt
SF7		Sub-horizontal and continuous reflections with medium to high amplitude	Log data unavailable		Submarine fans with debris/gravity flows
SF8		Subparallel to continuous reflections with medium amplitude	Log data unavailable		Canyon fill deposits
SF9		Subparallel and chaotic-to-continuous with weak amplitude	Log data unavailable		Canyon fill deposits
SF10		Subhorizontal and continuous reflections with very high amplitude	Log data unavailable		Submarine fans with coarse grained sediments.

Figure 24: Well and seismic facies based on seismic and GR log responses (After Escalona and Mann (2006)

4.3 Sequence stratigraphic framework of the Lower Cretaceous (Berriasian to Albian)

In order to get an overview of the Lower Cretaceous deposits, a regional composite seismic line is selected running from the Loppa High in the north, to the Hammerfest Basin in the south as shown in Figure 25. The strata, between BCU and K2 (K2 is one of the sequences from sequence stratigraphic framework for the LOCRA project interpreted by Marin et al. (2014) as shown in Figure 15), have been divided into three sequences (sequence 1, sequence 2 and sequence 3) based on the stratal lapping, the bounding surfaces and the presence of the clastic wedges. These sequences help in putting the clastic wedges in two broad systems: 1) wedges of early-rifting stage in sequence 1, and 2) wedges of late-rifting stage in sequence 3. Whereas, there are no clastic wedges in sequence 2.

4.3.1 Sequence 1

This sequence is bounded by the Base Cretaceous Unconformity (BCU) in the bottom and K1 (a flooding surface) from the top. This sequence contains two subsequences K0 and K1. BCU can be recognized by truncating reflectors against it as shown in Figure 25. K1 is a flooding surface which can be traced at the narrow shelf (faulted terrace) at some places and is eroding through the deposits of sequence 1, whereas it is missing at most of the places on the shelf. Bright reflections are observed in sequence K0 and lower part of K1. The reflectors in sequence K0 are onlapping against BCU on proximal side, whereas downlappings on the distal side have probably been eroded by channel incisions as indicated in Figure 25. Parallel reflections with high amplitude are downlapping on top of the downlapping reflections with onlaps on proximal side. Then, the system started retrograding until transgressive surface (K1) and finally reaching to the maximum flooding surface (MFS). The clastic wedges have been identified in this sequence which will be discussed in detail in coming sections.

4.3.2 Sequence 2

This sequence is bounded by maximum flooding surface (MFS) (interpreted as base of the fan) from the top and transgressive surface (K1) at the base as shown in Figure 25. It is mainly composed of retro-gradational onlapping reflections on proximal side, with truncating reflections against MFS on distal side. The majority of the reflection are continuous and transparent (weak amplitude) with the presence of a few bright and continuous reflections. Onlapping reflections on proximal side and truncations against MFS are an indication of transgressive deposits. These sediments were probably deposited when relative sea level was rising with limited sediment supply. The transparent (weak amplitude) reflections may indicate

the shale dominated lithology of probably deep marine environment. No clastic wedges have been observed in this sequence and it is generally dominated by deep marine environment of deposition.

4.3.3 Sequence 3

This sequence is bounded by MFS at the base and subaerial unconformity (K2) on the top as shown in Figure 25. A prograding pattern of reflections can be observed downlapping on the maximum flooding surface. The proximal side of these reflectors seem to be onlapping with the fault plane and even truncating against overlying unconformity. The reflections are parallel and continuous (broken at places) with weak to medium amplitude inclined towards south. Angle of these inclined reflections is around 15-20 degrees. Channel incisions can also be observed on top of this sequence with sediment fill of strong amplitudes. On the distal side in the deep basin, a wedge can be identified with parallel and continuous reflections. Reflections are onlapping on proximal side, downlapping on distal side and have doubly downlapping reflections at central part. They have very strong amplitude at the thicker part which dims out moving towards distal side.

Based on the sequence stratigraphic observations, it can be interpreted that the wedges in the deep basin and on the narrow shelf, in sequence 1, have been deposited in early phase of rifting (subsidence of the Hammerfest Basin and uplift of the Loppa High). The rifting caused a rapid fall in relative sea level which triggered erosional processes on the narrow shelf. The relative sea level rose as a result of decrease in rifting activities with time and transgressive deposits were dominant on the shelf. The shelf was flooded which gave rise to the deposition of wedges with overall prograding nature in sequence 3. This progradation was probably a response of local variations in relative sea level and change is sediment supply during the late-rifting stages. On the basis of these observations, the wedges have been grouped into two categories 1) wedges of early-rifting stage and 2) wedges of late- rifting stage. These wedges are discussed in detail in the next section.
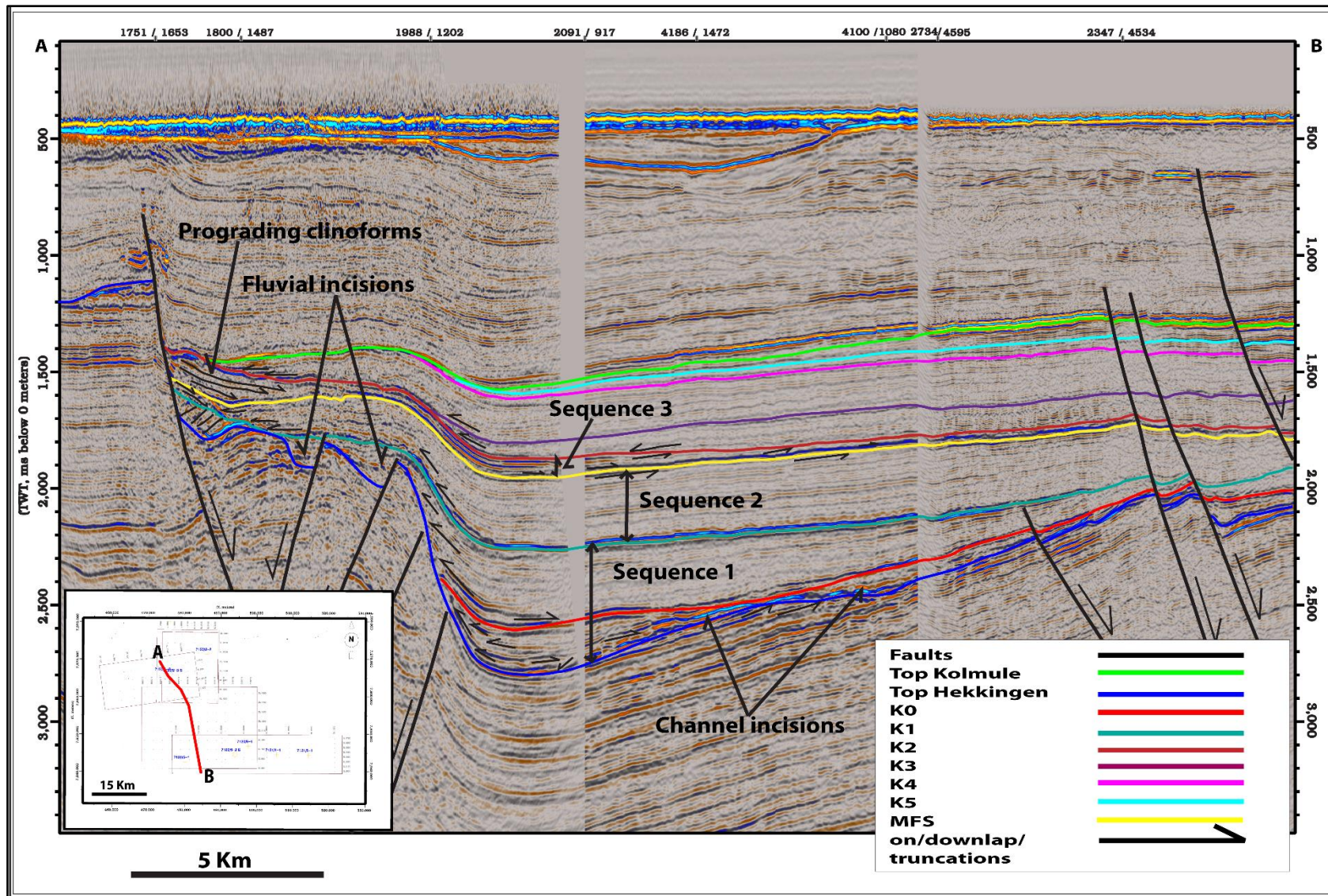
Figure 25: Seismic line for sequence stratigraphic framework classification of the wedges. The strata can be divided into three sequences on the basis of presence of clastic wedges. This division helps to classify the wedges into two main groups 1) wedges of early- rifting stage and 2) wedges of late-rifting stage

44

4.4 Characterization of clastic wedges

4.4.1 Wedges of early-rifting stage (Berriasian to Early Aptian)

These wedges are interpreted in deeper parts of the basin with equivalent wedges on narrow shelf. The wedges on the shelf have different seismic character and reflection geometries from those present on the basin floor. These wedges have been categorized into three main groups based on the location of deposition, internal seismic geometries and environment of deposition.

4.4.1.1 Type 1 Wedges

Observations

Well Character: Two wells 7120/1-2 and 7120/2-2 have penetrated these wedges. The upper part of the wedge in well 7120/1-2 has low to medium gamma-ray (GR) values, coarsening-up response with spikes. The medium values of GR indicate that the lithology is shale and silty-sand dominated as shown in Figure 26 (A). On the other hand, the lower part of the wedge shows smaller GR values with a blocky and fining-up overall response. The lower values of GR is an indication of sand dominated lithology. However, the wedge penetrated in well 7120/2-2 has medium to higher GR values with an overall spiky and fining-up response. Medium to higher values of GR can be interpreted as an indication of shale and silt sediments as shown by the core photo in Figure 26 (B). A small crossover of NPHI and density logs can be observed for the lower part of the wedge in well 7120/1-2 as shown in Figure 15. Whereas, values for NPHI and density log curves increase in well 7120/2-2 for the wedges. Synthetic response of the wedges in well 7120/1-2 is very smooth with minor reflections from the interior of the wedges. However, reflections can be observed from interior of the wedges in well 7120/2-2 (Figure 16)

Seismic character: The wedges in well 7120/1-2 are characterized by steeply dipping, discontinuous and chaotic reflections, dipping towards south in upper part of the wedge (SF2). The reflections have medium amplitude strength. The abrupt and chaotic behavior of the reflections indicate a high energy environment. They have alternating bright and relatively transparent (weak amplitude) reflections which further indicate the presence of alternating shale and sand layers. The lower part of the wedge (SF3) has relatively weak amplitude reflections dipping towards north (opposite to general depositional dip). On the other hand, the type 1 wedge (SF5) has chaotic, parallel and transparent reflections with weak amplitude at the location of well 7120/2-2 (Figure 27).

Thickness distribution: It can be observed that type 1 wedges are localized on the shelf with a time thickness of upto 200 milliseconds. They are bounded by fault plane of the main fault to the north and have dimensions of about 1.5 km by 2 km. Small scale depocenters can be identified along the main fault which are places of deposition for type 1 wedges with varying thicknesses. The dimensions increase moving towards the east where the wedges get thicker and broader. The eastern most wedge shows a pattern of different depocenters developed along the dip/flow direction as shown in Figure 28 at the location of well 7120/2-2.

Seismic attributes: Type 1 wedges show high values of variance, with a restricted circular to longitudinal shape, attached to the fault plane on the northern side. They show chaotic response on chaos attribute at well location 7120/1-2. Whereas, sweetness response is also lower for these wedges indicating higher amount of shale content. Lower part of the wedge is giving higher values of sweetness and lower values of chaos as shown in Figure 29. Highly chaotic response from the facies along the AFC may correspond to chaotic debris flow and slope apron deposits of type 1wedges.

Interpretation: Based on the observations, the upper wedge penetrated in well 7120/1-2 (SF2) is interpreted as footwall sourced slope aprons, debris/gravity flows with alternating high energy flows, ponded deposits and the lower part of the wedge (SF3) is interpreted as amalgamated fluvial channel fill sand as confirmed by GR response. The wedge in well 7120/2-2 (SF5), which is transparent, is interpreted as delta plain deposits with development of interdistributary bays which is also confirmed by GR response and core interpretations by Sandvik (2014) (appendix IV (Figure 60A)).

4.4.1.2   Type 2 wedges
Observations

Well character: These wedges are not penetrated by any of the wells drilled in the study area.

Seismic character: These wedges have been observed as onlaps on the bounding walls with weak to medium reflection strength. There are two different kinds of seismic facies (SF8 & SF9) with differing amplitude strengths, one with relatively strong (SF8) than the other (SF9) as shown in Figure 27. The medium amplitudes of the seismic facies SF8 may indicate the presence of silt to sand deposits whereas weak amplitudes of seismic facies SF9 may correspond to the shale dominant deposits.

Thickness distribution: The type 2 wedges are located away from the main fault and close to the shelf edge of the narrow shelf and have a time thickness ranging from 50 to 150 milliseconds. They are elongated features (mainly E-W and N-S directions) filled with fine to medium grained sediments deposited in the valleys/canyons/gullies .The gullies, canyons and valleys created depocenters along the faults which are the locations of deposition of these wedges. They have dimensions of approximately 2 km by 5 km and are found only on the western part of the narrow shelf as shown in Figure 28.

Seismic attributes: The type 2 wedges can be observed on the variance attribute map by low values of variance in the canyons along the faults as shown in Figure 29. The wedges are more differentiable in chaos and sweetness attribute maps as shown in Figure 29. The wedges can be seen as elongated bodies close to the shelf edge with higher sweetness values and lower values of chaos attribute.

Interpretation: Based on the observations, the wedges are interpreted as canyon fill deposits with different kind of sediment fills. The sediment with weaker amplitudes are probably deposited on distal side (SF9) whereas other is relatively closer to the source area which might be the reason of sand rich sediments for the later wedge (SF8). These wedges were probably deposited during the transgression times when shelf was flooded which explains the weak to medium amplitude of the reflections. No well has drilled through these wedges hindering the integration of seismic with well data.
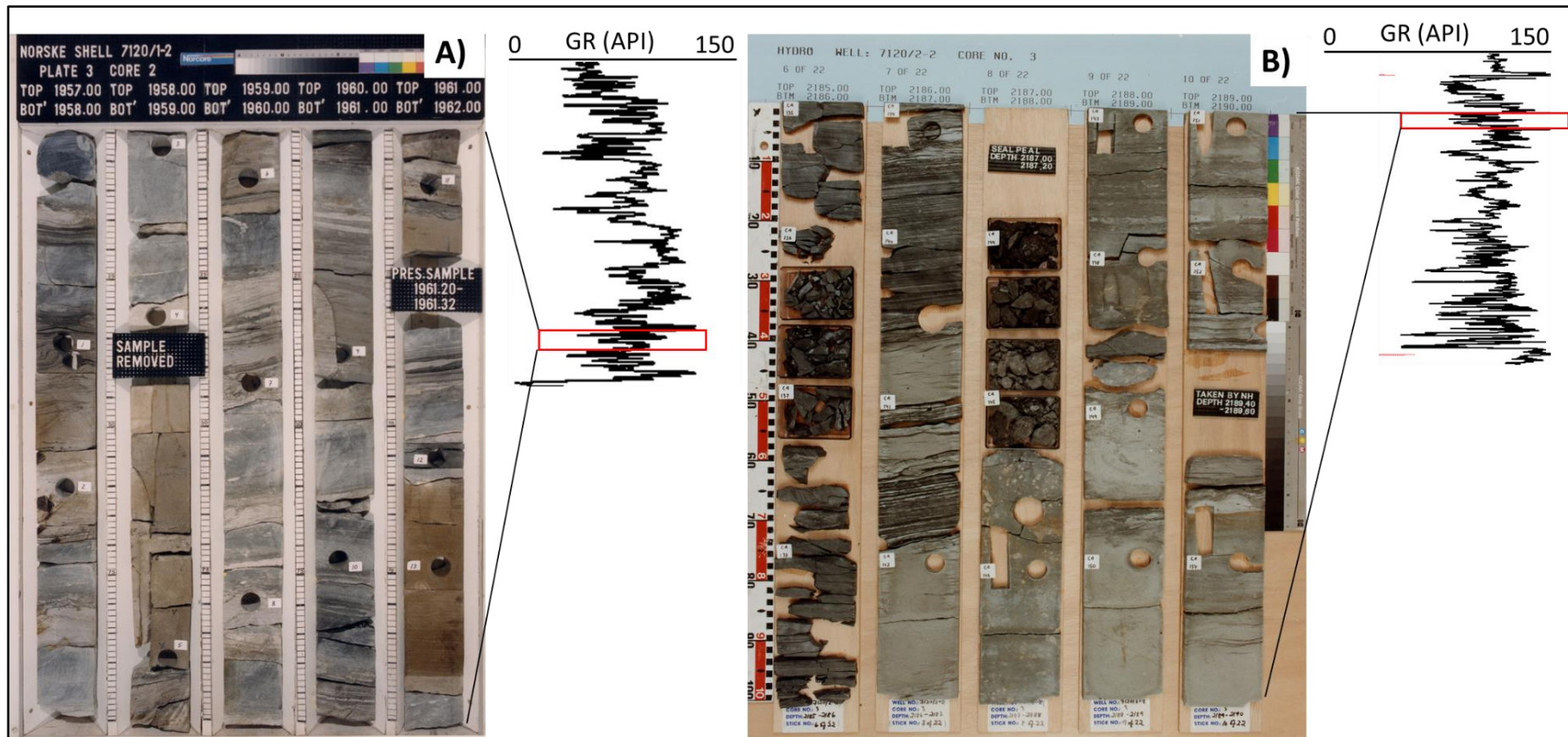
Figure 26: Core photos for type 1 wedges from well 7120/1-2 (A) and 7120/2-2 (B). Integration of log and core shows that the wedge in well 7120/1-2 is more sand prone than that of well 7120/2-2. The GR values for well 7120/1-2 are lower than that of well 7120/2-2, and it is proven by the core photos with mud-dominated lithology in the later well.
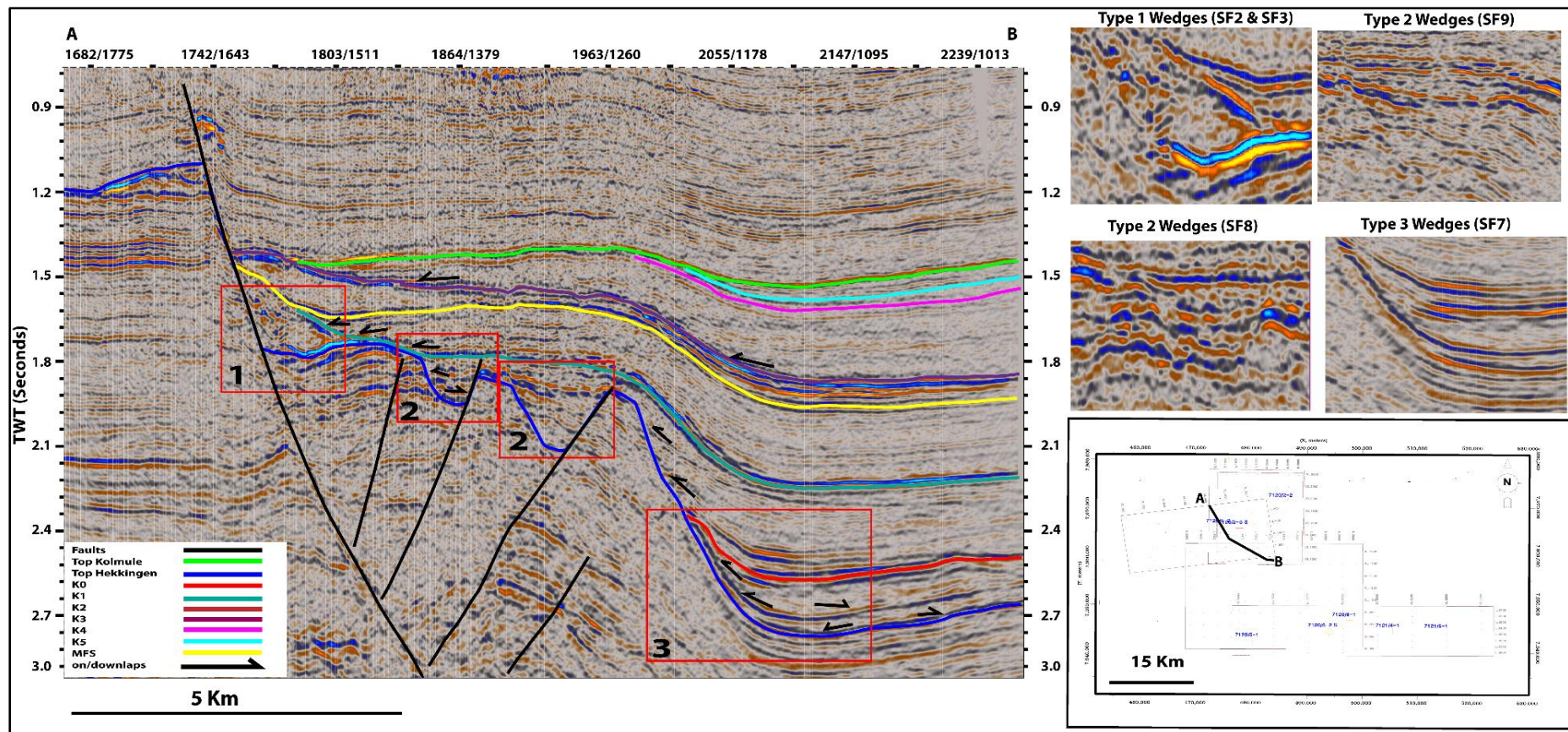
Figure 27: Composite seismic line showing wedges of early-rifting stage. Zoomed-in views of the wedges are shown on the right side to see the facies clearly. Type 1 wedges are characterized by chaotic, discontinuous and weak to medium amplitude in upper part and inclined, subparallel and continuous reflections with low amplitude in the lower. Type 2 wedges are facies of canyon fill with varying seismic response depending on the location of canyon related to the source area, wedges on the proximal side are characterized by subparallel to parallel and continuous reflections with high amplitude, whereas the one on the distal side shows inclined, parallel to subparallel, partially continuous and weak amplitude reflections. Type 3 wedge is characterized by parallel, continuous and high amplitude reflections.

49
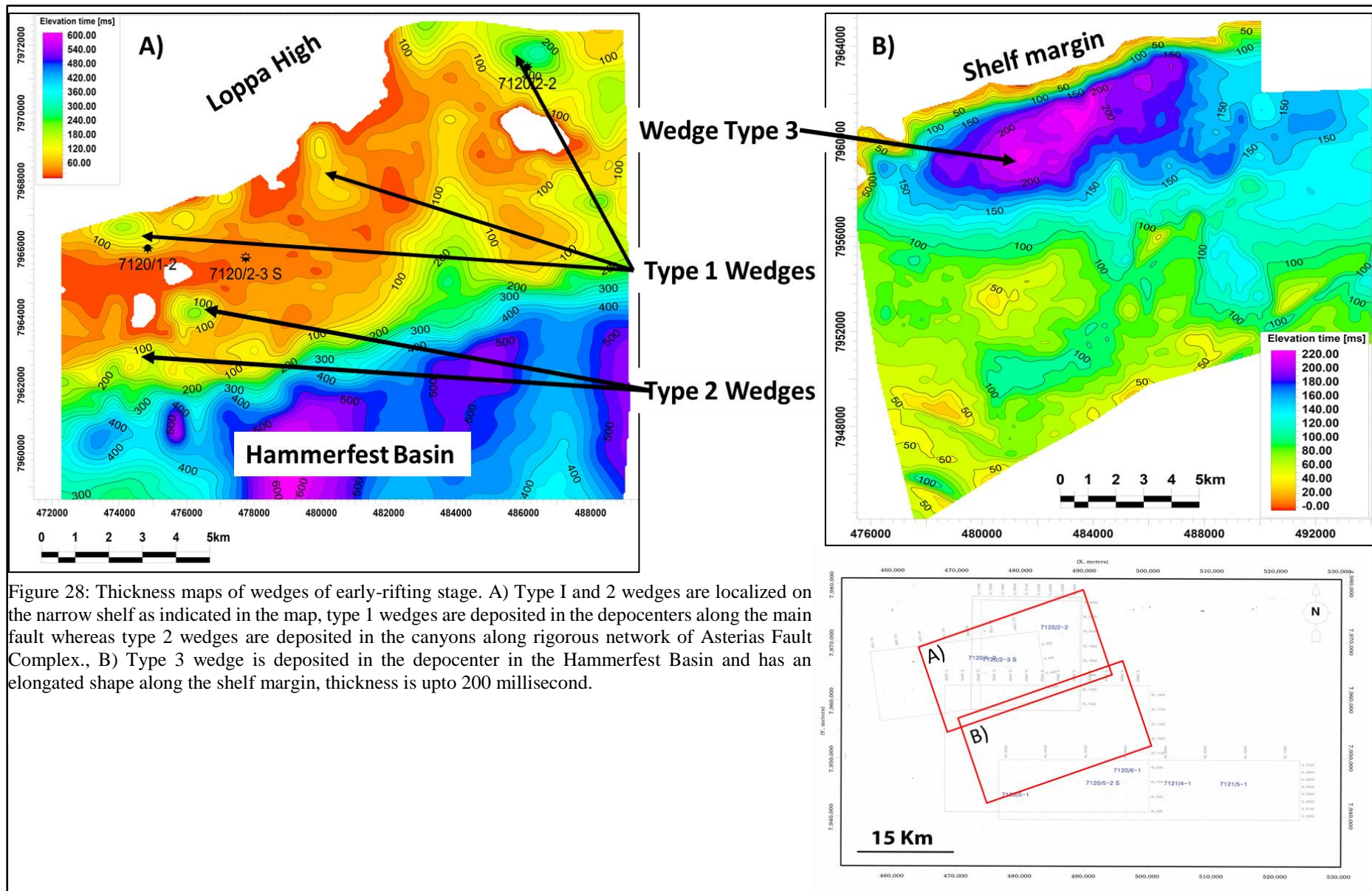
Figure 28: Thickness maps of wedges of early-rifting stage. A) Type I and 2 wedges are localized on the narrow shelf as indicated in the map, type 1 wedges are deposited in the depocenters along the main fault whereas type 2 wedges are deposited in the canyons along rigorous network of Asterias Fault Complex., B) Type 3 wedge is deposited in the depocenter in the Hammerfest Basin and has an elongated shape along the shelf margin, thickness is upto 200 millisecond.
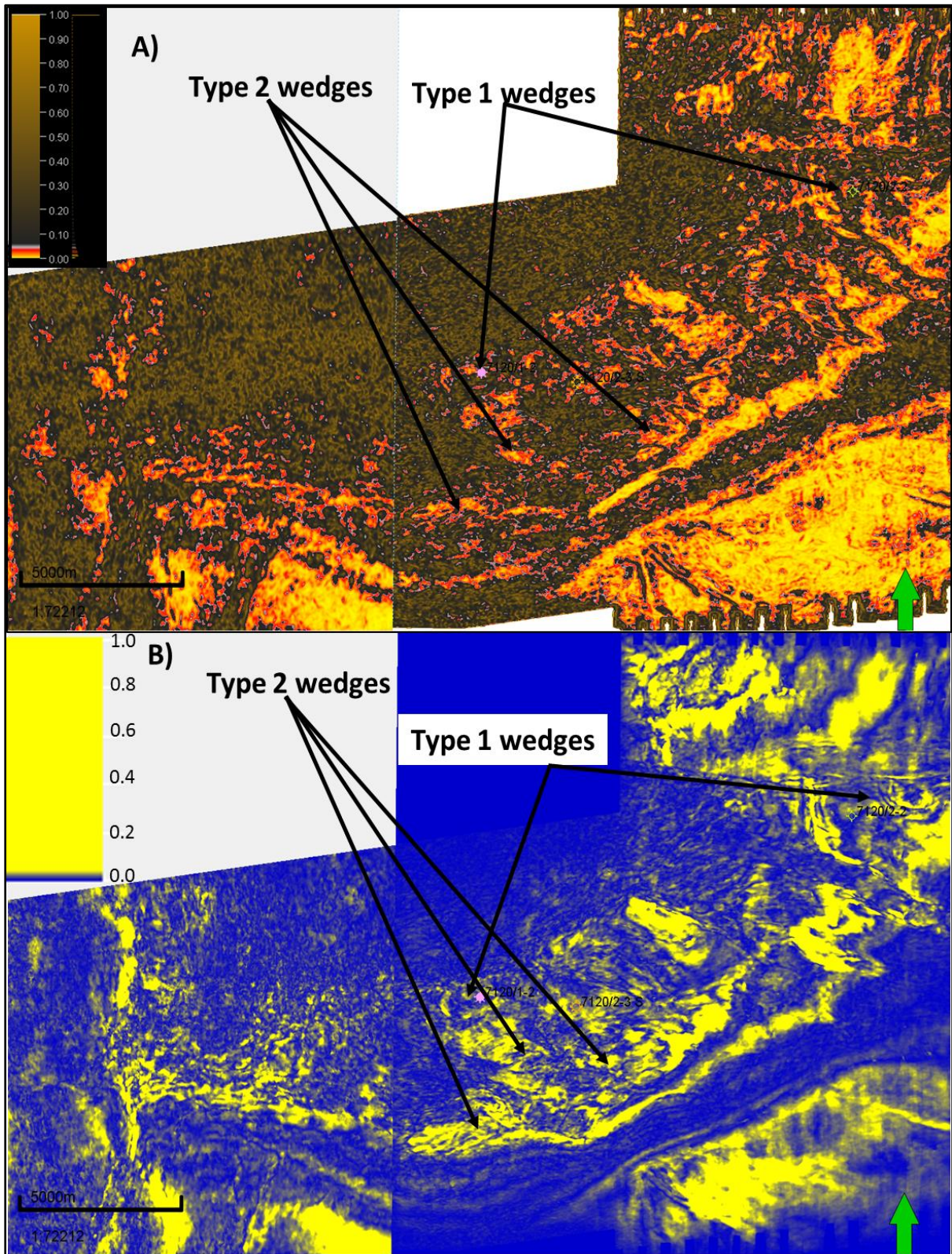
Figure 29: A) chaos attribute and B) sweetness attribute time slices at 1872 milliseconds. Type 1 wedges can be identified with higher values of chaos and lower values of sweetness along the main fault. Type 2 wedges are identified as elongated features close to the shelf edge with lower values of chaos and higher values of sweetness as indicated.

4.4.1.3 Type 3 wedge

Observations

Well character: These wedges have not been penetrated by the wells drilled in the study area until now.

Seismic character: The wedges are composed of very strong, parallel and continuous reflection facies with lappings on both proximal and distal margins. They consist of two kinds of stratal lapping, one with mound shape doubly downlapping and the other onlapping on proximal side and downlapping on the distal side as shown in the insets of Figure 27. The strong reflection amplitude may correspond to the presence of sand rich deposits. The second type of reflections are also observed which are downlapping on the doubly downlapping reflections with onlapping on proximal side. They also have strong amplitude but a bit discontinuous and subparallel. Channel incisions can also be observed on the seismic data as shown in Figure 30.

Thickness distribution: The type 3 wedge have been deposited on basin floor adjacent to the shelf edge. The time thickness of these wedges is upto 200 milliseconds with an increase in thickness from east to west. These wedges have elongated shape trending NE-SW, with main depocenter towards west as shown by higher thickness in the thickness map in Figure 28.

Seismic attributes: The variance attribute map indicates the presence of channelized feature as shown in Figure 31. The localized area is shown in combination with BCU two way time (TWT) structure map to highlight the type 3 wedge. Strong linear features with high variance values can be observed striking NE- SW. The boundaries of the linear features are showing higher values probably due to difference in variance of the deposits inside them as there are no fault discontinuities at this location as shown in seismic line in Figure 21. Whereas, the areas with very high values of similarity/low value of variance are observed appearing as specific geometric shapes. Other attributes have been used to resolve these transparent bodies successfully.

Type 3 wedge is characterized by a combination of different shapes such as fan, lobe and channel fills as shown in chaos map in Figure 32(A). These shapes are represented by low chaos values ranging from 0.01 to 0.05 approximately. All these shapes are observed to be originating from shelf to the northern side. Some of the low chaos value features are bounded by high chaos value features. These features are also interpretable on sweetness attribute map, however with less extents as shown in Figure 32 (B).

Interpretation: Based on the observations, wedges are interpreted as basin floor fans with associated prograding wedge. The doubly downlapping part of the wedge is interpreted as basin floor fan whereas the other part is probably the prograding wedge with downlaps on the basin floor fan. The basin floor fan has an intensive network of channel incisions on the distal side. These channels seem to feed the submarine fan from the NE direction. It can be concluded that the observed linear features are part of a channel belt with extensive incisions as shown in Figure 31. It can also be observed from the seismic line that the channels are bounded by overbank deposits such as levees. Variance attribute implies that the main source of sediments, for the basin floor fan, was from the NE at this stage. The areas with low variance values may be attributed as basin floor fan and channel lobes with a relatively homogeneous fill deposits. These features, however, are not interpretable with confidence on variance attribute map. Therefore, chaos and sweetness attributes were tested which delineated the fan and lobes with more clarity.

Chaos attribute delineate the channels as high chaos values sourced from NE whereas the channel lobes and submarine fan are easily interpretable in chaos attribute map. As sweetness is a good shale-sand discriminator (Hart, 2008), therefor it may be concluded from the map that the sweetness map has localized the sand rich areas in channel fill, submarine fan and lobes as indicated in Figure 32(B).
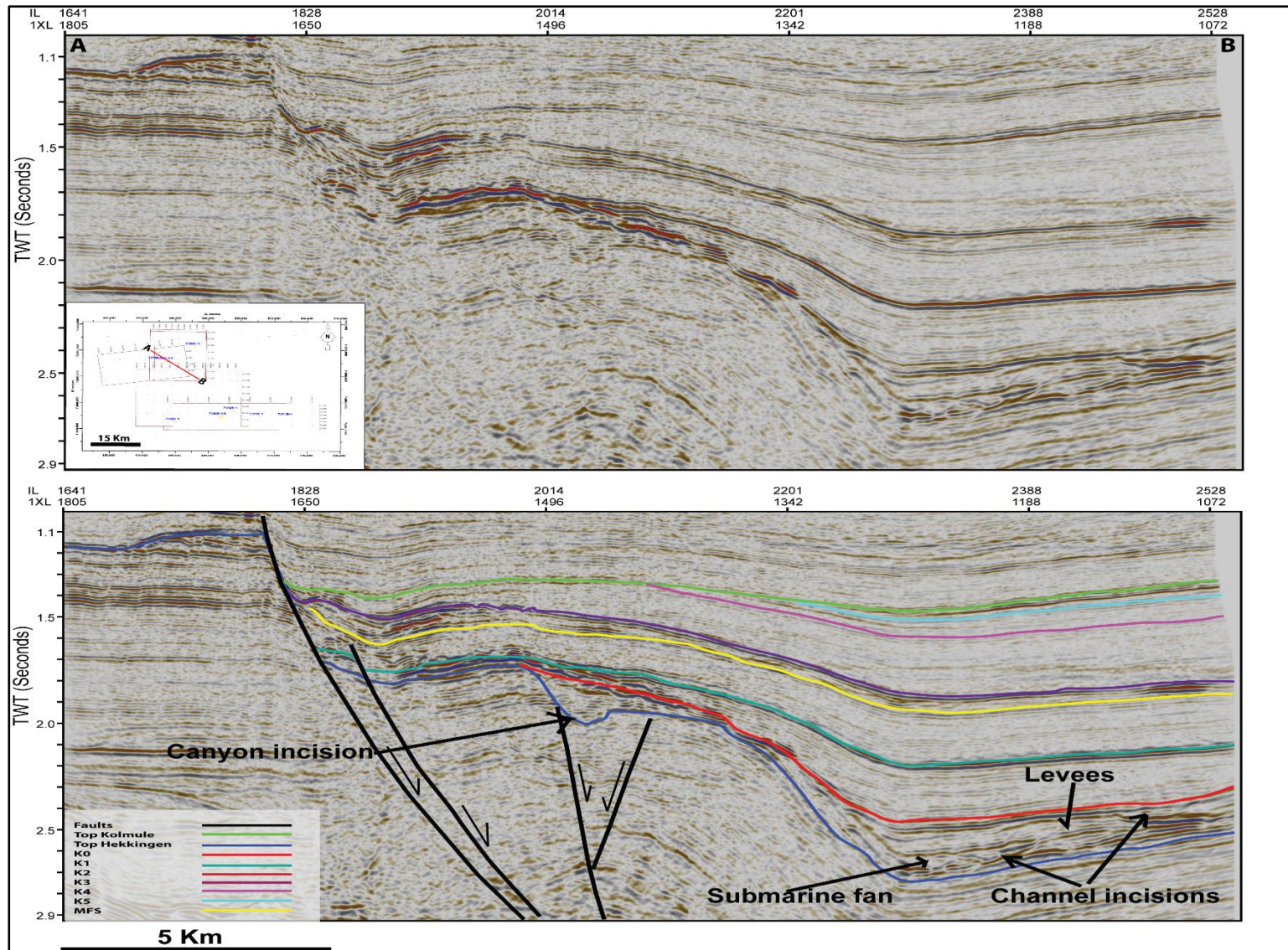
Figure 30: Uninterpreted (Top) and interpreted (bottom) seismic lines showing the channel incisions in deeper basin and canyon incision at shallower shelf margin.
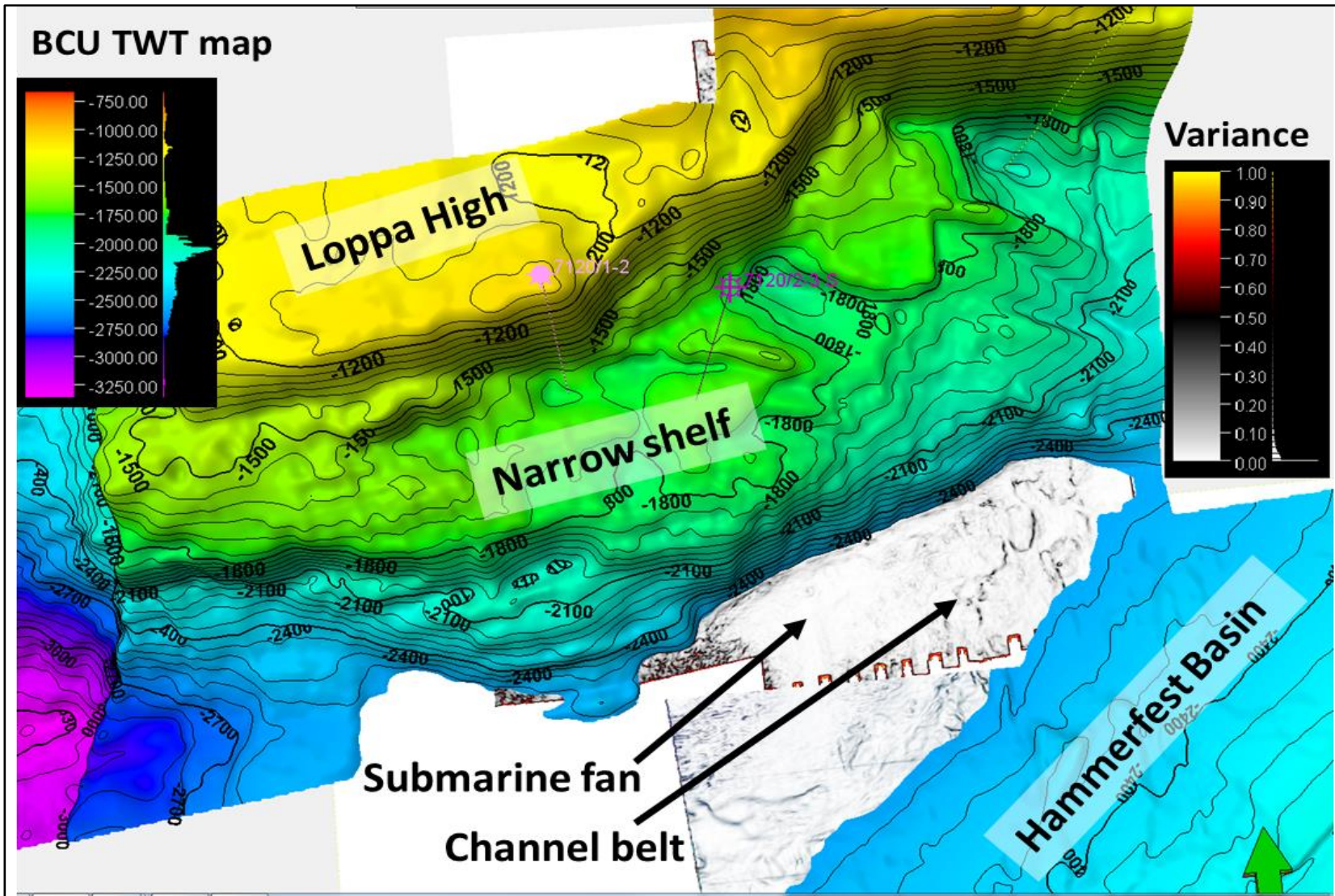
Figure 31: Variance attribute with BCU Two Way Time (TWT) map for type 3 wedge. The channel belt is quite visible on variance map originating from the narrow shelf margin in the northeast. Submarine fan is represented by very low variance (nearly zero) as indicated in the figure.
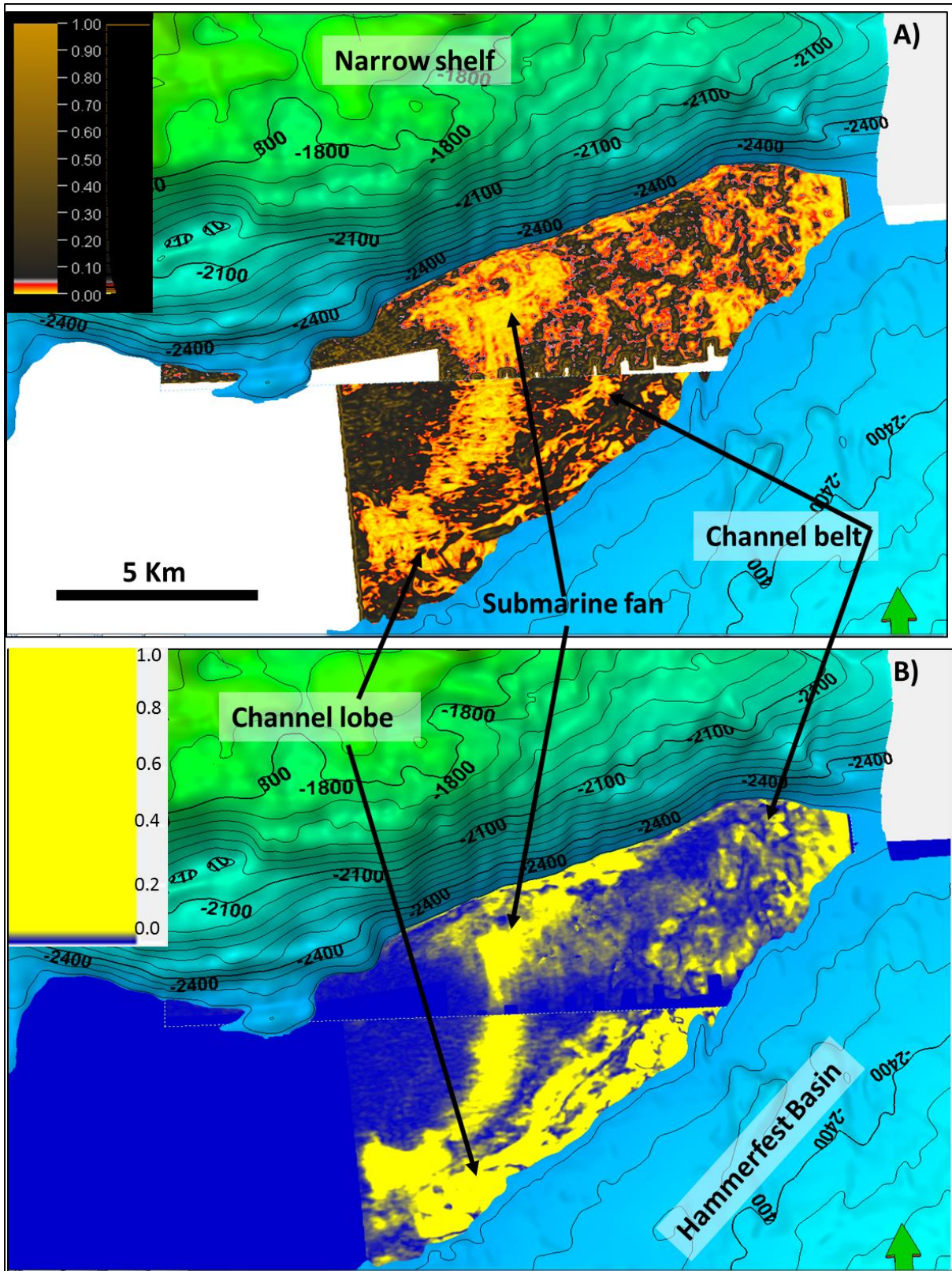
Figure 32: Seismic attributes with BCU TWT map for type 3 wedge A) Channel lobe, submarine fan and channels are seen clearly in chaos attribute, B) Sand prone areas are highlighted in sweetness attribute map with decreased size of high sweetness bodies.

4.4.2 Wedges of late-rifting stage (Early Aptian to Early Cenomanian)

These wedges were deposited when the narrow shelf was flooded because of the rise in relative sea level probably due to decreased tectonic activity. There was a relative abundance of sediment supply which was overcoming the rise in the relative sea level. These wedges are mainly grouped into two types, one on the shelf and the other in deep basin as shown in Figure 33 and Figure 34. They are bounded by maximum flooding surface (MFS) at bottom and a flooding surface (K2) on top as shown in Figure 33. Truncations and channel incisions can be observed on top of these wedges in the seismic data. They are divided into two types, wedges on the shelf are named as type 4 wedges and the ones deposited in deep basin are named as type 5 wedges.

4.4.2.1 Type 4 Wedges

Observations

Well character: These wedges are characterized by low to medium GR values. The response is smooth and blocky with minor spikes. The lower to medium values indicate a lithology dominated by silt and sand which is also proven by a core photo shown in Figure 34. A decrease in the value of sonic curve, increase in density and NPHI curves can be observed for the wedge in Figure 15. Top of the wedge is characterized by a trough whereas base is described by a peak amplitude using a reverse polarity wavelet. Reflections can be observed in the internal part of the wedge showing changes in lithology and energy of the environment (Figure 16).

Seismic character: The type 4 wedges (SF4) are the group of clastic wedges identified on the narrow shelf and are composed of seismically recognized foresets. The forsets are dipping at high angle (approximately 20 degrees) towards the south. These wedges are characterized by the wedge shaped clastic deposits with amplitude strength varying from weak to medium. The reflections are inclined, subparallel/parallel and continuous with downlappings on the distal side against MFS. These reflections are truncating on the proximal side which may be attributed to the erosion of topsets because of canyon incisions. These incisions have been observed, cutting and eroding through these deltas at some locations as shown in Figure 35. Seismic lines in inline and crossline directions are flattened at the base of the wedges to better interpret the reflection geometries. It can be observed that the reflections are dipping towards south at fairly high angles (approximately 20 degrees).

Thickness distribution: The type 4 wedges are found along the strike of the main fault with varying thicknesses. Two main depocenters can be observed, one at well location 7120/1-2 and

the other is at well 7120/2-2 as shown in Figure 34. They have dimensions of about 5 km by 10km. However, the eastern wedge (SF6) at the location of well 7120/2-2 is smaller. They have maximum thickness at these locations with minor wedges along the strike of the main fault separating the basin from the Loppa High. Thickness of main wedges ranges from 50 to 180 milliseconds as shown in Figure 34.

Seismic attributes: A lobate shape feature has been observed on the variance time slice at 1510 milliseconds as shown in Figure 36 (A). Various channel shape bodies can be identified, however one of them is very prominent running all the way from the Loppa High and ends near the shelf edge. The channel has been dissected by many south-dipping faults creating a chaotic response on the time slice because of the high values of variance. The linear features along the shelf margin can be identified with smaller values (0-0.1) of variance. They are surrounded by higher values (0.5-1) of variance. A time slice of chaos attribute (Figure 36(B)) at the same time shows the chaotic zone with higher values of chaos, whereas channel fill is less chaotic alongwith some other areas indicating the presence of various depositional features. Deposits with higher variance and chaos response along the main Asterias Fault Complex (AFC) are also observed. They might correspond to the type 1 wedges. Sweetness attribute time slice (Figure 37) at the same time reveals the details of the depositional features, and the shapes associated with channelized features are more pronounced. Moreover, the linear features along the shelf margin can be interpreted with more confidence and clarity.

Interpretation: Based on the observations, the wedges have been interpreted as wave dominated fan deltas (in micro-tidal coastal settings with a tidal range of less than 2 meters as indicated by core interpretations by Sandvik (2014) (Appendix IV(Figure 61A)) with eroded topsets and associated depositional elements such as channels, levees, crevasse splays and strandplains. The linear features observed near the shelf margin are interpreted as strandplains with brighter response in chaos and lower variance response (Figure 36). Strandplains indicate towards wave dominated environment of deposition. Crevasse splay can be interpreted on variance map with a well-defined shape while it is not so clear in chaos time slice probably because of heterogeneous kind of deposits. However, it is better resolved by sweetness attribute as shown in Figure 37. The progradational nature of the sediments indicate that the sediment supply was an important control (Coe, 2003). The canyons eroding through these deltas are probably one of the reasons of the eroded topsets. Progradation of the foresets implies that the wedges have been deposited during a short episode of highstand, generated because of quiescence in rifting. The amplitude strength of the reflections is an indication of relatively low

energy environments such as distal part of fan delta front with fine grained sand and intercalations of shale/silt probably deposited from the suspension sediments.
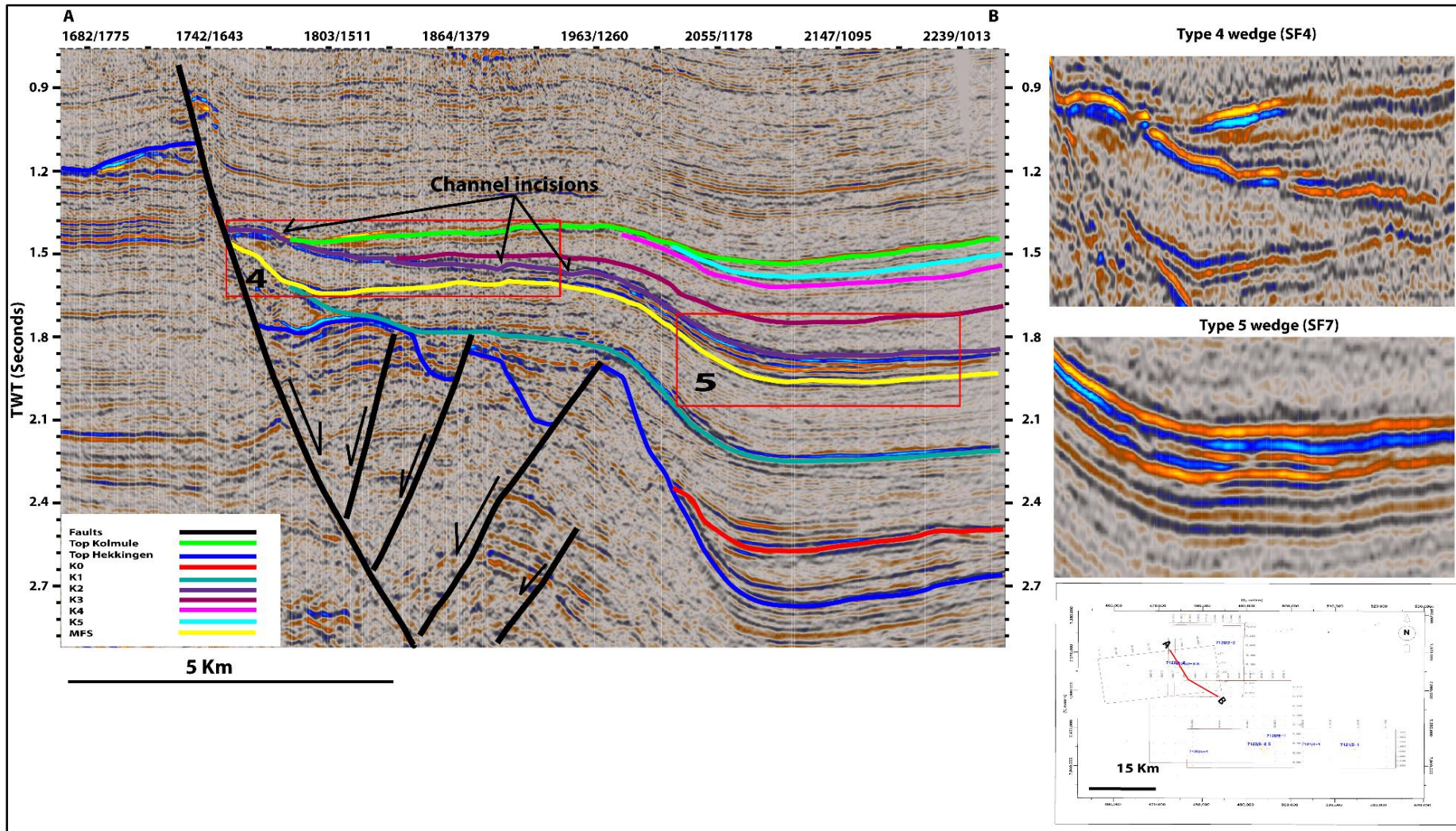
Figure 33: Composite seismic line passing through fan delta type 4 wedge and deep basin type 5 wedge. Notice the brighter reflectors for type 5 wedge which may indicate sand dominated lithology, whereas it is weak to medium for type 4 wedge probably because of the preservation of only distal part of the delta forsets.
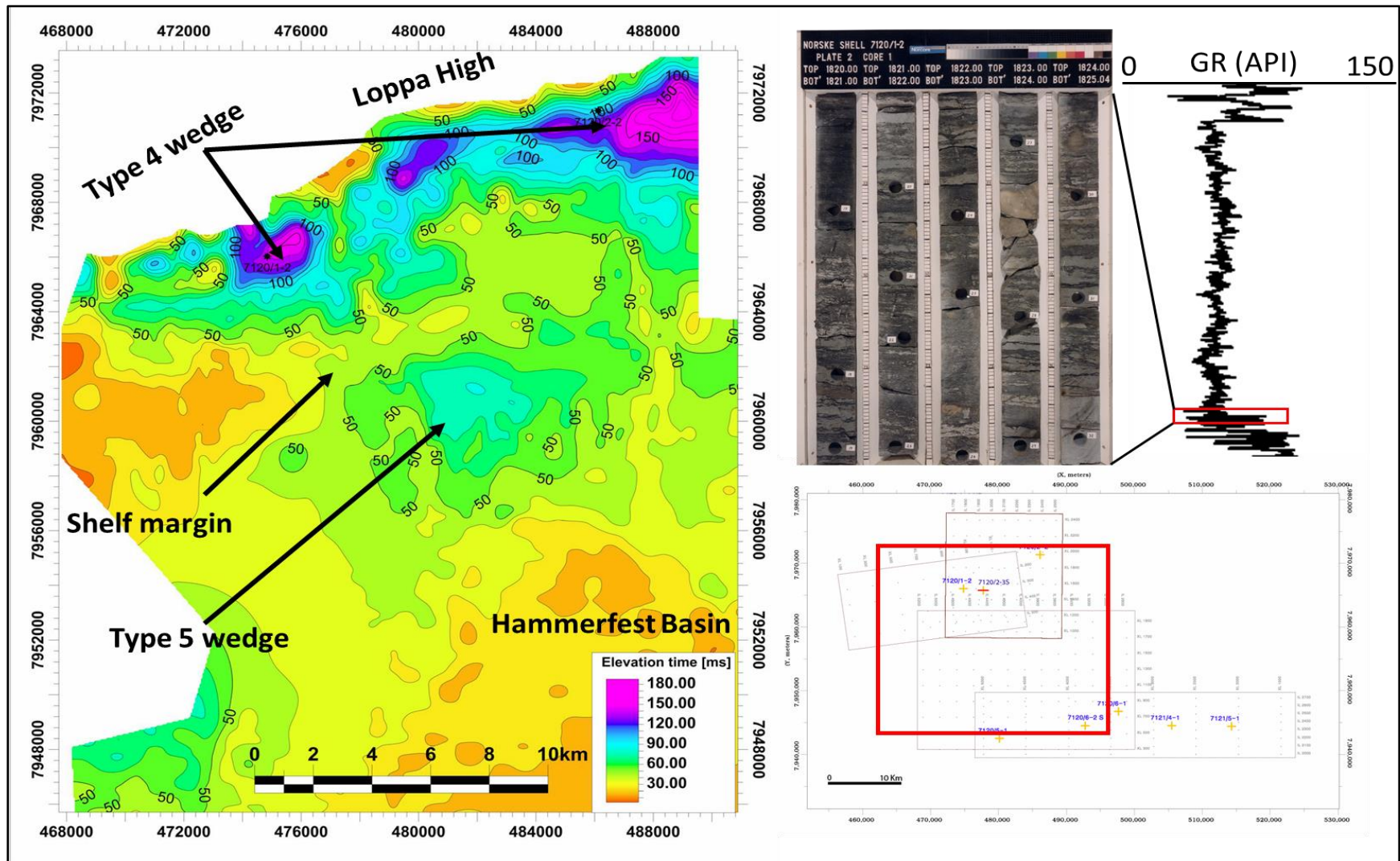
Figure 34: Thickness map of type 4 and 5 wedges. Various depocenters can be identified along the main fault and in the Hammerfest Basin. Core photo is from the lower part of type 4 wedge for the depth 1820 to 1825 meters. Alternating sand and silty shale packages can be seen in the core photo.
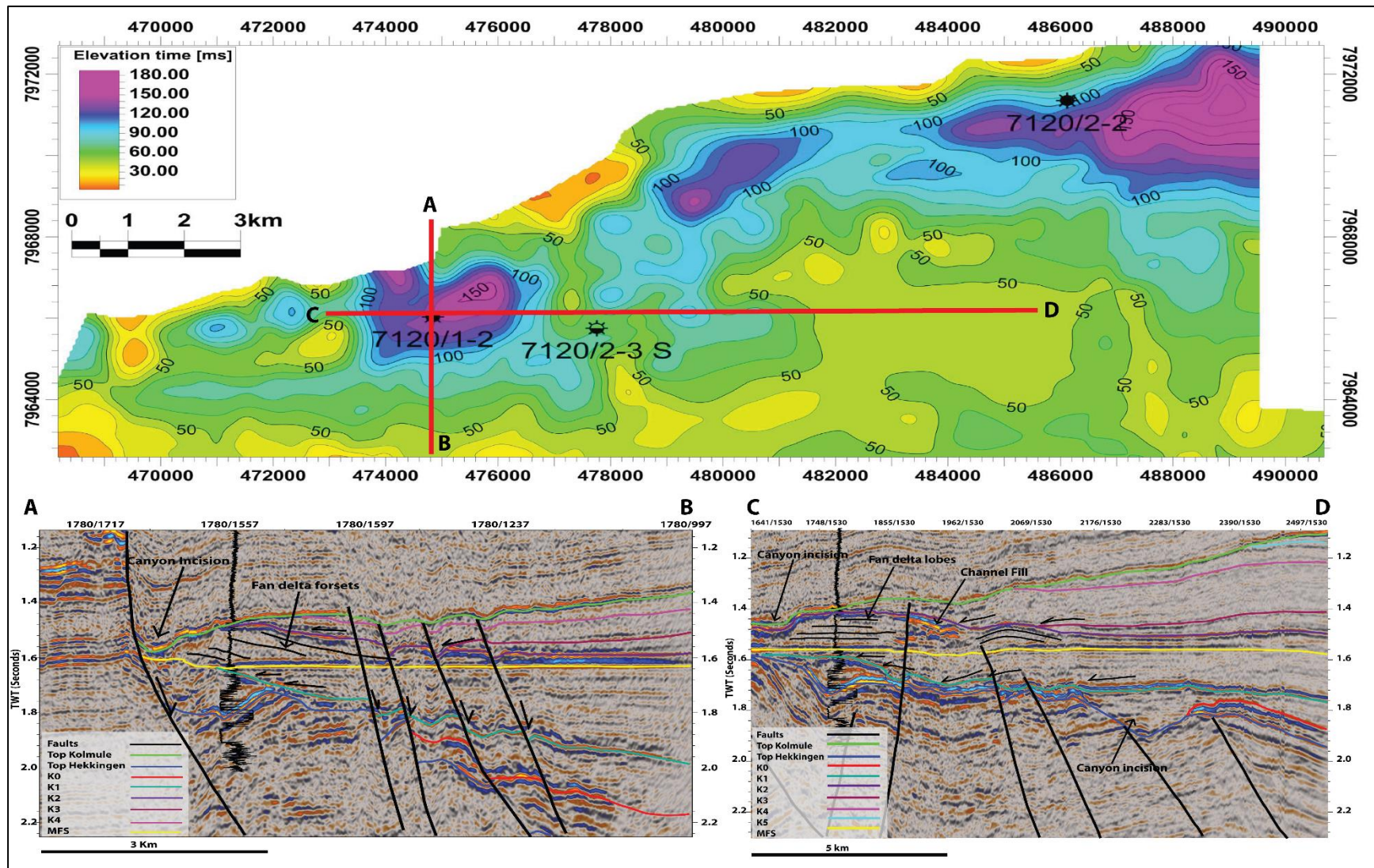
Figure 35: Type 4 wedge thickness map with inline and cross line. Seismic lines are shown for one of the wedges to elaborate dimensions of the wedge. Moreover they are flattened at the base of the wedge for interpretation of foresets angles (approximately 15-20 degrees)
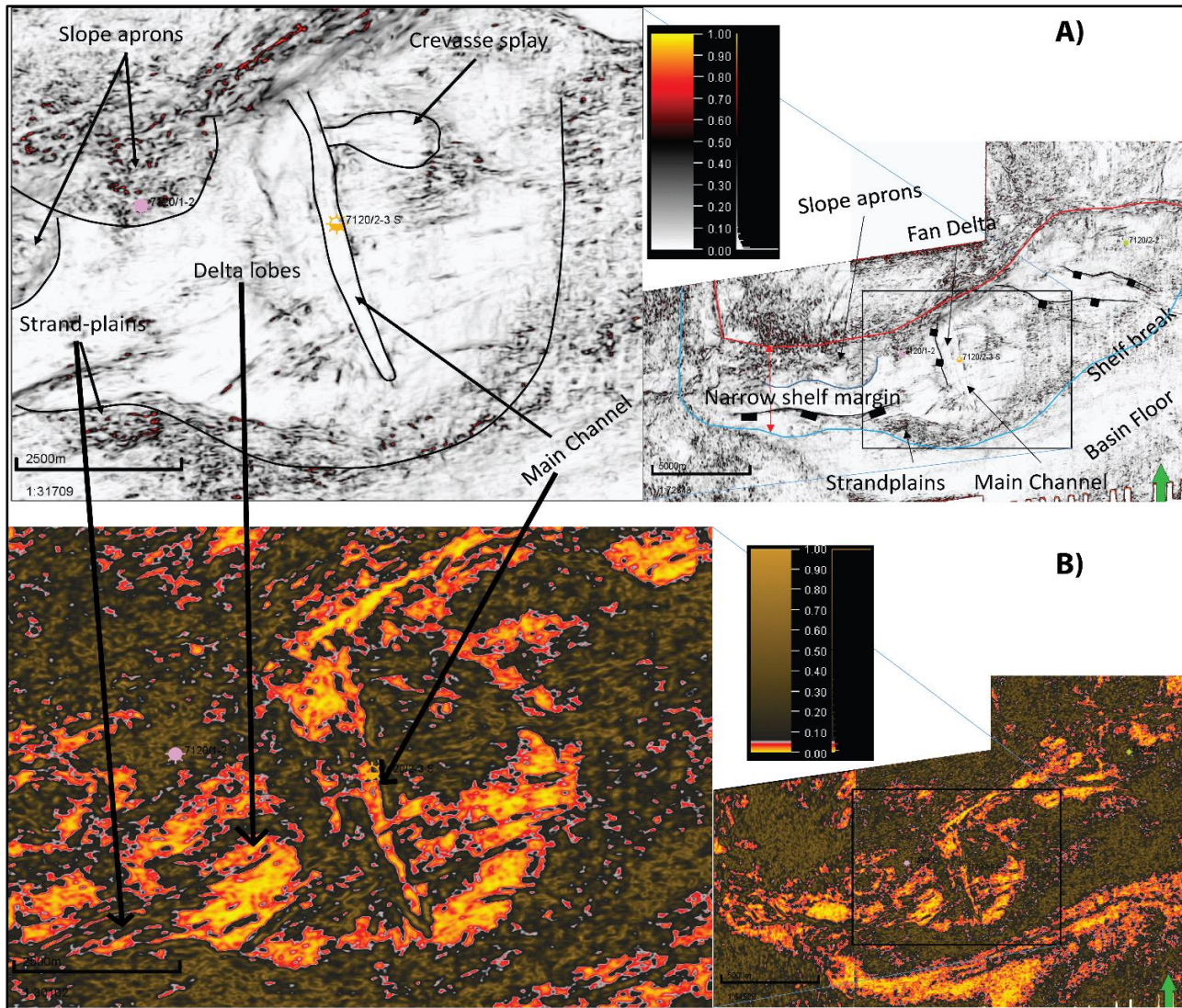
Figure 36: Type 4 wedge variance (A) and chaos (B) attribute time slices at 1510 milliseconds. Various depositional features can be marked on variance attribute map, whereas chaos attribute is separating and enhancing the features clearly into different parts based on the chaoticness of the deposits.
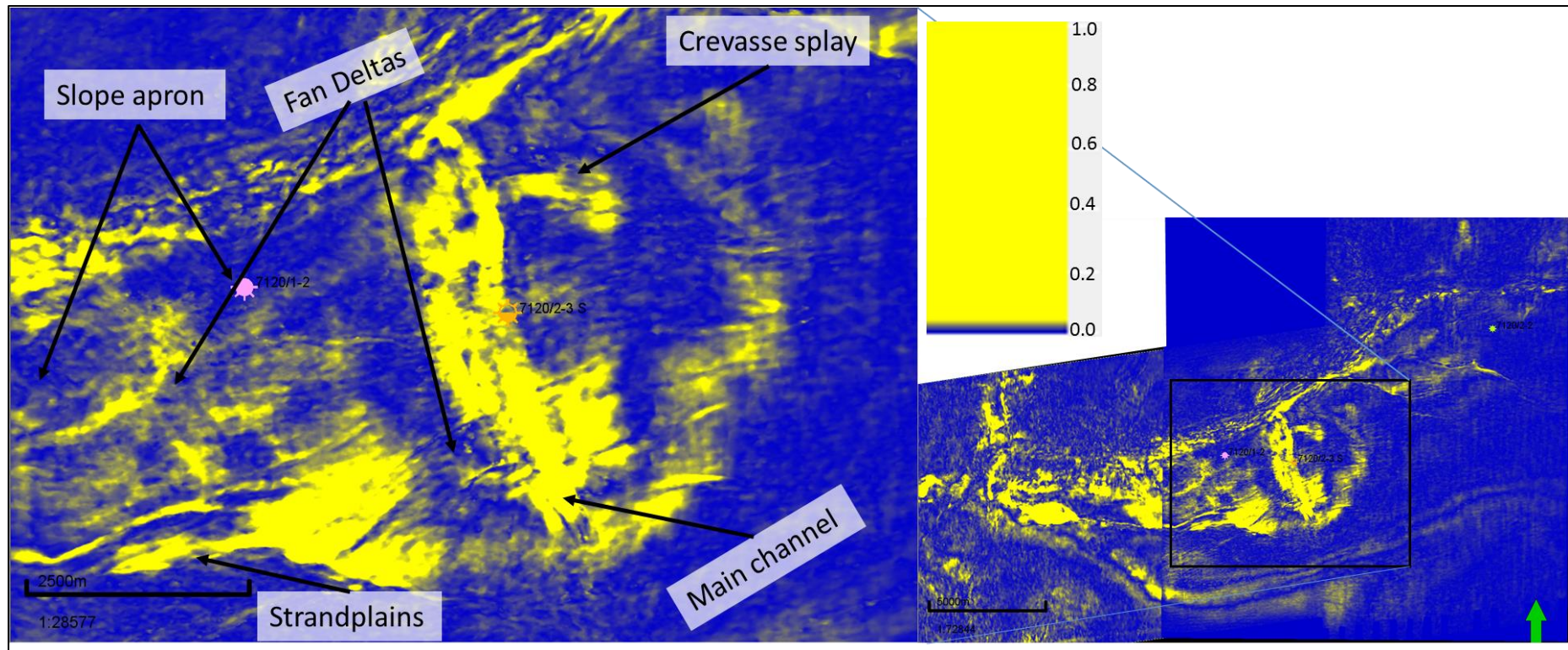
Figure 37: Sweetness attribute time slice at 1510 milliseconds. Notice that the crevasse splay and strandplains are resolved better than both variance and chaos attributes. The yellow areas show the higher values of sweetness which is associated with more massive and sand prone areas whereas blue color represent the low values corresponding to the shale prone areas. The response of the sweetness attribute is also used for localizing sand and shale dominated area. Channels and strandplains are sand dominated areas of the fan delta system, therefore they are represented by higher sweetness values. It can be observed in the inset figure to the right that the environment changes from sand to shale dominated moving from west to east, this has also been proven by rock physics analysis of the well data of wells 7120/1-2, 7120/2-3S and 7120/2-2 which is discussed in rock physics section.

4.4.2.2 Type 5 Wedge

Observations

Well character: This wedge has not been penetrated by any of the wells drilled to date in the study area.

Seismic character: This wedge is building out from the shelf through channel like features and traversing towards the east. The reflectors are downlapping on the distal margin with onlappings on the proximal side. Bidirectional downlapping has also been observed in the middle of the fan with weak to medium amplitude reflection as shown in section AB of Figure 39. A composite line CD in Figure 39 shows an arrangement of sheet like reflections without any clear stratal lapping. The reflection amplitude is strong, indicating the wedge is composed of coarse grained lithology.

Thickness distribution: The length and width of this wedge is approximately 7km and 4 km respectively and has time thickness of around 70 milliseconds as shown in Figure 38. It is characterized by a fan shape body as shown in Figure 38. The wedge is bounded by shelf edge and rotated footwall on the northern and southern sides respectively.

Seismic attributes: Variance, chaos and sweetness attributes show the fan from slightly different perspectives as shown in Figure 40 and Figure 41. A fan shape with very low variance values can be seen building out in variance time slice at 1864 milliseconds (Figure 40 (A)). Chaos attribute (Figure 40(B) shows the enhanced features of the fan with a clear shape. However, the boundaries are still not clearly differentiable. Sweetness attribute map reveals the fan geometry in detail. It may be noticed from the attribute maps that the sediment source is probably from narrow shelf via both channelized flow and debris/gravity flows. It is obvious from the attribute maps that the fan is bending towards east. The change in direction of the fan towards east may be interpreted as either affinity of sediment movement towards depocenter or the overall flow direction was eastward. It is an important point and needs more discussion which will be done in discussion section later. These wedges have not been drilled probably because of presence in the depocenter without any structural traps. Stratigraphic traps may be sought for exploration of hydrocarbons in these wedges.

Interpretation: Based on the observations, the wedge can be interpreted as basin floor fan with sediment source from the narrow shelf through channels and debris/gravity flows. Distal downlapping indicates the distal extents of the fan whereas bidirectional downlapping is an indication of a typical basin floor fan. Various attributes such as variance, chaos and sweetness

confirms the fan shape of the basin floor fan with a source from the shelf through canyon incisions.
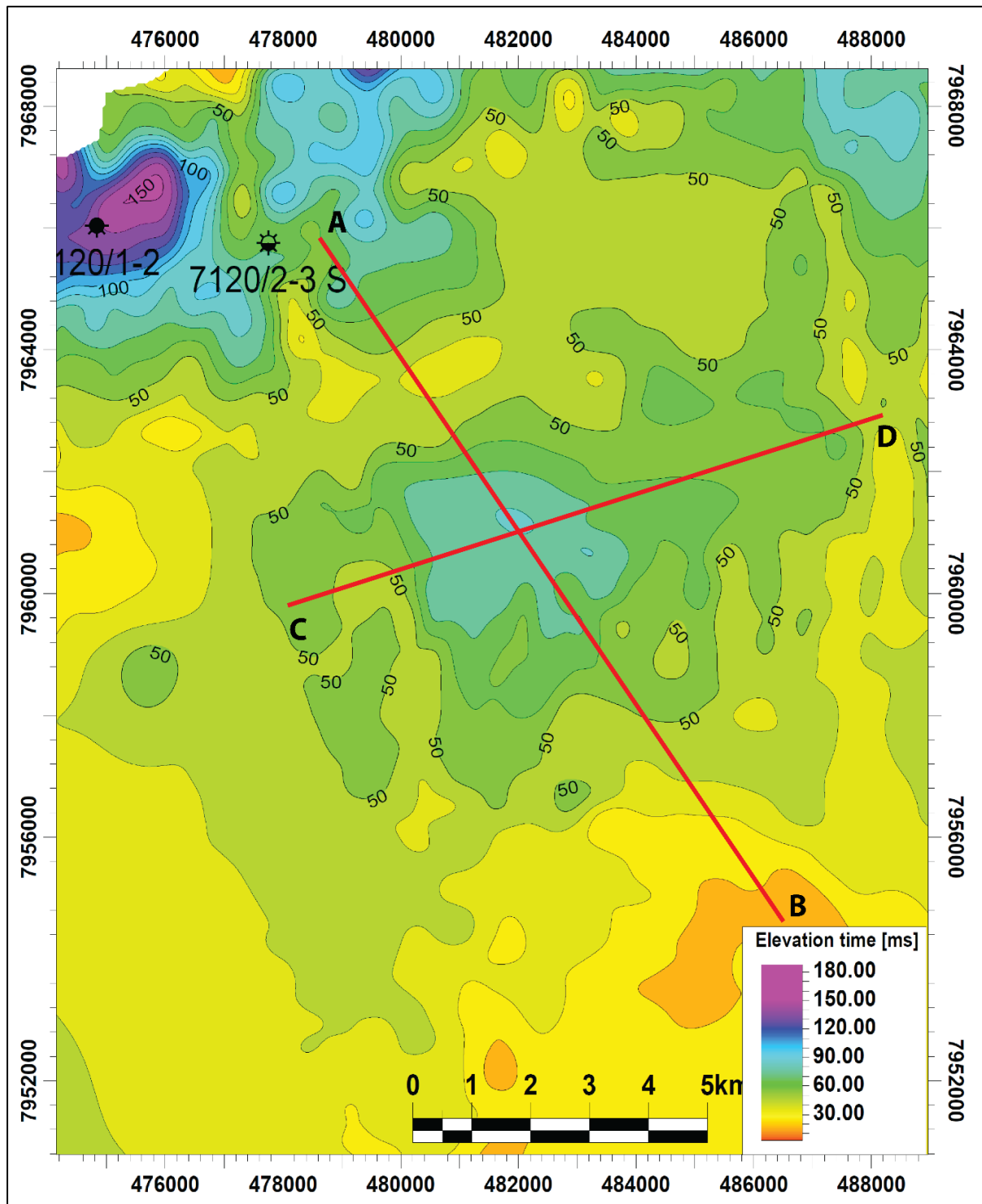
Figure 38: Thickness map of type 5 wedge showing dimensions and thickness variations of the fan.
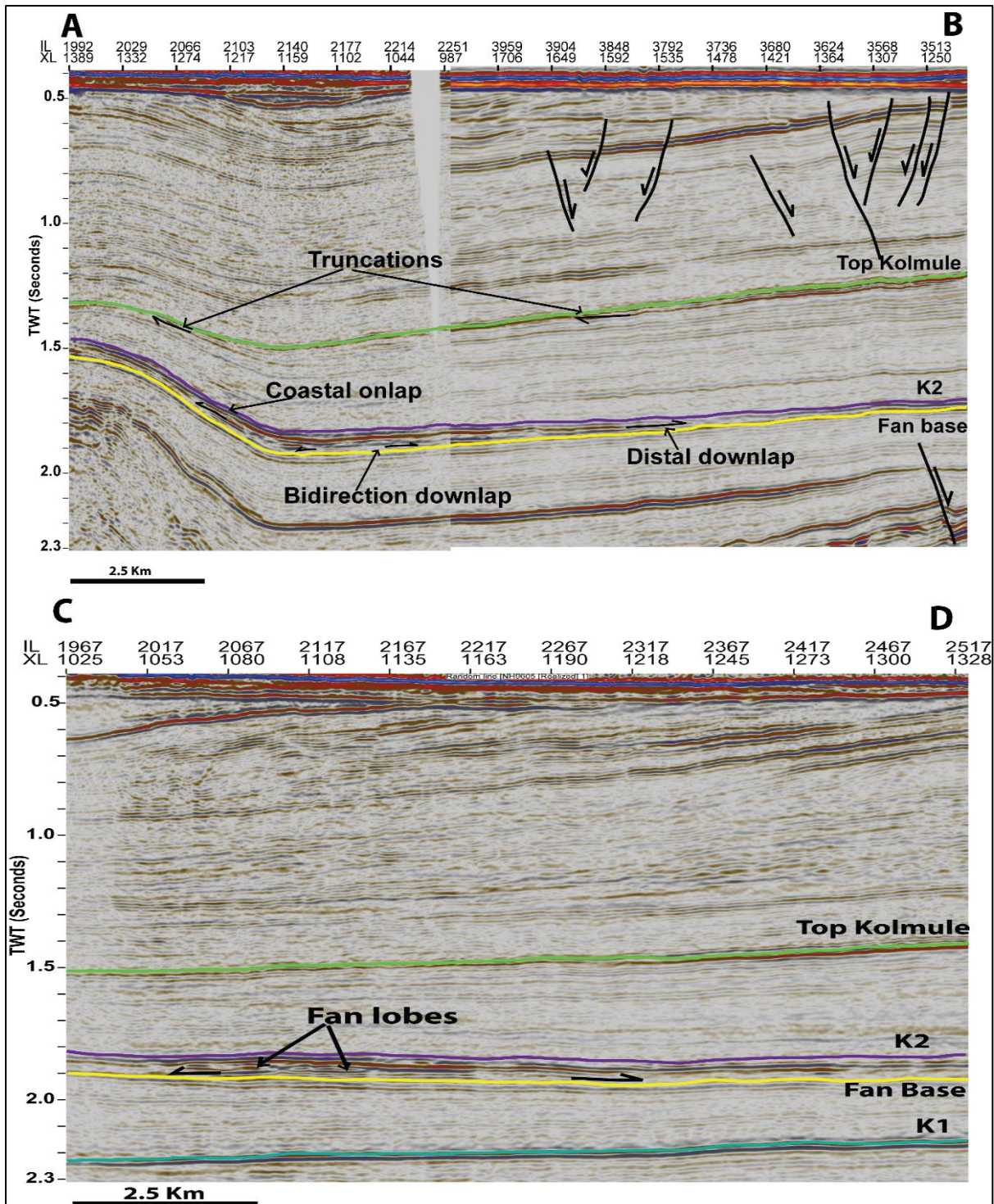
Figure 39: Composite seismic lines. AB) along dip showing onlapping, downlapping with interpretation of top and base of the fan, and CD) along strike showing fan lobes and bidirectional downlapping. Location of the lines is shown in Figure 38.
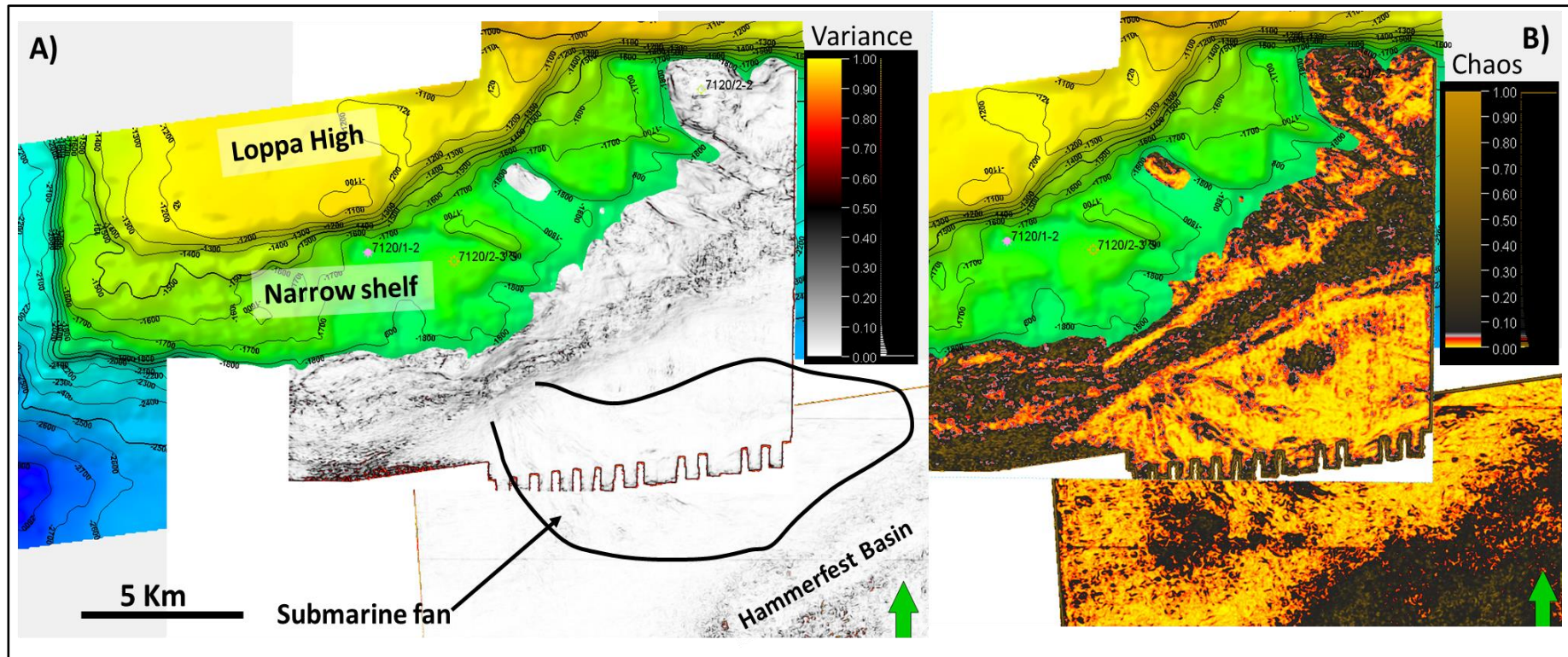
Figure 40: Type 5 wedge attribute time slices at 1864 milliseconds. A) Variance map along with TWT structure map at BCU level shows a submarine fan building out from the shelf and it bends eastward probably because of the depocenter being on that side. The channelized features can be observed originating from the shelf margin and feeding the fan. The fan has very small variance values which is making it difficult to interpret properly using variance attribute, B) Chaos map shows well-defined shape of the fan along with associated channels fanning out from northwest to southeast after leaving the shelf margin. Lower values of chaos show the homogeneity of the sediments. Channel boundaries are represented by higher values of variance and chaos.
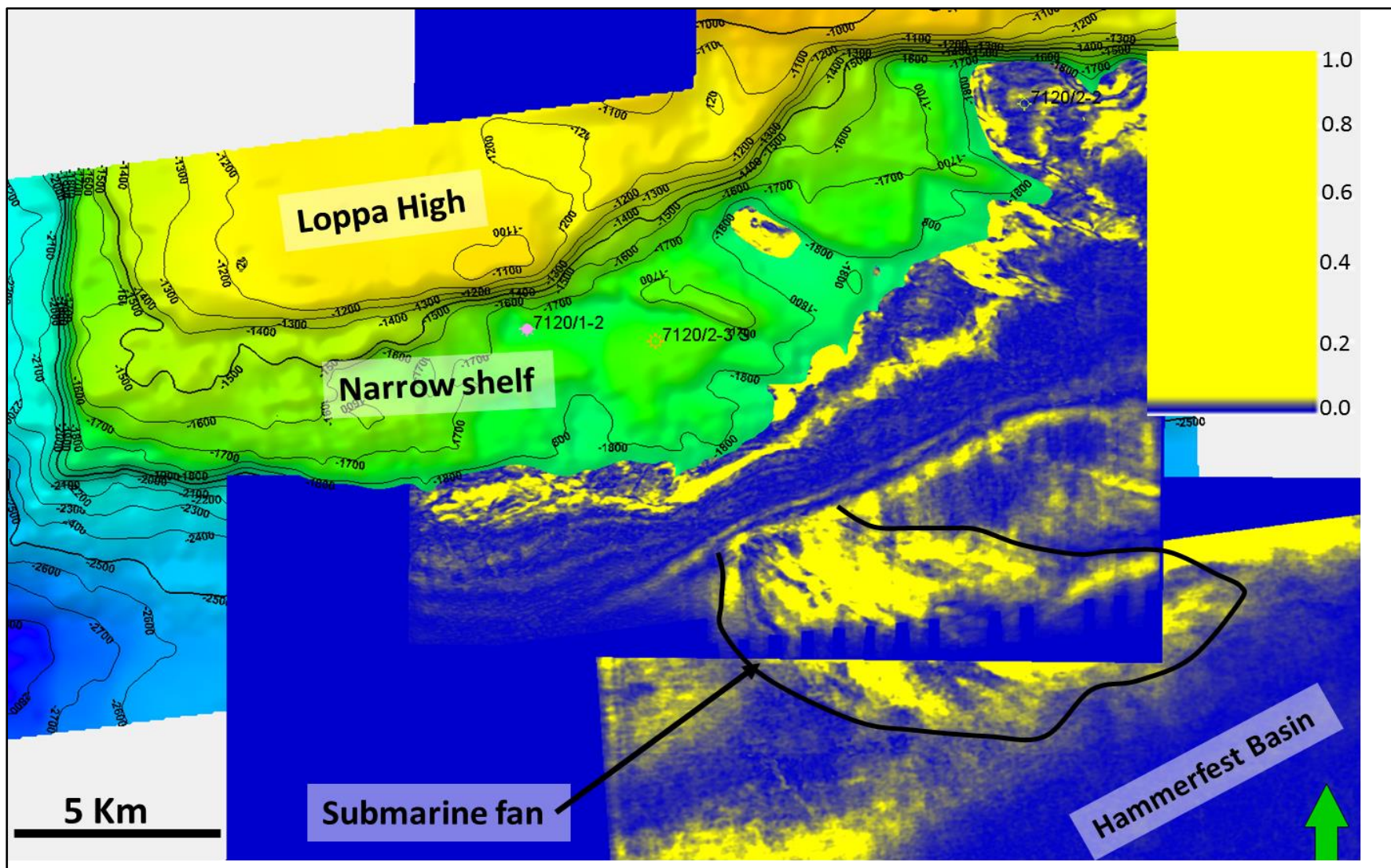
Figure 41: Sweetness attribute time slice at 1864 milliseconds. The fan is now narrower compared to the one resolved by chaos attribute and is more interpretable with clear boundaries. Sweetness responds to massive beds like sand with higher values of sweetness whereas lower values correspond to shale. The threshold value for sands has been chosen at around 0.05 sweetness units.

4.5   Rock physics analysis of the clastic wedges

Rock physics analysis of the wedges, penetrated by wells on the shelf, has been carried out. Only three wells have been drilled so far on the shelf and have encountered types 1 and 4 wedges. Well 7120/2-3S is drilled in 2013 on the channelized part of the type 4 wedge while well 7120/1-2 has penetrated the delta front part of the fan delta and type 1 wedge at deeper level.

4.5.1   Type 1 wedges

Observations: These wedges have been encountered in two wells, 7120/1-2 and 7120/2-2. Figure 42, Figure 43 and Figure 44 show the GR and P-wave velocities plotted against depth and the corresponding rock physics plots for these wedges on the right side of every figure. It can be observed that the wedges are characterized by mostly very low porosities (1 to 14%) and higher velocities as shown in Figure 43 (SF5) and 7 to 20 % for the upper part of the wedge in well 7120/1-2 (SF2). Comparatively higher porosities are confirmed by the sandy lithology as shown in thin sections in Figure 42 and by the core photos shown in appendix IV (Figure 59 (D)). However, the deeper part of the wedge in 7120/1-2 (SF3) shows different characteristics and have a porosity range of 12 to 23 %. Some data points fall on the friable sand model with most of the data below the model line for SF5. These wedges have very spiky GR response with periodical coarsening-up intervals which may be correlated with the points falling on the constant cement model. The proportion of shale is higher in the wedge encountered in well 7120/2-2 (SF5) as shown in Figure 43 and is supported by core photos in appendix IV (Figure 59 (C)). The thin sections in Figure 43 also confirms the presence of shale dominated lithology. On the other hand, the lower wedge in 7120/1-2 shows a blocky GR response with sharp spikes and almost all the data points fall on constant cement model (Figure 44). A shear reduction factor of 1 has been used to generate the constant cement model for this wedge.

Interpretation: The lower porosity wedges with data points scattered around friable sand model can be interpreted as silty shale with occasional spikes of relatively clean sand. The sand is mainly unconsolidated with minor amount of scattered cement between the grains causing further decrease in porosity. Whereas, the sandstone of lower part of the wedge in 7120/1-2 is a clean sand with porosity range of 12 to 23%. This sandstone has a higher amount of cement as indicated by Figure 44. This high porosity-high velocity sands have intercalations of shale as indicated by GR log in Figure 44. The sediments in well 7120/1-2, on western end, are sand prone and have sandy characteristics with minor cementation whereas sediments in well 7120/2-2, on the eastern side, are shale dominated and indicate a low energy depositional

environment than that in the east. These properties shows that the overall reservoir potential of these wedges is varying from bottom to top and from west to east. The deeper parts of the type 1 wedges in well 7120/1-2 have excellent reservoir quality with higher porosities (12 to 23 %).
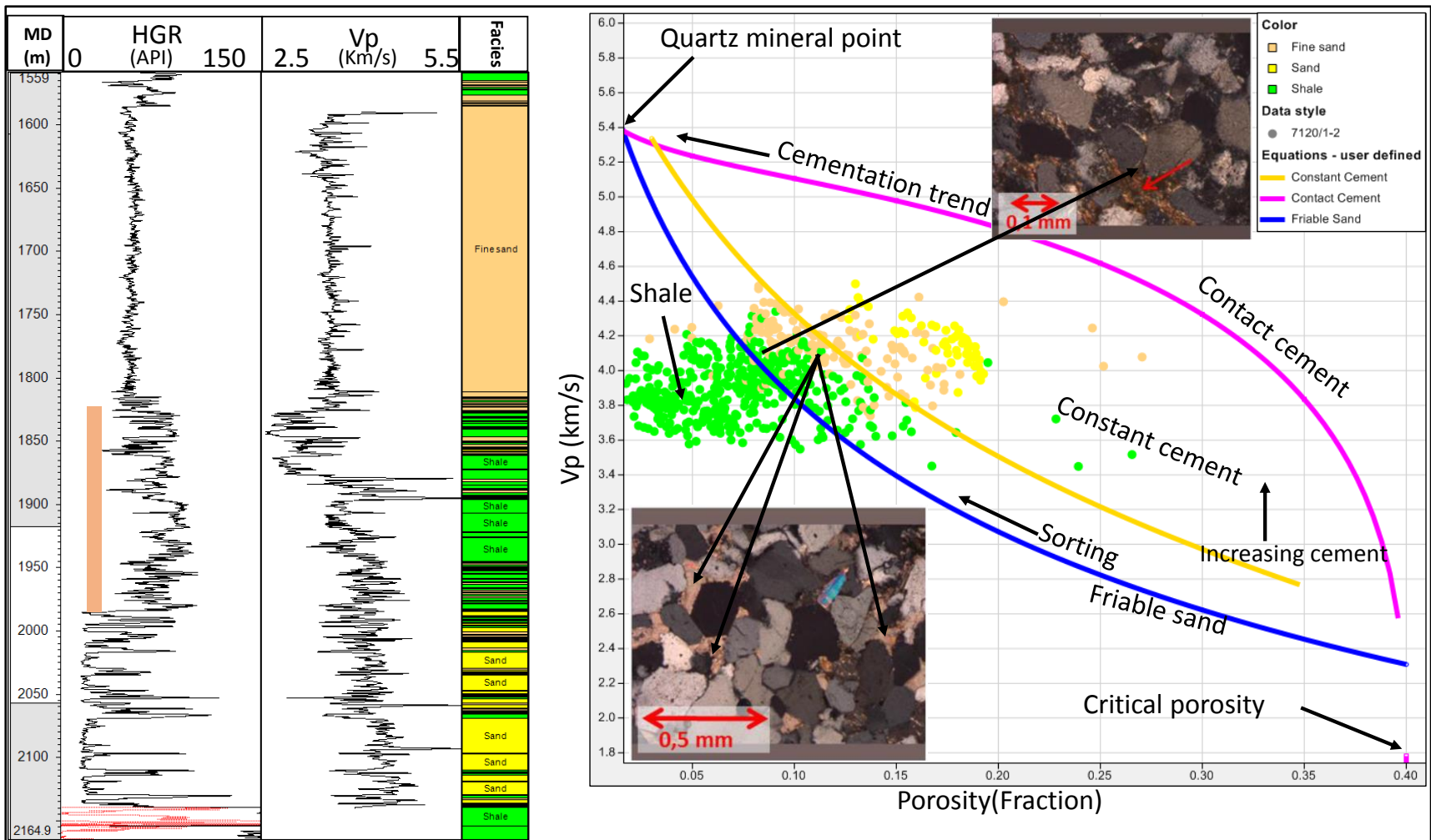
Figure 42: Rock physics analysis of upper part of type 1 wedge in well 7120/1-2. Gamma-ray (GR) and P-wave logs versus depth (left) show the location of the wedge with vertical orange color bar plotted in porosity-velocity plane (right). The porosity and Vp logs have been calculated from density and sonic logs respectively. The facies have been shown with different colors based on the GR values. Yellow color shows sand, orange color is for silty sands and green color indicates silty shale. Crossplot shows some good quality sand intercalations with a significant amount of cementation. The logs are shown only for an interval between Top Kolmule and Top Hekkingen. Thin section in bottom left shows carbonate cement at the depth of 1958.3 meters whereas the one on top right shows illitic matrix at the depth of 1962.15 meters. Thin sections are taken from Rodriguez (2015).
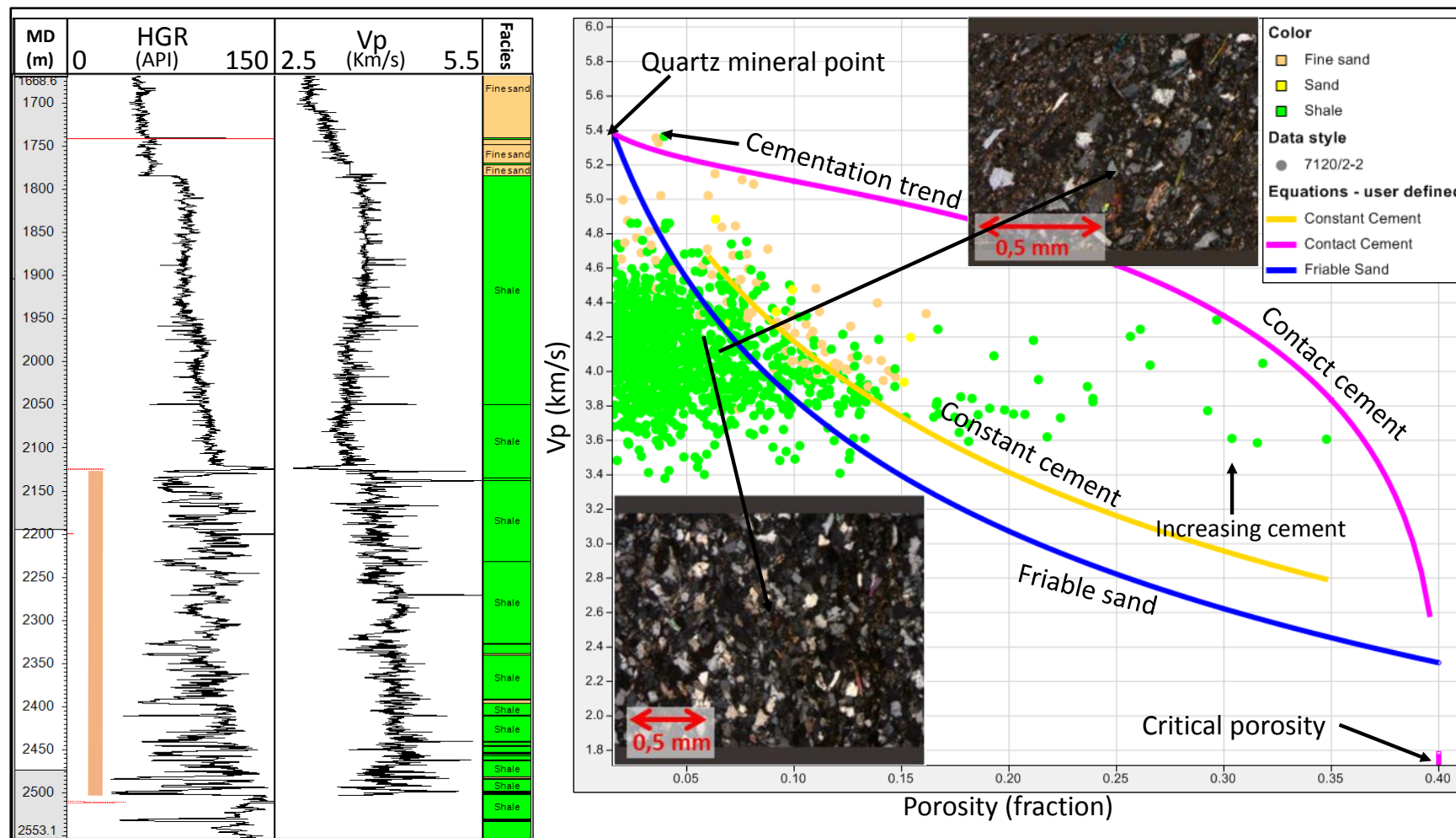
Figure 43: Rock physics analysis of type 1 wedge in well 7120/2-2. Left figure shows GR and Vp logs plotted versus depth, it shows that the GR values are higher for the wedge compared to well 7120/1-2. It is confirmed by the porosity-velocity plot on the right side, almost all the data points fall on the friable sand model and below it indicating shale dominant lithology. Porosity and velocity logs have been calculated from density and sonic logs respectively. The logs are shown only for Top Kolmule-Top Hekkingen interval. Thin section at bottom left shows feldspathic greywacke at the depth of 2186.75 meters. Top right thin section shows grains of muscovite in greywacke samples. Thin sections are taken from Rodriguez (2015).
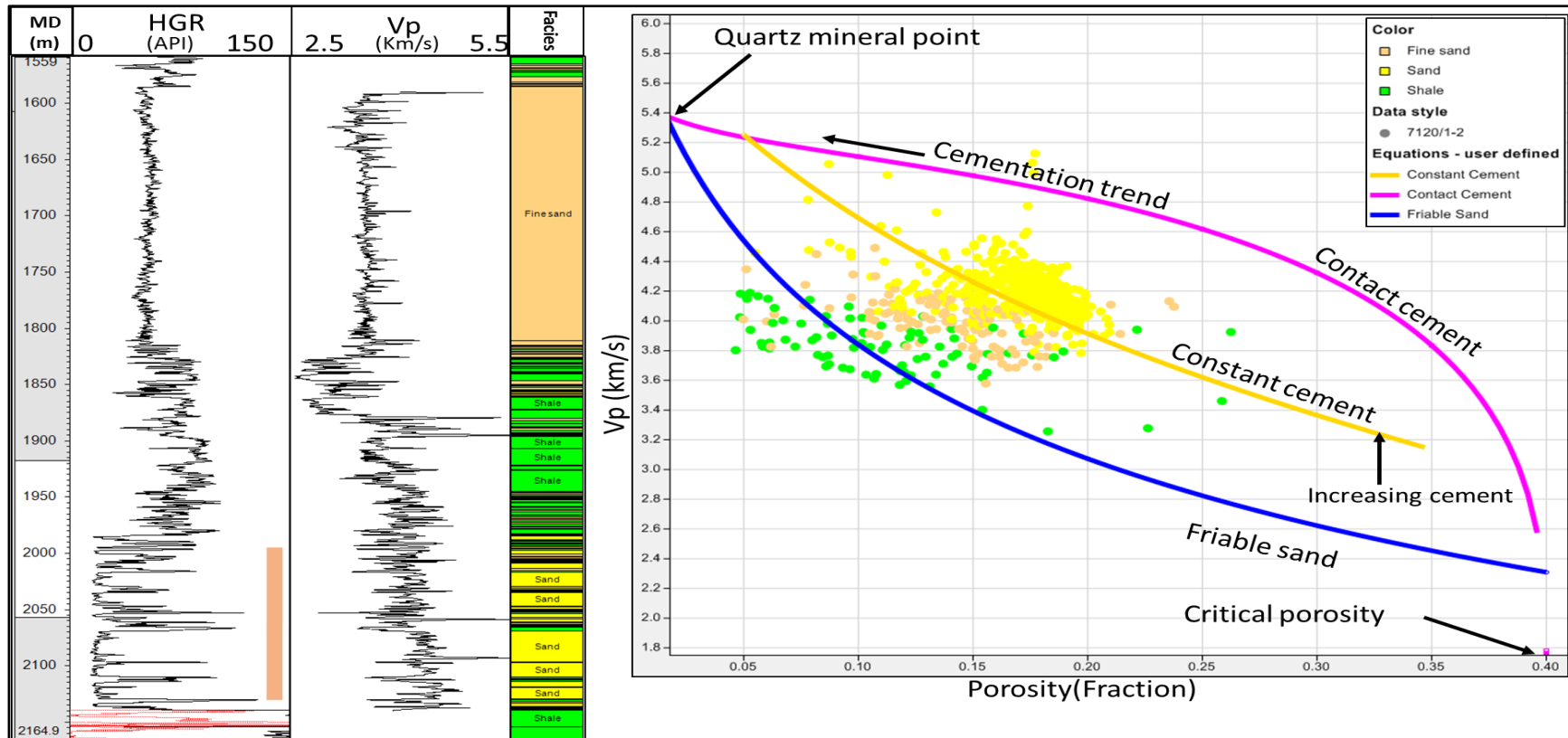
Figure 44: Rock physics analysis of lower part of type 1 wedge in well 7120/1-2. GR and p-wave velocity logs versus depth are shown to the left. GR shows a blocky response with spikes of very high GR values. Figure to the right shows a scatterplot in porosity-Velocity plane, the data points are plotted at higher porosity (between 12 to 22%) and on the constant cement model of shear reduction factor of 1. It indicates the higher amount of cement scattered between the grains, and it is medium to well sorted. The logs are shown only for Top Kolmule-Top Hekkingen interval.

4.5.2 Type 4 wedge

Observations: These wedges are interpreted as fan delta front containing prograding foresets type clinoforms with associated channel fills. The amplitude of the reflections is medium as discussed in previous sections. It can be observed from Figure 45 and Figure 46 that the GR response of the deltaic wedges in both of the wells 7120/1-2 and 7120/2-2 is very homogeneous with coarsening-up response. There is, however, a big difference between GR values of the wells indicating clam environment of deposition at the location of well 7120/2-2. The sequences in well 7120/1-2 are interpreted as delta foresets (SF4) whereas, the sediments of wedges at other well locations are distal in nature. GR response of the wedges in well 7120/2-2 (SF6) has a coarsening-up signature at bottom then changes to fining-up response towards top. The lower values of GR indicate that the wells probably have been penetrated on the distal margin of the delta or delta plain with fine grained dominated sediments. Data points of well 7120/2-2 fall on the friable sand model line and below it with lower values of porosities (1 to 10%) which indicates shale dominated silts. Data points from well 7120/1-2 falls on the constant cement model (generated using shear reduction factor of 0.25) which shows small amount of cement in the sediments. The porosity values are slightly higher than that of well 7120/2-2 ranging from approximately 10 to 20% with relatively better sorting as shown in Figure 46

Interpretation: The wedge encountered in well 7120/2-2 is mostly shale dominated as confirmed by core photo in Appendix IV (Figure 60(A)). On the other hand, the wedge encountered in well 7120/1-2 is sandy with good reservoir porosities (10 to 20%). The core photos are from the basal part of the wedge and shows alternating layers of sand and shale with some coal layers as shown in Appendix IV (Figure 60(B)). The higher amount of shale volume in core photos indicates that the well is drilled on distal part of the delta probably on bottomsets. It can be concluded that the wedge encountered in well 7120/1-2 is of medium sorting with a small amount of cement scattered between the grains causing porosity reduction. Whereas, wedge encountered by well 7120/2-2 is predominantly shale with minor intercalations of sand with very low porosity (1 to 10%). This also supports the decreasing sand proportion of the system moving from west to east. Wedges on the western side have reservoir quality sands compared to the eastern side along the strike. The type 4 wedge in 7120/1-2 is well sorted with porosity mainly affected by diagenetic processes whereas the one in well 7120/2-2 is poorly sorted and porosity has been affected mainly by poor sorting.
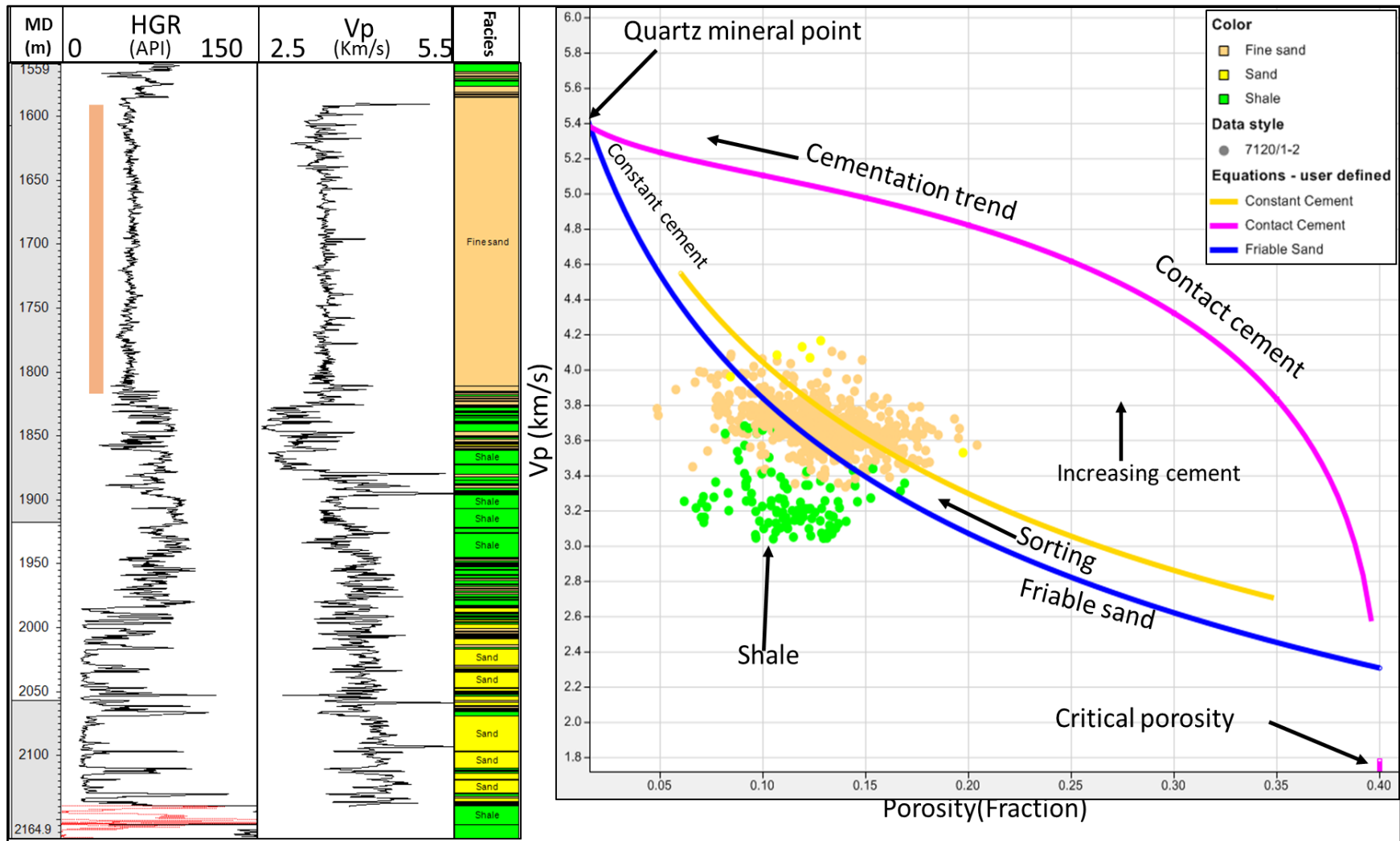
Figure 45: Type 4 wedge rock physics analysis for well 7120/1-2. Right side shows GR and Vp logs versus depth, Wedge shows lower GR values with blocky shape indicating the homogeneity of the sediments. The crossplot to the right is between porosity and velocity data and most of the data points are falling on the constant cement model of shear reduction factor of 0.25. It shows a small amount of cement between the grains. Porosity and velocity are calculated from density and sonic logs. The logs are shown only for the Top Kolmule-the Top Hekkingen interval.
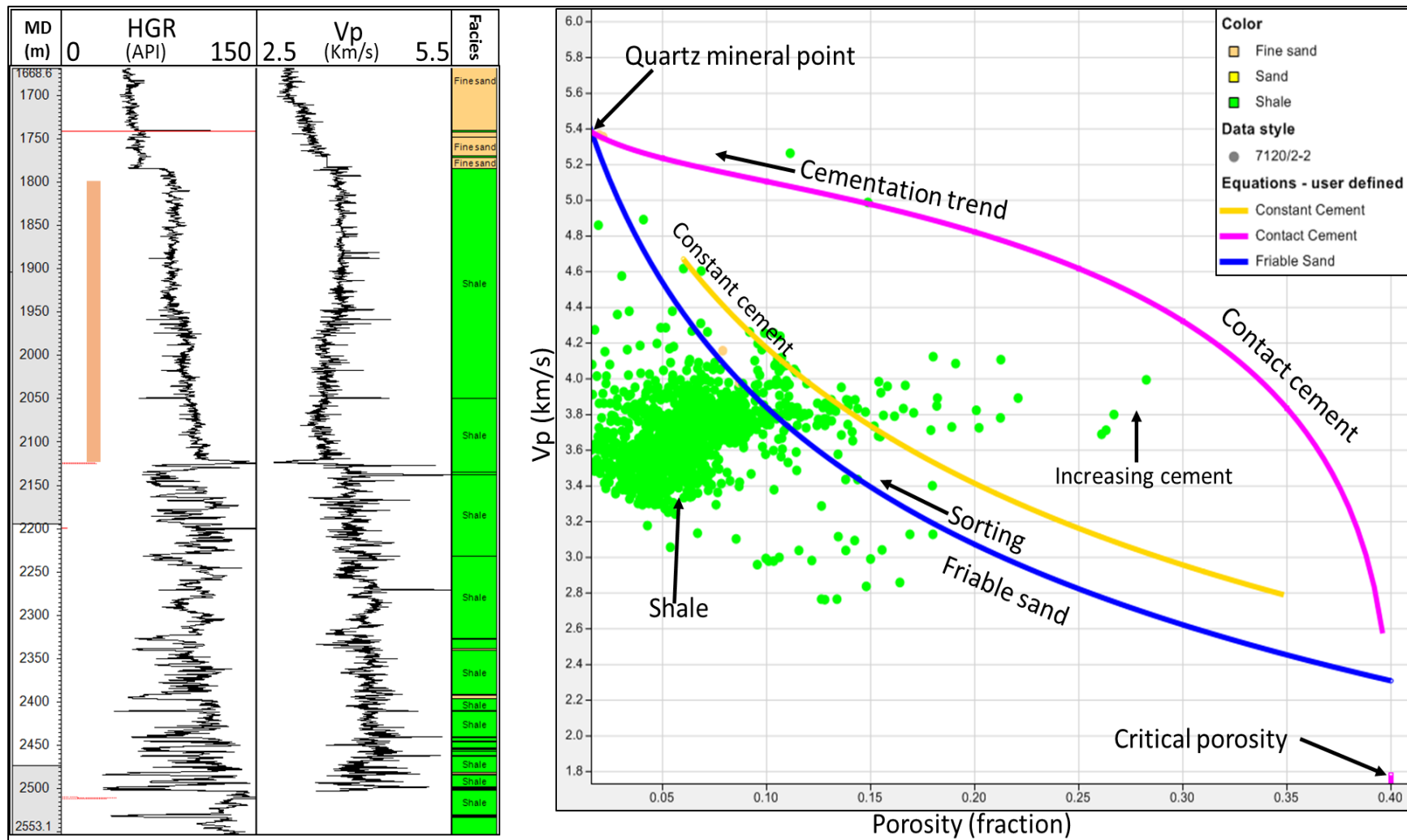
Figure 46: Type 4 wedge rock physics analysis for well 7120/2-2. Left hand side figure shows GR and Vp logs versus depth indicating the zone that has been analyzed in the porosity-velocity plane to the right side. Almost all of the data is plotted below friable sand model with only few on the constant cement model with a shear reduction factor of 0.25. It shows that the wedge is shale dominated which is also confirmed by the core photos in appendix IV.

4.5.3 Rock physics analysis of well 7120/2-3S (Skalle)

This well was drilled in 2013 to explore the petroleum potential of the Lower Cretaceous clastic wedges. It penetrated the channelized part of the type 4 wedge and shows a nice coarsening-up deltaic GR response topped by a blocky response from GR as shown in Figure 47. The upper part of the wedge was found to be gas filled with brine saturated basal part (NPD, 2013).

Observations: Rock physics analysis has been carried out for the wedge and most of the data points are fitting the constant cement model (with a shear reduction factor of 0.4) as shown in Figure 47. The scatter has a porosity range of 7 to 27%. GR response for the wedge shows a coarsening-up response first which then changes to blocky response on top before repeating it again in the upper part. Some data points also fall on the friable sand model probably corresponding to the data of higher GR values between two episodes of deltaic deposits.

Interpretation: The sands are interpreted to be cemented intermediately as indicated by the constant cement model. The sorting trend indicates that the sands are well sorted indicating high energy of depositional system. The reduction of porosity is not only because of depositional origin such as sorting and grain packing, but a significant amount of contact cement and scattered cement also adds to it. The overall reservoir quality of the sandstone is very good with porosity (7 to 27 %) preservation partly because of presence of cement at the contacts of the grains.
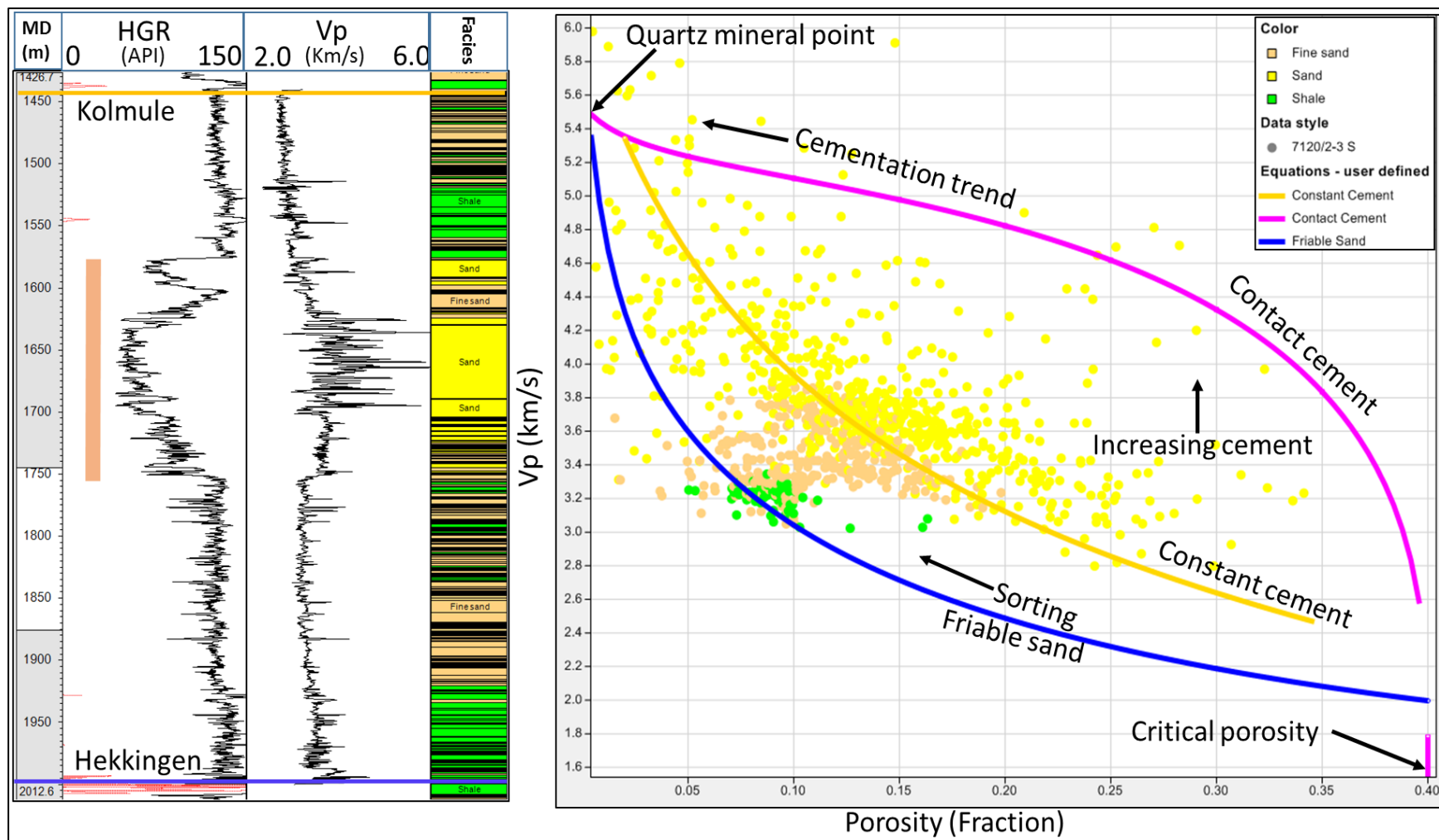
Figure 47: Rock physics analysis of channelized part of type 4 wedge in well 7120/2-3S. GR and Vp logs to the left show the zone of analysis and is plotted in porosity-velocity plane to the right side. Almost all the data points fall on the constant cement model line generated using shear reduction factor of 0.4. It indicates a medium to high amount of cement between the grains. Moreover, the porosity ranges from around 7 to 27 % and within a range of very well sorting. The porosity and p-wave velocity have been calculated using density and sonic logs. Only the Lower Cretaceous interval is shown in the well logs.

4.5.3.1 Rock physics template

A rock physics template provides a link between elastic properties and reservoir properties of the rocks (Avseth and Veggeland, 2015). Well data can be crossplotted followed by superimposing rock physics template, which help interpreting various geological trends from the data such as shale content, cement volume and porosity as shown by brown arrows in Figure 48.

Observations: The data has been crossplotted in the acoustic impedance (AI)-Vp/Vs plane and the friable sand model has been superimposed to interpret possible geological trends from the template. Three different trends can be observed in the template, 1) data points falling on the shale trend, 2) data falling on the brine sand trend and, 3) the data points falling between 100% brine line and 100% gas saturation line.

Interpretation: Some data points follow a trend with higher Vp/Vs ratios and low acoustic impedance which are interpreted as shale and shown as green points. These are falling on the shale trend as shown in Figure 48. The data points falling on 100% brine line are brine saturated sand whereas the points located below this line are gas saturated sand with different gas saturations moving down to the 100% gas saturation line. Different geological trends are also interpreted from this template as follows;

1. Increasing cement volume
2. Increasing content of shale
3. Decreasing effective pressure
4. Increasing porosity
5. Increasing gas saturation

It can be interpreted from the scatterplot that the sand and shale data points are differentiated. The sand can further be divided into brine and gas sand using the above defined trends.
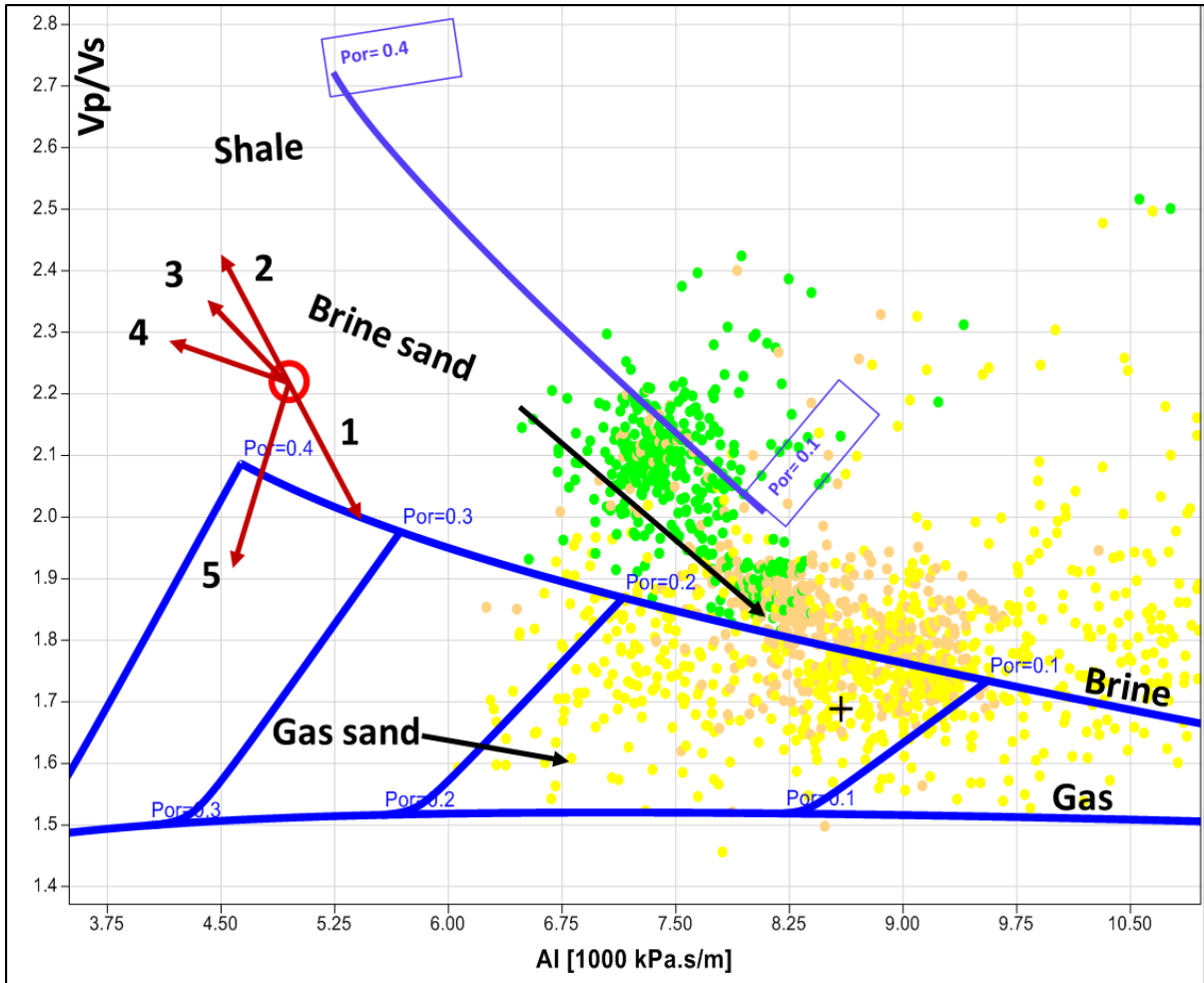
Figure 48: Rock physics template analysis for well 7120/2-3S. A cross plot Acoustic Impedance versus Vp/Vs superimposed with rock physics template. Gas sand can be observed close to 100% gas saturation line as encountered in the well. The brown arrows define various geological trends 1) increasing cement volume, 2) Increasing shaliness, 3) Decreasing effective pressure, 4) Increasing porosity and 5) Increasing gas saturation. Friable sand model has been computed at 20 Mpa with mineralogical data from well logs. Shale trend has been drawn manually to depict the changes in shale properties.

5 Discussion

5.1 Structural control on deposition of clastic wedges along the southern margin of the Loppa High

The sediments were derived from the uplifted footwall of the Loppa High to the north and northeast. The complex faulting system, known as Asterias Fault complex (Figure 21) to the south of the Loppa High, controls the drainage patterns and sedimentation as proven by Type 1 and 2 wedges and their internal geometries. The narrow shelf was highly faulted at the time of deposition of the Lower Cretaceous sediments. Different trends of the faults on the shelf were responsible for the deposition of different kind of wedges depending on the tectonic activities, sediment supply and changes in relative sea level. Moreover, the fault family 2 (F2) act as bypass mechanisms for the sediments supply to the deep basin (Figure 49). Type 1, 2 and 3 wedges are the one influenced more by this structural complexity. Whereas, type 4 and 5 wedges are less affected by this faulting on the shelf. However, thickening and thinning of the wedges is still controlled by the topographic features created by the faulting on the narrow shelf.

5.2 Controls on sediment flux

Sediment flux is controlled by either climate (favorable conditions for weathering and erosion) or tectonic movements(sedimentation adjacent to an active fault) (Coe, 2003). The sediment supply is partly controlled by both the processes in the study area. In the beginning, a rapid rate of early-rifting stage provided ideal conditions for weathering and erosion processes on the Loppa High and narrow shelf area. The weathering and erosion generated canyons/gullies and fluvial incisions on the narrow shelf as shown in Figure 49. The sedimentation took place in the accommodation space created adjacent to the active Asterias Fault Complex and in the deeper Hammerfest Basin. The sediments were transported to deep basin traversing through the gullies and canyons and deposited as submarine fans. Secondly, erosional processes were restricted to the footwall upland areas during the late-stage of rifting when tectonic activity was relatively quiescent and narrow shelf was flooded. Most of the sediments were depositing on the narrow shelf along the strike of the main fault. This gave rise to the deposition of fan deltas along the strike of the main fault (Figure 49).
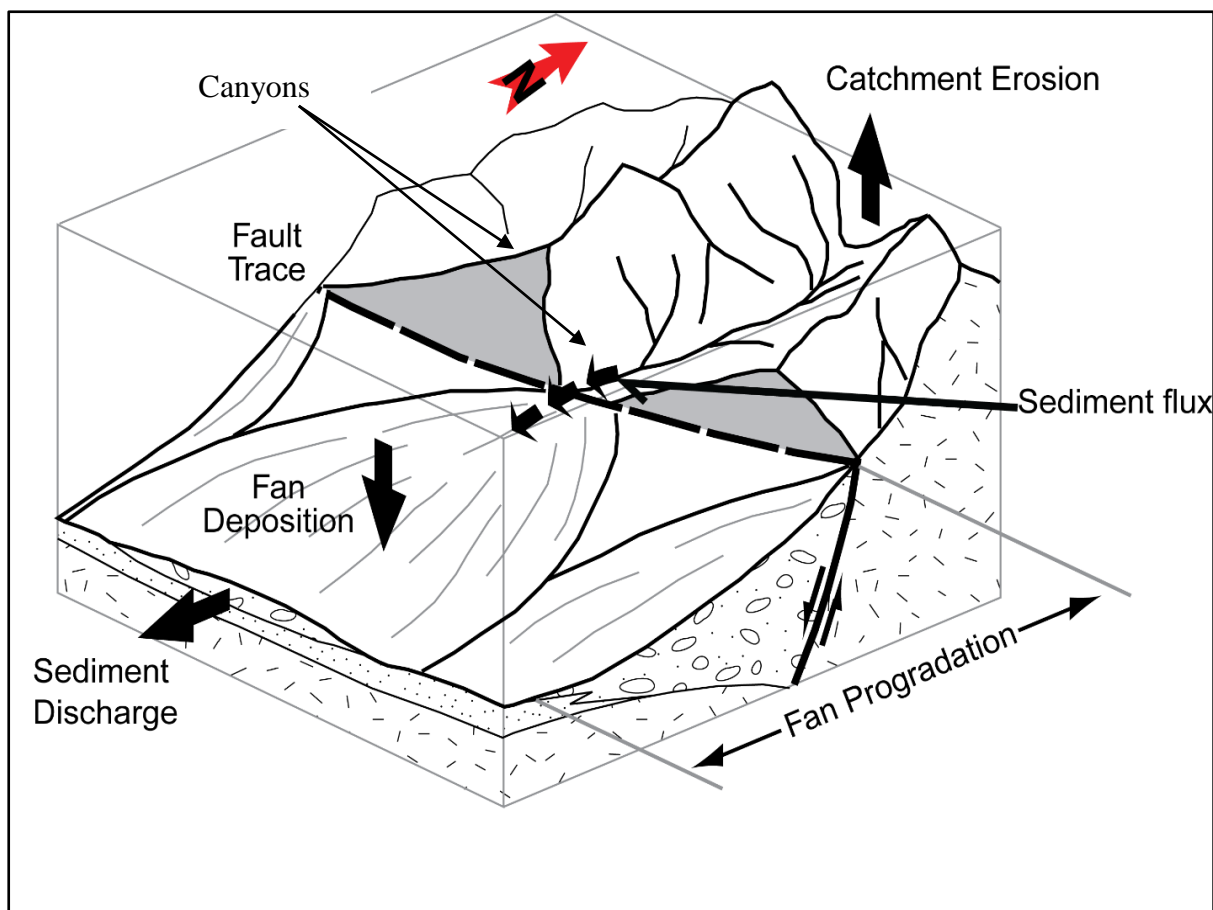
Figure 49: Controls on sediment flux in the southern margin of the Loppa High modified from Allen and Densmore (2000).

5.3 Seismic attribute workflows

Form the observations, it is evident that the seismic attribute workflows are key in both qualitative and quantitative interpretation of depositional environment. It is obvious from Figure 50 that the shape of the fan delta in thickness map is similar to the morphology resolved by sweetness attribute map at corresponding depth. The main channel running north-south can be interpreted on both the thickness map and sweetness attribute time slice. Attributes further resolve the sub-depositional environment such as crevasse splays strandplains etc. This proves that seismic attributes could be very helpful in interpretation of depositional environment in case of lack of/limited availability of core data which is the main tool for environment of depositional environments. However, attributes should be used in combination with well log and seismic facies to finally interpret the environments.
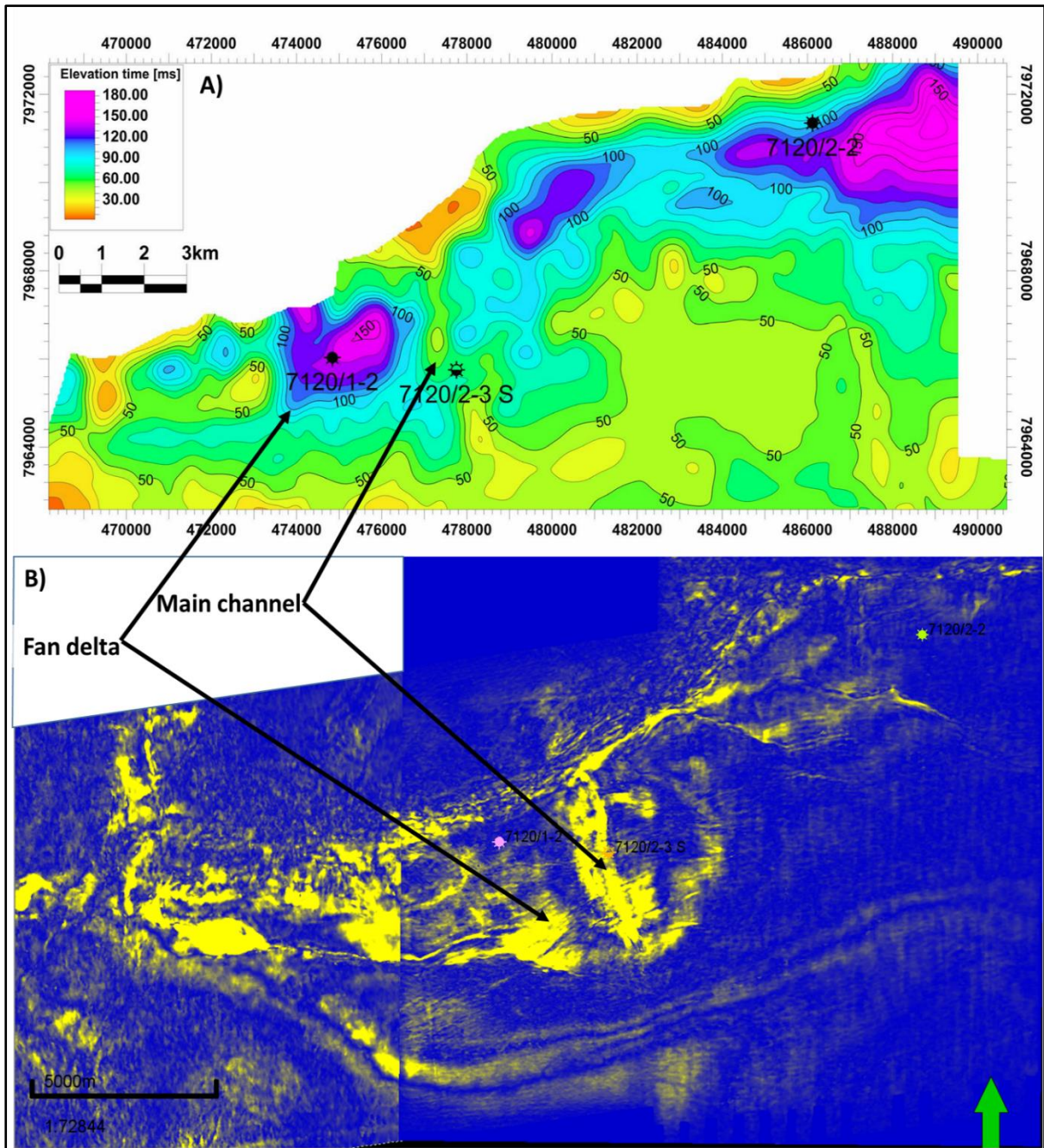
Figure 50: A) Thickness map of fan delta deposit shows fan delta with a lobate shape, B) Sweetness attribute time slice at 1510 milliseconds is showing the similar lobate shape fan delta. It proves the significance of the appropriate seismic attributes for interpretation of depositional environments.

5.4 Evolution of clastic wedges along the southern margin of the Loppa High

5.4.1 Phase 1: Clastic wedges of early-rifting stage (Berriasian to Lower Barremian)

The main phase of subsidence and uplift existed during the Middle Jurassic to Early Cretaceous (Aptian-Albian) times (Faleide et al., 1993) This subsidence (of the Hammerfest Basin) and the uplift (of the Loppa High) resulted into drop in the relative sea level, which exposed the narrow shelf area (faulted terrace), triggering erosional processes. The sediment supply from highland areas, to the north and northeast, was dominantly medium to fine grained with occasional storms as indicated by GR log response. The shelf area, intensely faulted due to Asterias Fault Complex, was acting as a bypass area for the sediments to the deeper basin. The faulted terrace was containing a complex of valleys/canyons which were acting as sediment bypass mechanism to deep basin. This possibly resulted into deposition of three types of wedges on different parts of the basin (Figure 51A): 1) Slope aprons, ponded deposits and gravity failure deposits along and in the vicinity of the main fault, 2) basin floor fans in the relatively deeper Hammerfest Basin and 3) wedges deposited in the canyons on the faulted terrace (narrow shelf) during transgression. The deep marine fans are interpreted to be sourced from eastern side (in addition to the canyons directly from shelf) through a wide channel belt as shown in Figure 51A and also indicated by fan shape on attribute maps as shown in Figure 32 and 33. There could be two possible reasons of this type of building of fan from east to west, 1) the sediments were moving to the depocenter to the west and 2) the general flow and input of the sediments was from the eastern side generating a flow direction of sediment from the east. However, the observations from the data support the earlier possibility.

The deposition of basin floor fans in deep basin is in confirmation with the interpretation of Seldal (2005) about the wedges that they are deposited in the deep basin environments with good reservoir quality (average porosity range of 13 to 17 %). However, detailed analysis of these wedges helped in differentiating them to be deposited in different depositional environments (shallow marine and deep marine), not deep marine only. On the other hand, Sandvik (2014) interpreted them as coastal plain and offshore transition zone (with a minor tidal influence) deposits in wells 7120/2-2 and 7120/1-2 respectively. Type 1 wedges in well 7120/2-2 are interpreted as delta plain deposits based on the well log and seismic facies which is in confirmation with Sandvik (2014). However, the same type of wedges in well 7120/1-2 are interpreted as footwall derived debris flows, slope aprons, ponded deposits and amalgamated fluvial channels which are not in confirmation with the interpretations of Sandvik (2014). The reason probably is that the core interpretations are from basal part of the

85

wedges which might be the bottomsets of the fan delta as indicated by shale deposits with minor stringers of sand as shown in core photo in appendix IV (Figure 59(B)).

Finally, the type 1 and 2 wedges are interpreted to be deposited in coastal plain, slope aprons/ponded deposits/debris flows andcanyon fill deposits respectively on the faulted terrace (shelf). Type 3 wedge deposited in deep marine environments as wedge shaped bodies of coarse grained sediment.

5.4.2   Phase 2: Clastic wedges of late-rifting stage (Barremian to Albian)

The rifting activities were ending at this stage causing a gradual rise in relative sea level which may be attributed to rift quiescence period. The faulted terrace (narrow shelf) was flooded due to the rise in relative sea level during the Aptian-Albian because of the reduced tectonic activity such as subsidence and uplift. This resulted into a change of basin margin environment from erosional to progradational on the shelf (faulted terrace). This was the time of deposition of fan deltas along the strike of the main fault with sediment source from the footwall uplands (Figure 51B). The deposition of fan deltas resulted into development of wedge shaped clastic bodies ending near the shelf edge which was approximately 5 km away from the footwall uplands in the Lower Cretaceous times. Development of numerous fan deltas along the strike of the main fault, from different point sources, created interdistributary bays. Interdistributary bays and delta plains are the places of deposition of fine grained sediments as can be observed from the core interpretation of well 7120/2-2 in appendix IV (Figure 51(A)). Transparent (weak amplitude) seismic reflections from the wedges penetrated in well 7120/2-2 might indicate that the sediment supply was medium to fine grained.

The sediments were also bypassing to the deeper basin through a network of canyons/gullies and channels from the western side of the delta front. The shape of the fan can be seen diverting from the west to east. Again, there could be two possibilities for the diversion of sediment flow from the west to the east (Figure 51B): 1) the sediments were moving to the depocenter located to the eastern side, and 2) the general flow and input of the sediments was from the western side generating a flow direction of sediment from the west. First possibility seemed to be correct based on the observation from the data as shown in Figure 51B. This episode of deposition was followed by a period of non-deposition/hiatus and erosion. This is indicated by truncating reflectors against the erosional surface on top of the deltaic deposits. After the deposition of these wedges, the system changed to a full-fledged transgressive environment and is dominated by fine-grained deposits.
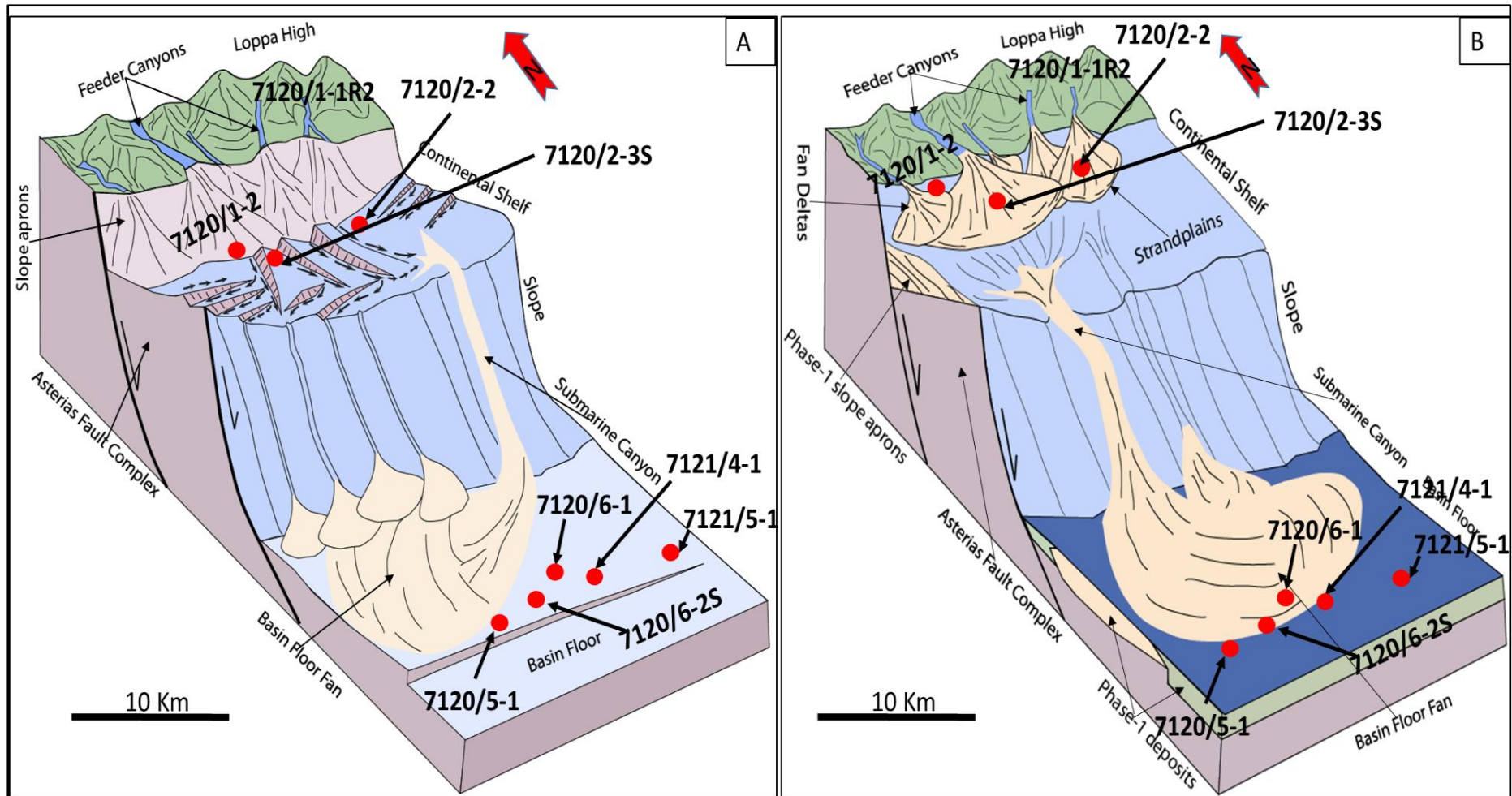
Figure 51: Conceptual depositional models. A) Phase-1 where erosion was happening on the narrow shelf area and sediment were able to cross the narrow margin to deep basin through a rigorous network of canyons/gullies on the faulted terrace. B) Phase-2 where narrow shelf was flooded and sediments were depositing as fan deltas in addition to bypassing to the deep basin through slumps and debris flows via canyons. Red dots show approximate locations of the wells used in this study.

5.5 Reservoir properties of the clastic wedges

Reservoir quality of the wedges has been studied by Seldal (2005) based on the evaluation of well logs. Petrophysical evaluation was carried out by Rodriguez (2015) to evaluate the reservoir properties of the wedges encountered in wells 7120/1-2 and 7120/2-2 along-with other wells. Both of these studies concluded that the quality of the reservoir is good with porosity ranges of 13-17 %. Minor amount of carbonate cement has been found during thin section analysis by Rodriguez (2015). Further on, rock physics analysis has been carried out, in this study, for evaluation of the reservoir properties of these clastic wedges which gives different results depending on the depositional environment.

The type 4 wedge (SF4), deltaic deposits, shows very good quality (porosity range 7-20%) of sands with a considerable amount of cement as interpreted in Figure 45. The presence of contact cement is beneficial for keeping the grains intact at contact points and hence preserving the porosity resulting into increase in reservoir quality. It also causes the increase in velocity of the sand which results into increase in the acoustic impedance. On the other hand, the presence of constant cement, distributed between the grains, act as degrading process for porosity and reduce reservoir potential of the wedge. However, amount of cement is low to medium which indicates that the grains are intact and the decrease in porosity is not significant for these wedges. That is probably one of the reasons of preservation of porosities despite a burial depth of more than 3000 meters and then uplift of around 1500 m as proposed by Rodriguez (2015). Furthermore, presence of a fair amount of cement may cause a drastic change in the seismic response due to increased acoustic impedance of the sand layer compared to non-cemented sand layer. Therefore, a cemented sand underlying shale unit might give a brighter seismic response than that of non-cemented sand underlying the same shale unit. This phenomenon is also confirmed by the bright reflections from top of this wedge as shown in Figure 52. It can be observed from the figure that the amplitude of the reflections depend on the amount of cement as indicated by the rock physics crossplots on the right side of each seismic line. Weak to medium amplitude reflections in Figure 52A can be attributed to the presence of the less amount of cement in silty sand. The high amplitude seismic response in Figure 52B shows the presence of relatively well cemented clean sand, causing a significant difference in acoustic impedance. It gives an indication of the change in seismic response because of presence of cement in the sand. However, a proper AVO analysis, using pre-stack seismic data, is necessary to validate the difference in amplitude of the seismic reflections.
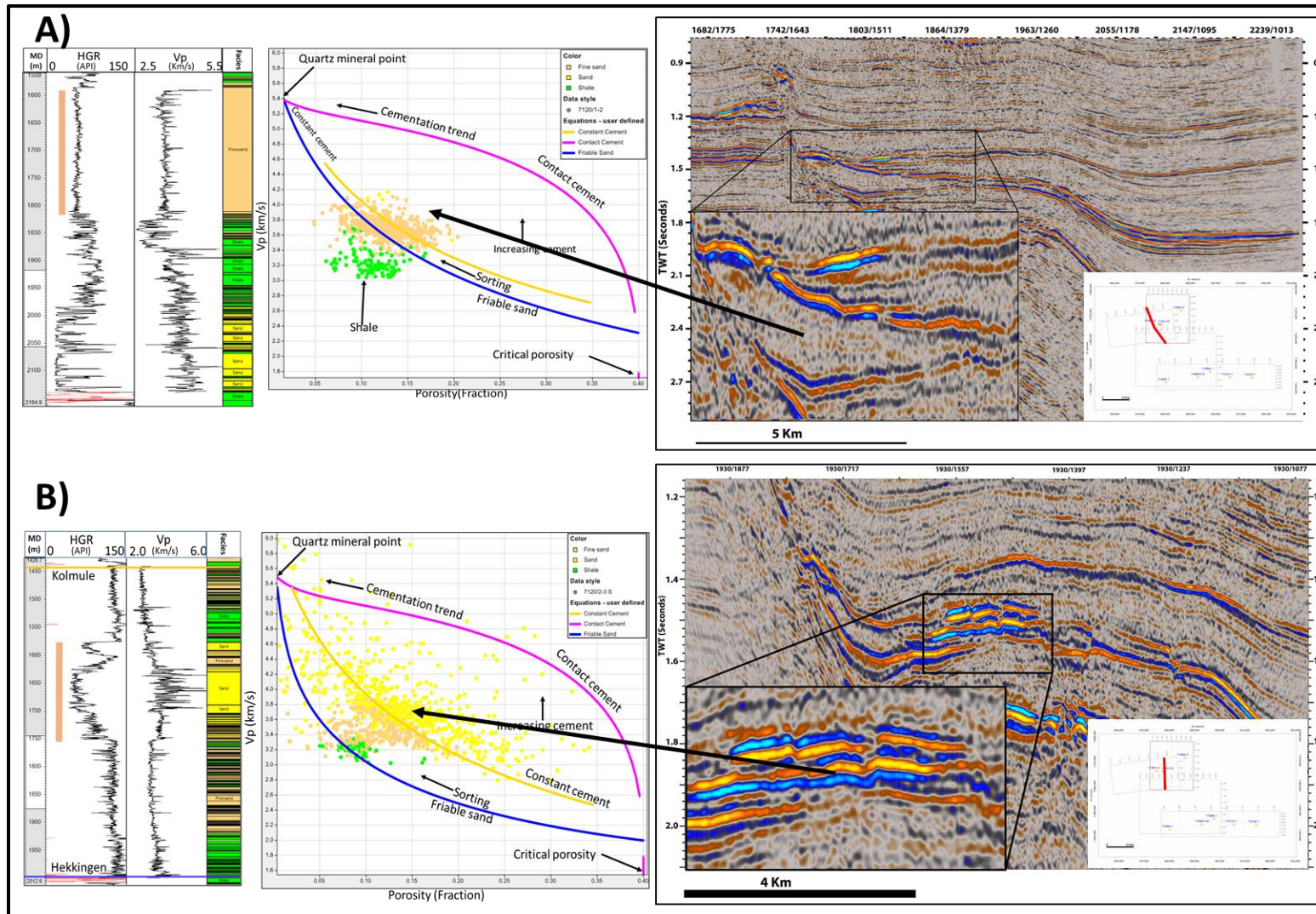
Figure 52: Seismic response of the type 4 wedge at wells 7120/1-2 (A) and 7120/2-3S (B). The data points for 7120/2-3 S falls on the constant cement model indicating higher amount of cement also confirmed by the brighter seismic response as shown. Whereas, the data points fall on the constant cement model but closer to the friable sand model which indicates relatively lower amount of cement and is confirmed by relatively weaker seismic reflections.

89

Type 1 wedges show varying rock physics response in wells 7120/1-2 and 7120/2-2. Most of them are composed of friable sand and silty shale as proposed by the location of scatterplots in porosity-velocity plane in Figure 42 and Figure 43. However, the lower part of the type 1 wedge (SF3) in well 7120/1-2 shows excellent reservoir quality with porosity range of 12 to 22% and medium to high amount of contact cement along with constant cement as shown in Figure 44. Contact cement is good for porosity preservation even at greater depth while constant cement reduce the porosity and reservoir potential of the rocks. On the other hand, these wedges in well 7120/2-2 (SF5) show poor quality sands with almost all the data plotted on and below friable sand model as shown in Figure 43.

Analysis of the wedge encountered in the lower part of the Kolmule Formation, in well 7120/2-3S, points out that the channelized parts of the fan deltaic deposits have excellent reservoir properties with porosity ranging from 7 to 27%. The amount of cement is medium to high as indicated by the constant cement model.

The cementation is partly confirmed by the compaction trends of the wells as shown in Figure 53. The change of compaction trend from mechanical into chemical compaction happens at around 2 km depth with a temperature of about 70 degrees Celsius (Avseth et al., 2010). However, in the study area the transition depth is shallower as shown in Figure 53. The mechanical compaction changes into chemical compaction at around 1500 meters (7120/2-3S), 1600 meters (7120/1-2) and 1800 meters (7120/2-2). This change in transition depth indicates the threshold depth where onset of cementation is likely to be happening for each well location. Notice that the transition depth is deeper for well 7120/2-2 indicating the rocks will be cemented at slightly greater depths at this location.

The compaction trend of the well 7120/2-3S is at shallower depth indicating cementation is highly likely to be found at relatively shallower depths. The results of rock physics analysis (carried out for the wells) are in accordance with the compaction trends. The type 4 wedge (SF1) found in well 7120/2-3S is more cemented at equivalent depths in comparison to those encountered in other wells corresponding to the seismic facies SF4 and SF6 in wells 7120/1-2 and 7120/2-2 respectively. The wedges of type 1 in well 7120/1-2 (SF2 and SF3) are deeper than wedge type 4 (SF4) in the same well and have higher amount of cement as shown in Figure 42, Figure 44 and Figure 45. However, the same wedge in well 7120/2-2 (SF5) shows very small amount of cement at even higher depth values.

Diagnosis of the cement in clastic wedges may help in understanding the seismic behavior of the wedges. The amount of cement decreases from bottom to top in the wells, and also while moving from west to east from well 7120/1-2 to 7120/2-2. It reveals the possible reasons of the reduction in porosity (depositional or diagenetic) which helps understanding the reservoir properties of the wedges. The reduction in porosity at well locations 7120/1-2 and 7120/2-3S is controlled mainly by diagenetic processes such as cementation, compaction. On the other hand, porosity is reduced mainly because of deteriorating sorting at well location 7120/2-2. However, both of these processes are partly contributing to the porosity reductions in all of the wells. Hence, it could be very helpful in planning exploration activities keeping the depositional and diagenetic trends in mind.
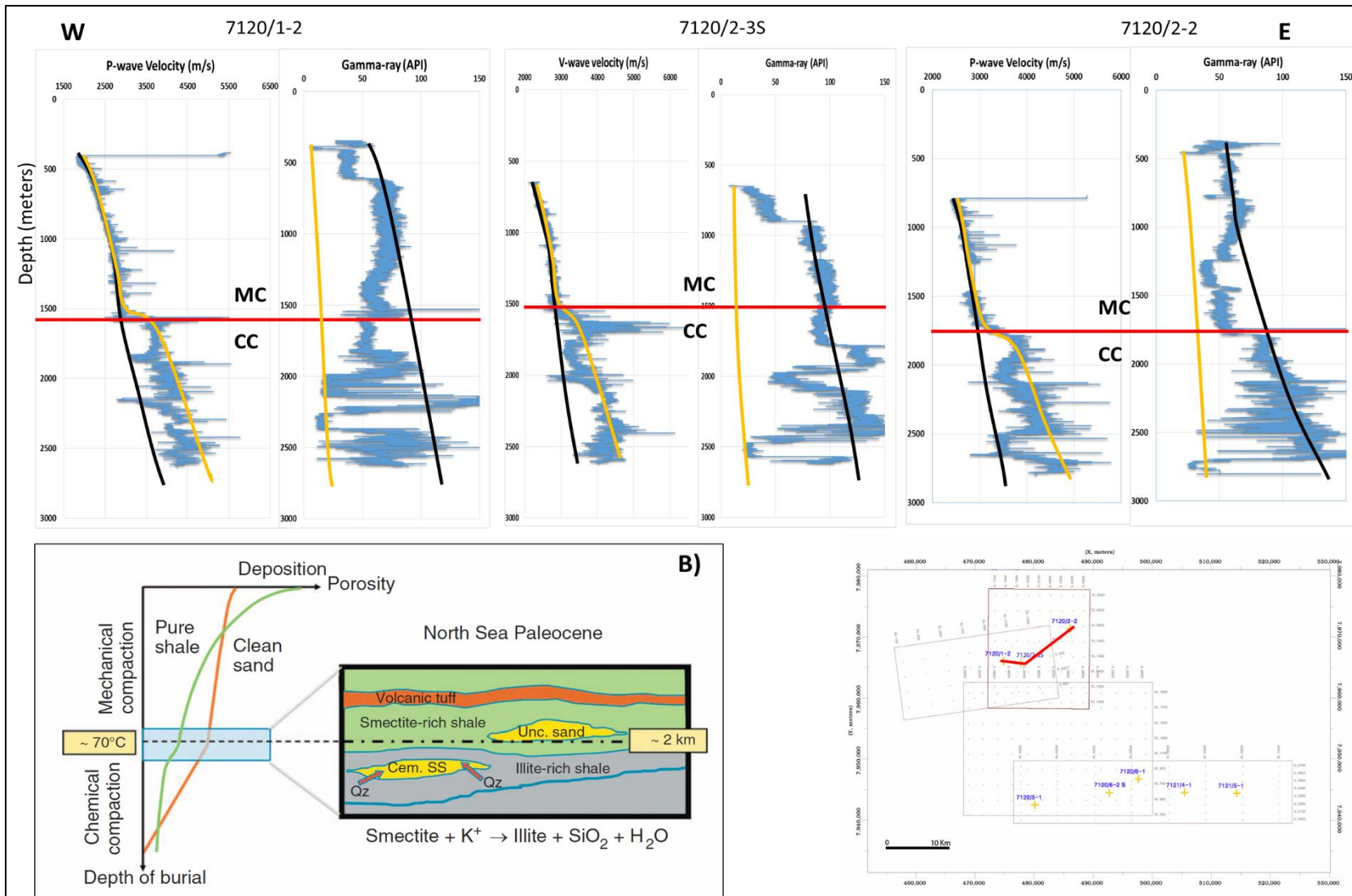
Figure 53: Compaction trends for sandstone (orange line) and shale (black line). Mechanical compaction changes into chemical compaction below depth of approximately 1500 meters and sandstone is expected to be cemented below transition zone notice depth of around 1800 m for well 7120/2-2. MC= mechanical compaction, CC= chemical compaction (adapted from Avseth et al. (2010)

5.6 Present day analogues for wedges of type 4

Type 4 wedges are interpreted to be deposited in wave dominated fan deltaic settings with medium to high reservoir quality. It is supported by the presence of strandplains and typical lobate shape of the fan delta on seismic attribute time slices. The wave dominated behavior of the coastline resulted into development of strandplains which could be a potential target of exploration. These kind of wave dominated fan deltas are found worldwide, however the ones in the southwest Jamaica and the central Japan could be the best present day analogues for the one interpreted in this study as shown in Figure 54.

5.6.1 Kurobegawa fan delta, central Japan

It is modern fan delta of arcuate morphology at the mouth the Kurobe River in the Toyama Bay of Japan. It is a wave dominated fan delta indicated by the development of strandplains along the coastal areas. It has features such as abandoned and braided channels, delta plain, crevasse splays and strandplains similar to as observed in the fan deltas of type 4 wedge.as shown in Figure 54A.

5.6.2 Yallahs Fan delta, southwest Jamaica

This is a wave-dominated lobate shape fan delta with an area of around 11 sq. km as shown in Figure 54B. It has a gradient of about 15 m /km and dips towards sea (Wescott and Ethridge, 1980). It is smaller than the fan delta observed in this study but present the similar characteristics such as very closely located highlands (Blue Mountains) lobate shape, channels, strandplains and basinward thinning wedge shaped geometry.

A comparison of the fan delta from this study and the modern ones is presented in Figure 54. The similarities such as delta plain, channels and strandplains can clearly be observed as indicated in the figure.
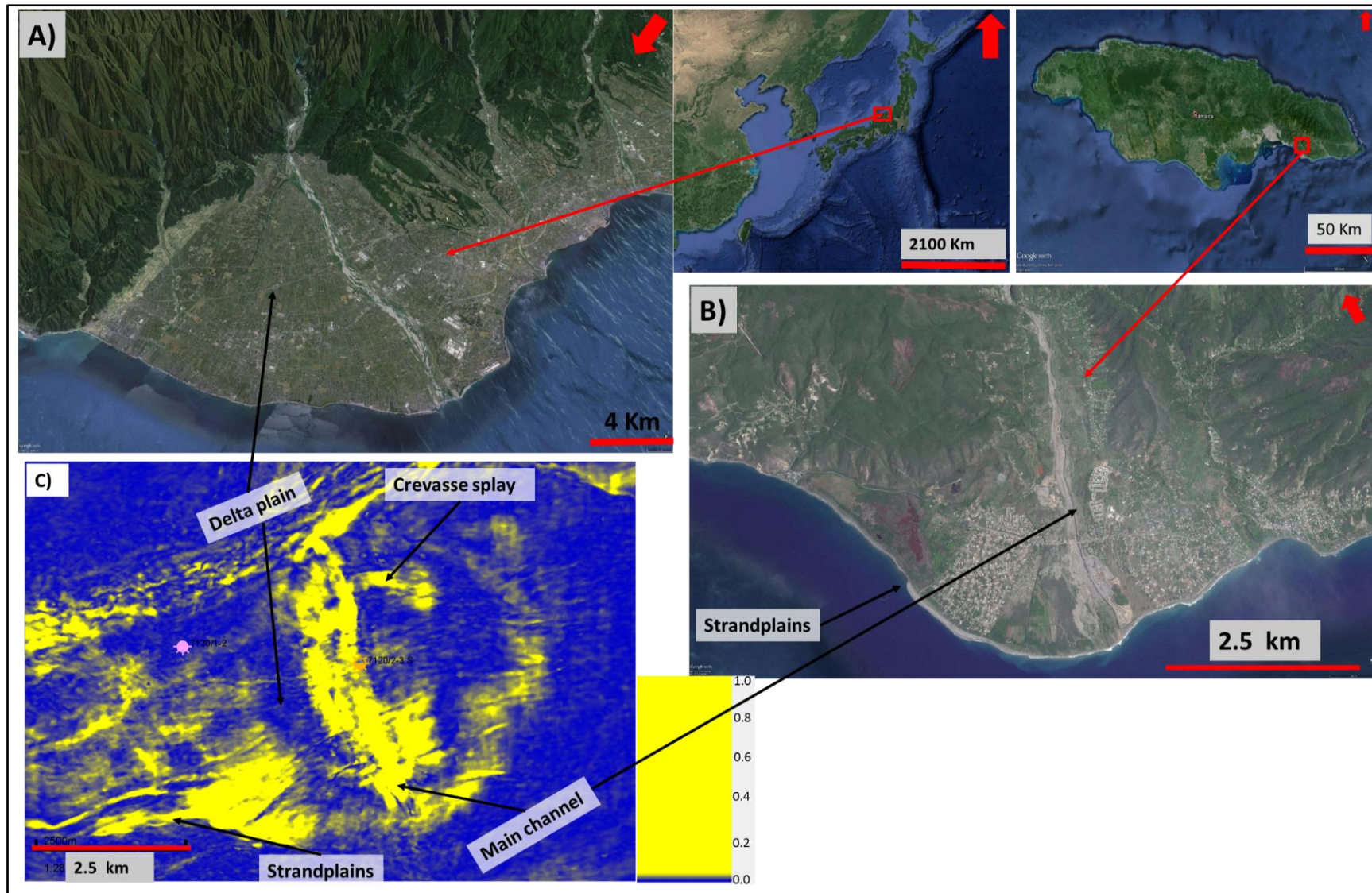
Figure 54: A) Kurobegawa fan delta, central Japan and B) Yallahs fan delta, southwest Jamaica and C) fan delta interpreted in the study area. These fan deltas are the most closely related analogues with nearly the similar dimensions and depositional settings as indicated.

6 Conclusions

An integration of well logs, seismic facies and seismic attributes is essential for interpretation of depositional environment of clastic wedges in the southwestern Barents Sea. Seismic attribute workflows (structural smoothing followed by coherence, chaos and sweetness) are useful for defining the depositional environment based on qualitative observation of the shape of the depositional elements. Rock physics analysis is helpful in diagnosing properties of sand such as volume of cement, sorting/porosity trends and shale proportion. The main conclusions drawn from the study are;

1. The wedges are divided in two main groups depending on the level of tectonic activities 1) Wedges of initial-rifting phase deposited on the erosional basin margins when narrow shelf was exposed and erosional processes were dominated, carrying sediments to the deeper part of the basin and, 2) wedges of late-rifting stage, deposited at the time of flooding of narrow shelf.

2. The deep basinwedges are the basin floor fan deposits, deposited during both initial and late stages of rifting, with potential reservoir quality sediments which is indicated by high amplitude reflections.

3. Wedges observed on the narrow shelf are deposited in a range of environments, 1) slope aprons and debris flow, 2) fan delta wedges with channel fills and over bank deposits such as crevasse splays and alongshore strandplain, 3) canyon fills, and 4) ponded deposits.

4. Type 4 wedges have a good reservoir potential as indicated by rock physics analysis compared to that of type 1 wedges.

5. Proportion of sand decreases going from west to east as observed in well data and seismic attributes which indicate relatively calm environment in the east during the Early Cretaceous times. It implies that the wedges found in the western part have better reservoir quality than those present in the eastern side.

6. Different seismic attributes respond to depositional elements differently depending on the internal properties, shapes and relationship with the structural trends. Coherence attribute delineate minor faults and channel boundaries with a subtle help in identification of fan deltas and associated depositional features (channels, crevasse splay, strandplains, floodplain etc), submarine fans and submarine channel system. Chaos attribute delineate internal sediment fill of the depositional elements on the basis of homogeneity/heterogeneity. Whereas, sweetness attribute is sensitive to sand and

shale dominated sediments and better resolve the features such as crevasse splays, strandplains and submarine fans.

7. The wedges with relatively clean and well sorted sand are cemented whereas those with deteriorating sorting and more shale content are friable (behave as rock only under pressure conditions otherwise individual grains).

8. Diagnosis of cement in sands of wedges, especially in deltaic wedges, implies that the seismic response of the wedges is stronger compared to those made of friable and less cemented sands.

7 Future Work

Rock physics models have been proposed for the sands of each wedge. However, the seismic response of the wedges could not be tested properly, to confirm the seismic response from the top and bottom of the wedges, because of unavailability of pre-stack seismic data. It would be interesting to validate the seismic response predicted by rock physics modeling in this study conditioned availability of pre-stack seismic data.

Furthermore, lithology and fluid cubes could not be generated because of limited time available during this study. This study could be expanded by generating the cubes for detailed analysis of the wedges from reservoir potential and fluid saturation point of views.

8 Appendices

8.1 Appedix I

Fluid saturation, mineral content (Vshale) and porosity logs generated using Interactive Petrophysics (IP) senergy software for well 7120/2-3S as shown below in CPI plot.

Following formulas have been used for calculations of PHIE and Sw

PHIE = PHID-V_{sh}*PHIDsh, PHID = Density porosity and PHIDsh = Density-porosity of shale

Where,

PHID = (ϱma – ϱb)/(ϱma – ϱf)

PHID$_{sh}$ = (ϱma – ϱsh)/(ϱma – ϱf)

Where ϱma = Density of matrix, ϱb = Bulk density of the rock and ϱf = Density of the fluid and ϱsh = Density of shale

 And water saturation

Sw = (1/Rt^0.5)/(((Vsh^(1-Vsh/2))/Rsh^0.5)+((PHIE^(m/2))/(a*Rw)^0.5))

Rsh = Resistivity of shale from the log. , Rw = Resistivity of water, Vsh = Volume of shale, Rt = formation resistivity, PHIE = effective porosity
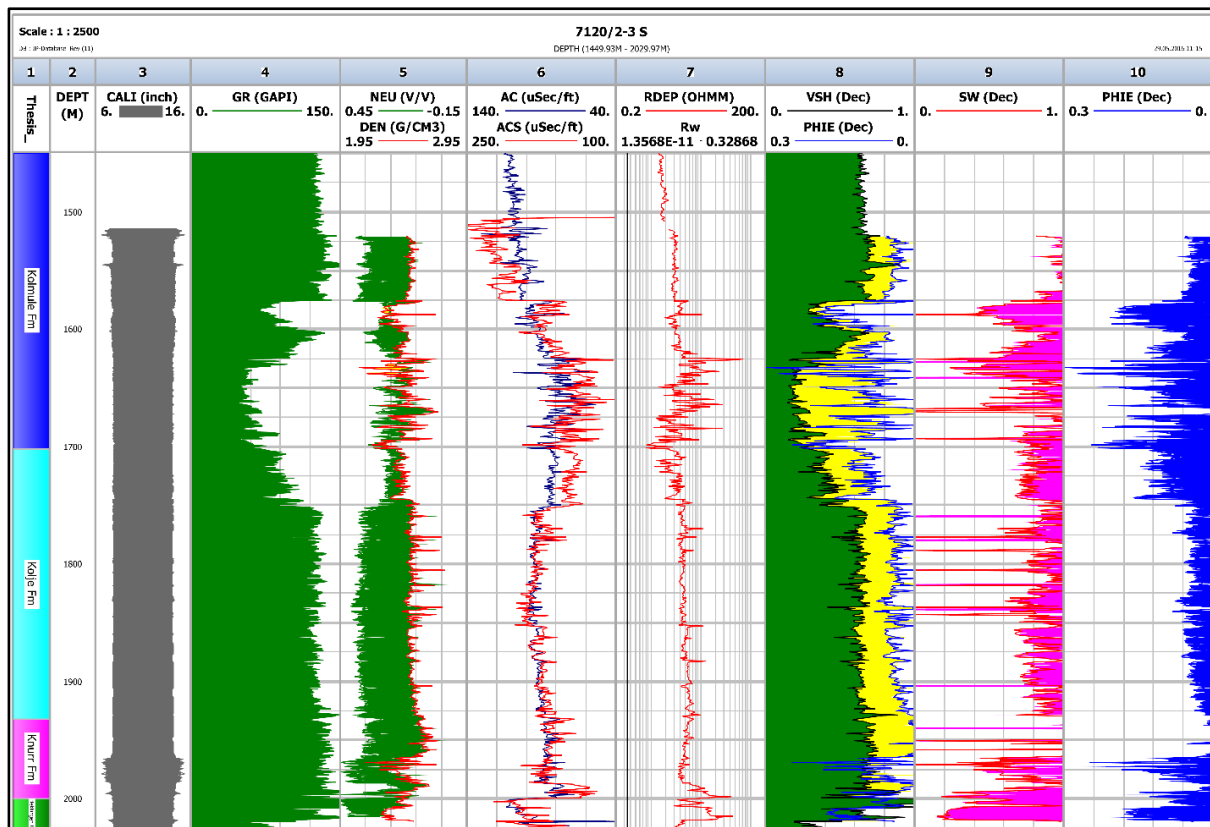
Figure 55: Porosity, water saturation and Vshale logs generated using IP senergy software.

8.2 Appendix II

The neutron-density plots for analysis of homogeneity of the clastic wedges are shown below.
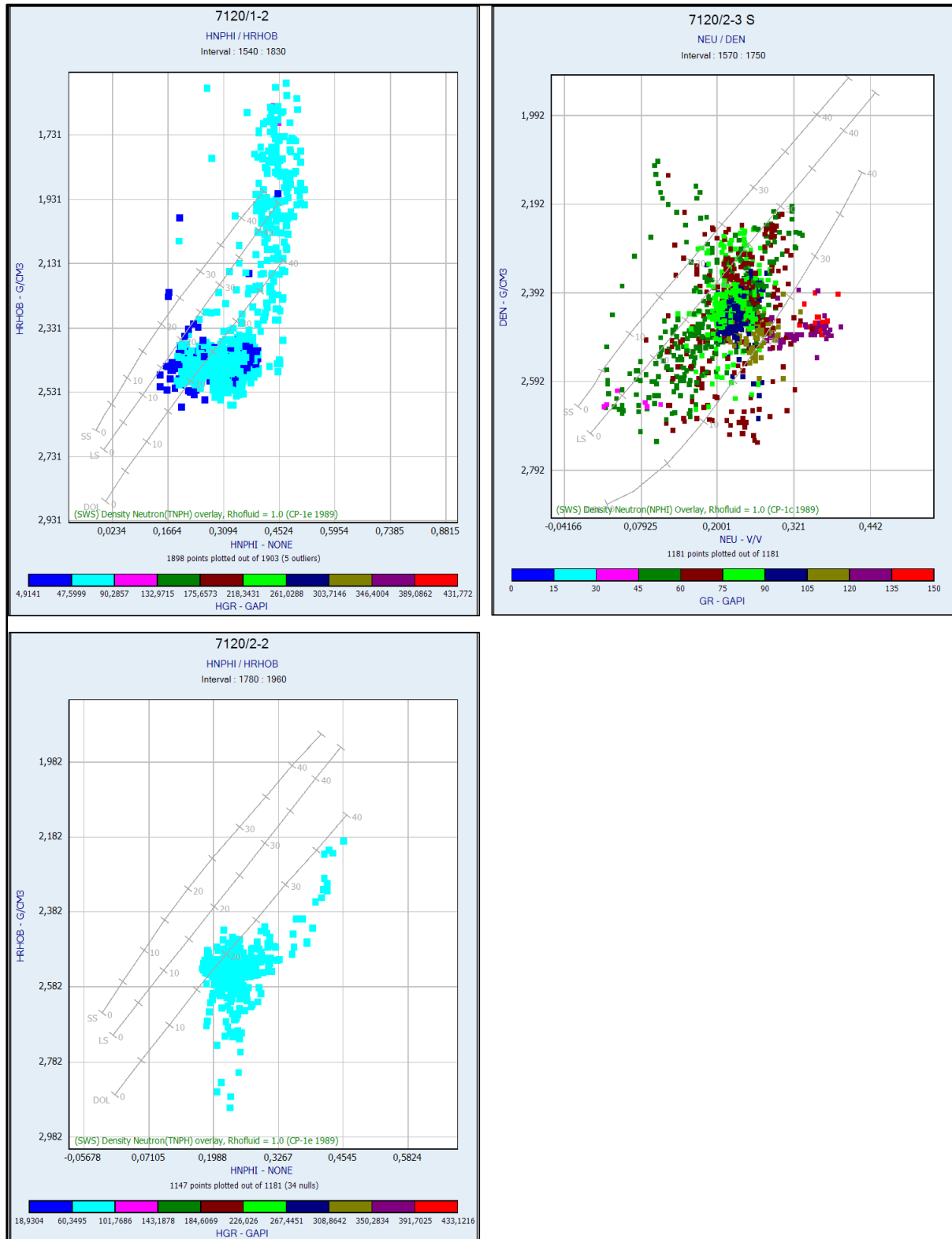
Figure 56: Neutron-density crossplot for wedge type 4 in the well drilled though it. Notice the shale content increase as we move from west to east.
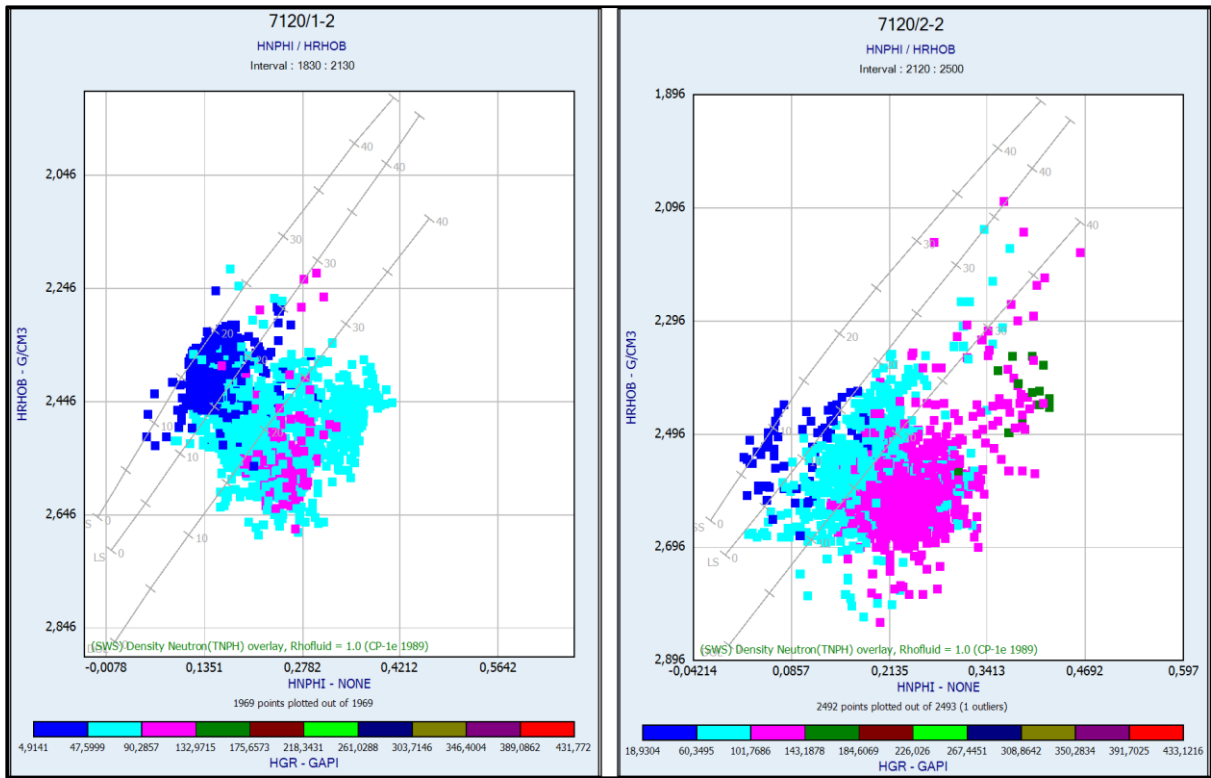
Figure 57: Wedge type 1 neutron-density crossplot showing heterogeneity of the wedges with clean sand on one hand to pure shale on the other.

8.3 Appendix III

Interactive electro-facies generation for well 7120/2-3S using Blueback interactive facies generator using GR value cut-offs.
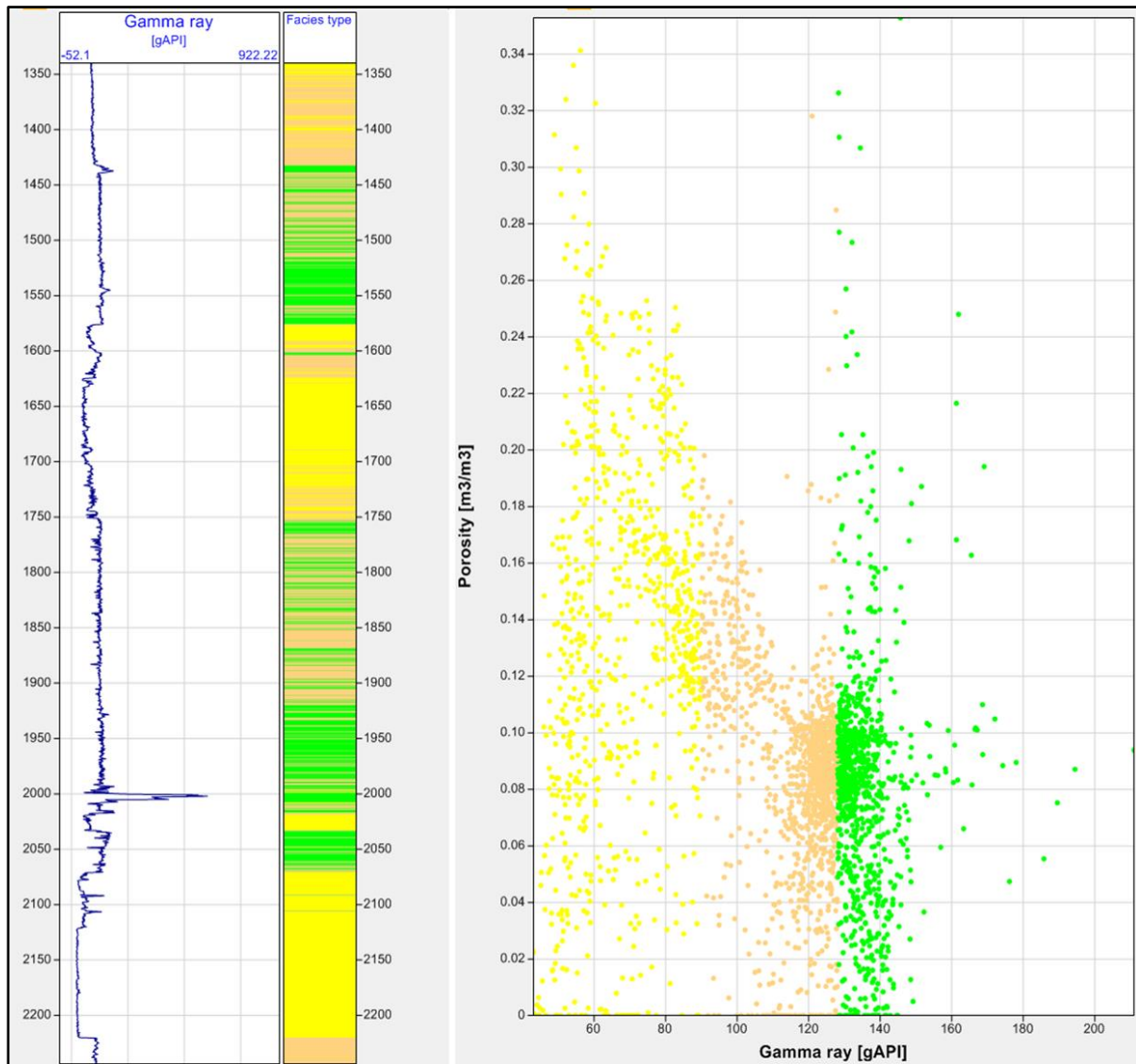
Figure 58: Interactive facies based on the values of gamma-ray (GR).

8.4 Appendix IV

Core photos and interpretations for different wedges are shown below

Figure 59: Core photos for part of the wedges, A) Wedge type 4 well 7120/2-2, and B) Wedge Type 4 well 7120/1-2, C) Wedge type 1 well 7120/2-2 and, D) Wedge type 1 well 7120/1-2. The overall behavior of the wedges is similar to these photos.

Figure 60: Core interpretation well 7120/2-2. A) Upper part of wedge type 1 is interpreted as coastal plain deposits whereas wedge type 4 is interpreted to be deposited in offshore transition zone , B) Lower part of the wedge type 1 is interpreted as offshore transition zone (Sandvik, 2014).

Figure 61: Core interpretation well 7120/1-2. Both wedge type 1 and 4 are interpreted as offshore transition deposits (Sandvik, 2014).

9   References

Allen, P. A., and A. Densmore, 2000, Sediment flux from an uplifting fault block: Basin Research, v. 12, p. 367-380.

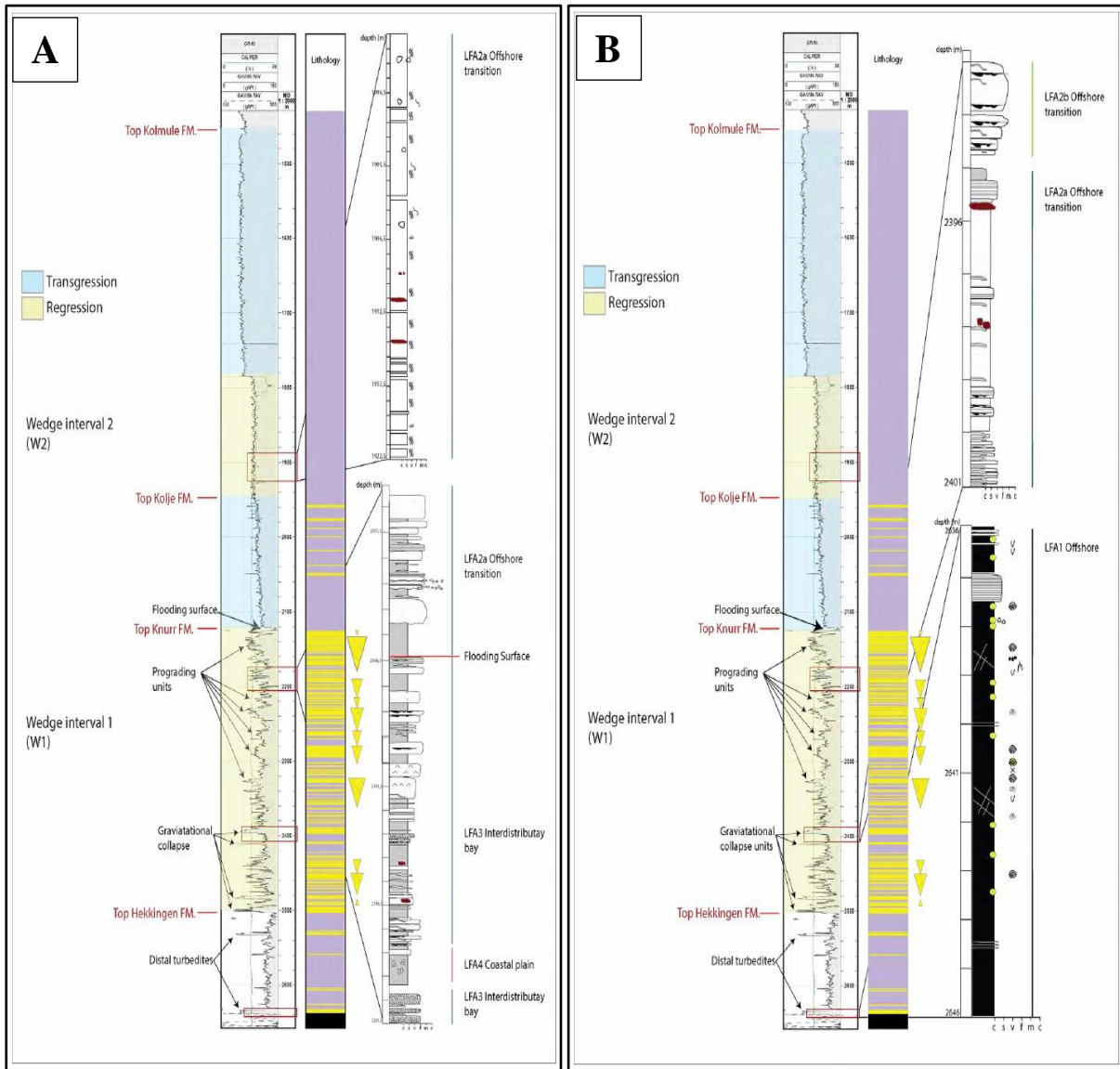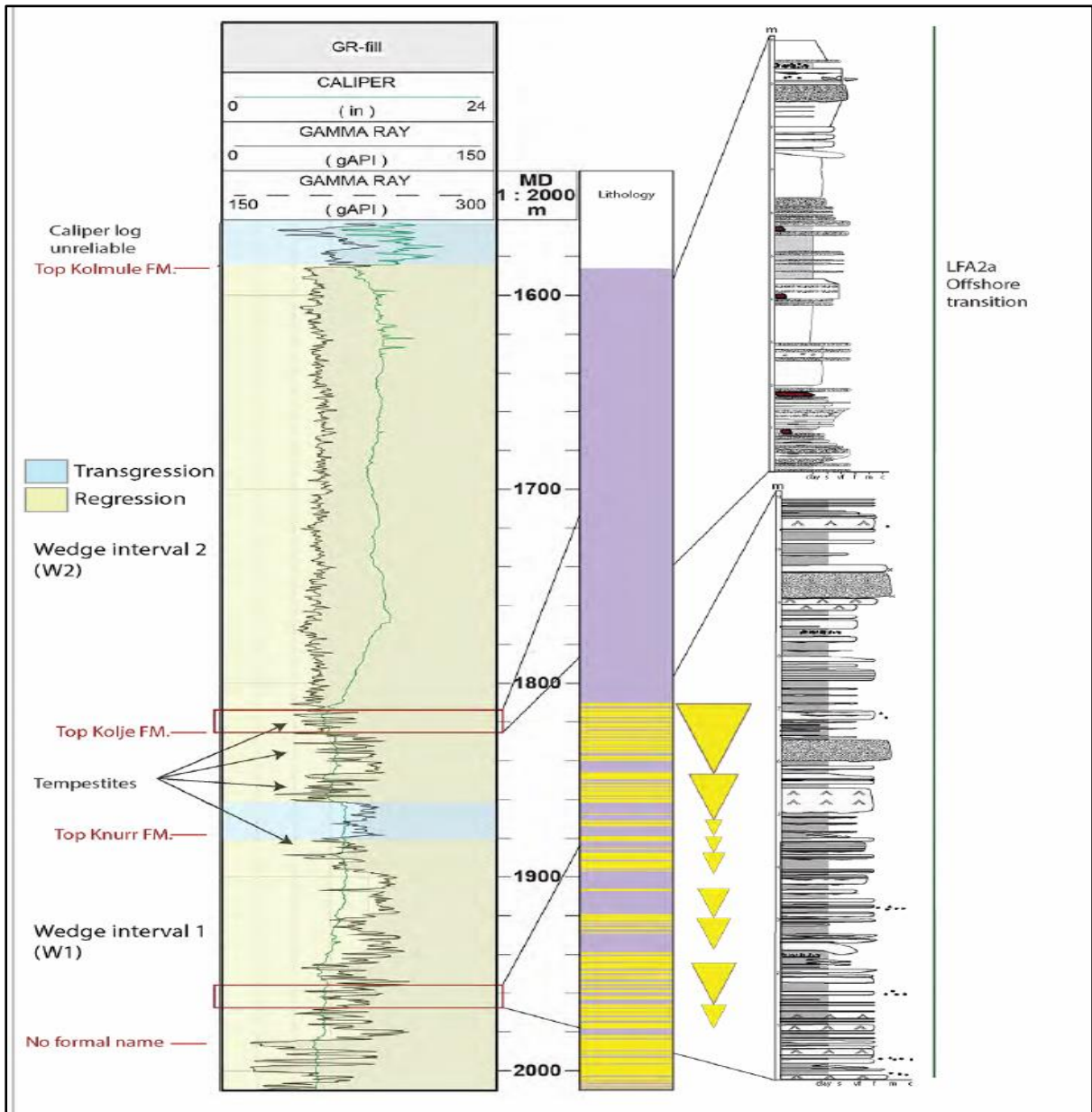Avseth, P., J. Dvorkin, G. Mavko, and J. Rykkje, 2000, Rock physics diagnostic of North Sea sands: Link between microstructure and seismic properties: Geophysical Research Letters, v. 27, p. 2761-2764.

Avseth, P., A. Jørstad, A.-J. van Wijngaarden, and G. Mavko, 2009, Rock physics estimation of cement volume, sorting, and net-to-gross in North Sea sandstones: The Leading Edge, v. 28, p. 98-108.

Avseth, P., T. Mukerji, and G. Mavko, 2005, Quantitative Seismic Interpretation: Quantitative Seismic Interpretation, by Per Avseth and Tapan Mukerji and Gary Mavko, pp. 376. ISBN 0521816017. Cambridge, UK: Cambridge University Press, March 2005., p. 376.

Avseth, P., T. Mukerji, G. Mavko, and J. Dvorkin, 2010, Rock-physics diagnostics of depositional texture, diagenetic alterations, and reservoir heterogeneity in high-porosity siliciclastic sediments and rocks—A review of selected models and suggested work flows: Geophysics, v. 75, p. 75A31-75A47.

Avseth, P., and T. Veggeland, 2015, Seismic Screening for Hydrocarbon Prospects using Rock-Physics Attributes: ASEG Extended Abstracts, v. 2015, p. 1-1.

Bahorich, M., and S. Farmer, 1995, 3-D seismic discontinuity for faults and stratigraphic features: The coherence cube: The leading edge, v. 14, p. 1053-1058.

Brown, A. R., 1996, Seismic attributes and their classification: The leading edge, v. 15, p. 1090-1090.

Chopra, S., and K. J. Marfurt, 2005, Seismic attributes—A historical perspective: Geophysics, v. 70, p. 3SO-28SO.

Coe, A. L., 2003, The sedimentary record of sea-level change, Cambridge University Press.

Dalland, A., D. Worsley, and K. Ofstad, 1988, A Lithostratigraphic Scheme for the Mesozoic and Cenozoic and Succession Offshore Mid-and Northern Norway, Oljedirektoratet.

Dvorkin, J., and M. A. Gutierrez, 2002, Grain sorting, porosity, and elasticity: Petrophysics, v. 43.

Dvorkin, J., and A. Nur, 1996, Elasticity of high-porosity sandstones: Theory for two North Sea data sets: Geophysics, v. 61, p. 1363-1370.

Dvorkin, J., and A. Nur, 2002, Critical-porosity models: MEMOIRS-AMERICAN ASSOCIATION OF PETROLEUM GEOLOGISTS, p. 33-42.

Dvorkin, J., A. Nur, and H. Yin, 1994, Effective properties of cemented granular materials: Mechanics of materials, v. 18, p. 351-366.

Escalona, A., and P. Mann, 2006, Sequence-stratigraphic analysis of Eocene clastic foreland basin deposits in central Lake Maracaibo using high-resolution well correlation and 3-D seismic data: AAPG bulletin, v. 90, p. 581-623.

Faleide, J. I., F. Tsikalas, A. J. Breivik, R. Mjelde, O. Ritzmann, O. Engen, J. Wilson, and O. Eldholm, 2008, Structure and evolution of the continental margin off Norway and the Barents Sea: Episodes, v. 31, p. 82-91.

Faleide, J. I., E. Vågnes, and S. T. Gudlaugsson, 1993, Late Mesozoic-Cenozoic evolution of the south-western Barents Sea in a regional rift-shear tectonic setting: Marine and Petroleum Geology, v. 10, p. 186-214.

Fanka, W. R. T., 2012, Rock physics study of poorly consolidated sandstone in the North Sea, Norwegian University of Science and Technology Trondheim, 76 p.

Ferguson, C. J., A. Avu, and G. Paton, 2010, Seismic analysis workflow for reservoir characterization in the vicinity of salt: first break, v. 28.

Fjeld, T. L., 2014, Seismic characterization of lower cretaceous clastic wedges in the Tromsø Basin, University of Stavanger 59 p.

Gabrielsen, R., 1984, Long-lived fault zones and their influence on the tectonic development of the southwestern Barents Sea: Journal of the Geological Society, v. 141, p. 651-662.

Halland, E., J. Mujezinovic, F. Riis, A. BJØRNESTAD, I. MELING, I. GJELDVIK, I. TAPPEL, M. BJØRHEIM, R. RØD, and V. PHAM, 2014, CO 2 Storage Atlas: Norwegian Continental Shelf: Norwegian Petroleum Directorate, PO Box, v. 600.

Hart, B. S., 2008, Channel detection in 3-D seismic data using sweetness: AAPG bulletin, v. 92, p. 733-742.

Hoy, R. G., and K. D. Ridgway, 2003, Sedimentology and sequence stratigraphy of fan-delta and river-delta deposystems, Pennsylvanian Minturn Formation, Colorado: AAPG bulletin, v. 87, p. 1169-1191.

Hwang, I., S. Chough, S. Hong, and M. Choe, 1995, Controls and evolution of fan delta systems in the Miocene Pohang Basin, SE Korea: Sedimentary Geology, v. 98, p. 147-179.

Marin, D., A. Escalona, A. Kayukova, A. Stoupakova, and A. Suslova, 2014, Characterization of Lower Cretaceous seismic clinoforms in the SW Barents Sea: Implication to sand prone bodies prediction.

Matthews, N., U. Zimmermann, E. Mostafa, C. Rudd, L. Støle, T. J. Lapen, and R. Andreasen, 2015, Provenance data from Mesozoic rock successions in the Hammerfest basin: NGF Winter Conference.

McPherson, J. G., G. Shanmugam, and R. J. Moiola, 1987, Fan-deltas and braid deltas: varieties of coarse-grained deltas: Geological Society of America Bulletin, v. 99, p. 331-340.

Mindlin, R. D., 1949, Compliance of elastic bodies in contact: ASME Journal of Applied Mechanics, v. 16, p. 10.

NPD, 2013, Factpages, Wellbores, Norwegian Petroleum Directorate (NPD), Norway, p. Wellbore.

Radovich, B. J., and R. B. Oliveros, 1998, 3-D sequence interpretation of seismic instantaneous attributes from the Gorgon Field: The Leading Edge, v. 17, p. 1286-1293.

Reading, H. G., 2009, Sedimentary environments: processes, facies and stratigraphy, John Wiley & Sons.

Rodriguez, I., 2015, Petrophysical characterization of the Lower Cretaceous clastic wedges in the northwestern Barents Sea, University of Stavanger 1-117 p.

Sandvik, S. E., 2014, Description and comparison of Lower Cretaceous deposits from Svalbard and the southern Loppa High, University of Bergen, 121 p.

Sattar, N., C. Juhlin, and N. Ahmed, 2012, Seismic stratigraphic framework of an Early Cretaceous sand lobe at the slope of southern Loppa High Barents Sea, Norway, AAPG, p. 17.

Seldal, J., 2005, Lower Cretaceous: the next target for oil exploration in the Barents Sea?: Geological Society, London, Petroleum Geology Conference series, p. 231-240.

Tyler, N., and W. A. Ambrose, 1985, Facies architecture and production characteristics of strandplain reservoirs in the Frio Formation, Texas, Texas Univ., Austin (USA). Bureau of Economic Geology.

Weimer, P., R. M. Slatt, and R. Bouroullec, 2007, Introduction to the petroleum geology of deepwater settings, AAPG/Datapages.

Wescott, W. A., and F. G. Ethridge, 1980, Fan-delta sedimentology and tectonic setting--Yallahs fan delta, southeast Jamaica: AAPG Bulletin, v. 64, p. 374-399.